# KSU S4M: Settlement Stabilization through Structural Strengthening and Monitoring of KDOT Bridge 059-045 Shawnee Drive over I-135

Abdul H. Halim
Hayder A. Rasheed, Ph.D., P.E., F.ASCE
Caleb Mitchell, M.S.
Habiburrahman Ahmadi, Ph.D.

*Kansas State University Transportation Center*

Kansas
Department of Transportation

| 1. Report No. KS-20-03 | 2 Government Accession No. | 3 Recipient Catalog No. | |
|---|---|---|---|
| 4 **Title and Subtitle** KSU S4M: Settlement Stabilization through Structural Strengthening and Monitoring of KDOT Bridge 059-045 Shawnee Drive over I-135 | | 5 **Report Date** March 2021 | |
| | | 6 **Performing Organization Code** | |
| 7 **Author(s)** Abdul H. Halim, Hayder A. Rasheed, Ph.D., P.E., F.ASCE, Caleb Mitchell, M.S., Habiburrahman Ahmadi, Ph.D. | | 8 **Performing Organization Report No.** | |
| 9 **Performing Organization Name and Address** Kansas State University Transportation Center Department of Civil Engineering 2118 Fiedler Hall Manhattan, KS 66506-5000 | | 10 **Work Unit No. (TRAIS)** | |
| | | 11 **Contract or Grant No.** C2089 | |
| 12 **Sponsoring Agency Name and Address** Kansas Department of Transportation Bureau of Research 2300 SW Van Buren Topeka, Kansas 66611-1195 | | 13 **Type of Report and Period Covered** Final Report May 2016–April 2022 | |
| | | 14 **Sponsoring Agency Code** RE-0719-01 | |
| 15 **Supplementary Notes** For more information write to address in block 9. | | | |

16 **Abstract**

The Bridge 059-045 at Shawnee Drive over I-135 is a reinforced concrete box girder structure constructed in 1965 to connect the rural Shawnee Drive across the Interstate I-135 near McPherson, KS, in between Salina and Wichita. The bridge was observed during annual inspection in 1998 to have experienced some settlement due to its proximity to a sinkhole. This settlement progressed to noticeable levels in 2012 necessitating a semi-annual elevation profile survey that was consistently conducted by KDOT. In April 2016, KDOT determined that the bridge requires a detailed analysis to determine the safety and suitability of the bridge to stay open to traffic. Accordingly, a project was started by Kansas State University to perform a detailed finite element analysis to assess the level of distress in the bridge due to the continuous differential settlement caused by the active sinkhole deep in the soil under the bridge. Detailed finite element analysis was performed in this study revealing the fact that some structural components in this bridge are still safe while others have reached their ultimate envelope capacity, thus, suggesting the closure of the bridge to general traffic.

An estimated cost for strengthening is given in Section 5.2.5 of this report. Knowing that the strengthening will only extend the bridge's life up to May 2022, considering the settlement rate, it is recommended to demolish the bridge instead of strengthening it.

| 17 **Key Words** Bridges, Box girder bridges, Settlement (Structures), Finite element method, Structural analysis | 18 **Distribution Statement** No restrictions. This document is available to the public through the National Technical Information Service www.ntis.gov. | |
|---|---|---|
| 19 **Security Classification (of this report)** Unclassified | 20 **Security Classification (of this page)** Unclassified | 21 **No. of pages** 136 | 22 **Price** |

Form DOT F 1700.7 (8-72)

This page intentionally left blank.

# KSU S4M: Settlement Stabilization through Structural Strengthening and Monitoring of KDOT Bridge 059-045 Shawnee Drive over I-135

Final Report

Prepared by

Abdul H. Halim
Hayder A. Rasheed, Ph.D., P.E., F.ASCE
Caleb Mitchell, M.S.
Habiburrahman Ahmadi, Ph.D.

Kansas State University Transportation Center

# NOTICE

# DISCLAIMER

# Abstract

The Bridge 059-045 at Shawnee Drive over I-135 is a reinforced concrete box girder structure constructed in 1965 to connect the rural Shawnee Drive across the Interstate I-135 near McPherson, KS, in between Salina and Wichita. The bridge was observed during annual inspection in 1998 to have experienced some settlement due to its proximity to a sinkhole. This settlement progressed to noticeable levels in 2012 necessitating a semi-annual elevation profile survey that was consistently conducted by KDOT. In April 2016, KDOT determined that the bridge requires a detailed analysis to determine the safety and suitability of the bridge to stay open to traffic. Accordingly, a project was started by Kansas State University to perform a detailed finite element analysis to assess the level of distress in the bridge due to the continuous differential settlement caused by the active sinkhole deep in the soil under the bridge. Detailed finite element analysis was performed in this study revealing the fact that some structural components in this bridge are still safe while others have reached their ultimate envelope capacity, thus, suggesting the closure of the bridge to general traffic.

An estimated cost for strengthening is given in Section 5.2.5 of this report. Knowing that the strengthening will only extend the bridge's life up to May 2022, considering the settlement rate, it is recommended to demolish the bridge instead of strengthening it.

# Acknowledgments

# Table of Contents

# List of Tables

# List of Figures

# Chapter 1: Introduction

## 1.1 Overview

The Bridge 059-045 at Shawnee Drive over I-135 is a reinforced concrete box girder structure constructed in 1965 to connect the rural Shawnee Drive across the Interstate I-135 near McPherson, KS, in between Salina and Wichita. The bridge was observed during annual inspection in 1998 to have experienced some settlement due to its proximity to a sinkhole.

## 1.2 Background

The settlement of Bridge 059-045 in McPherson County has been monitored since October 2012. Settlement at this location is expected to have been occurring since the bridge was built. The Kansas Department of Transportation (KDOT) believes that the settlement is caused by abandoned oil wells in the area. In the 1920s there were few regulations on oil production, which led to rapid withdrawals from the areas. The wells were drilled through many layers in order to reach the oil, which included sandstone, groundwater, shale, and thick salt deposits. Since the oil was removed so quickly, the sites ran out of oil and were abandoned. According to KDOT Regional Geologist Neil Croxton, "Whatever plugging was done, if anything was done, was not successful" (Dedo & White, 2017). The ineffective plugging allowed for the ground water to get past the shale, which protects the salt layer from the water. The water then dissolved the salt layer, which created voids underground and lead to gradual settlement over time.

When the bridge was built in 1965, nine borings were taken around the location of the bridge. These were used to determine the soil conditions under the bridge in order to design the depth of the piles and to find the depth of the bedrock. In 2017, 23 borings were taken to determine how the soil layers and the depth of the bedrock had changed since the bridge was originally built. Figure 1.1 shows the drop in bedrock elevation from 1965 to 2017.
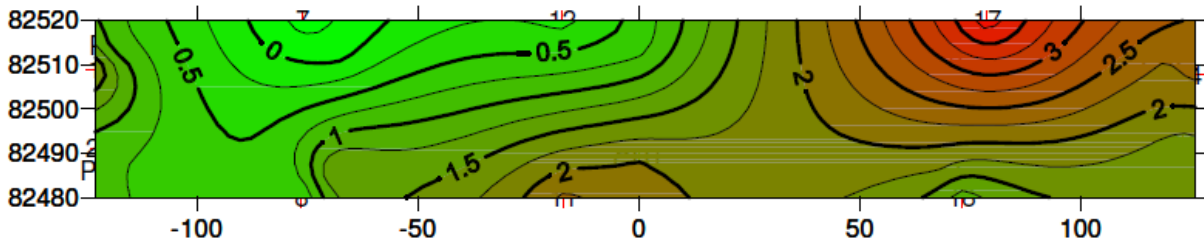
**Figure 1.1: Drop in bedrock elevation at the bridge footprint**

The drop in the bedrock ranges from zero feet on the west side of the bridge to over 3 feet on the east side. This drop in the bedrock shows how the settlement of the bridge was able to take place over time, but it is not an accurate measurement of how the bridge itself is settling. Starting in 2012, survey crews from KDOT have taken survey shots of the bridge to determine how it has settled from its original state. The change in elevation of the bedrock provides a good guide as to what the bridge settlements are, but it is not exact. There is no change in bedrock elevation at Abutment 1 and there is no settlement at Abutment 1 according to the survey data, but this exact correlation is not always the case. The change in bedrock elevation would suggest that the highest settlement values would be on the north side of the bridge at Pier 3 and Abutment 2, while in reality the largest settlement values are at Pier 2 and Pier 3 on the south side of the bridge. Figure 1.2 shows the settlement profile of the bridge in April of 2017.
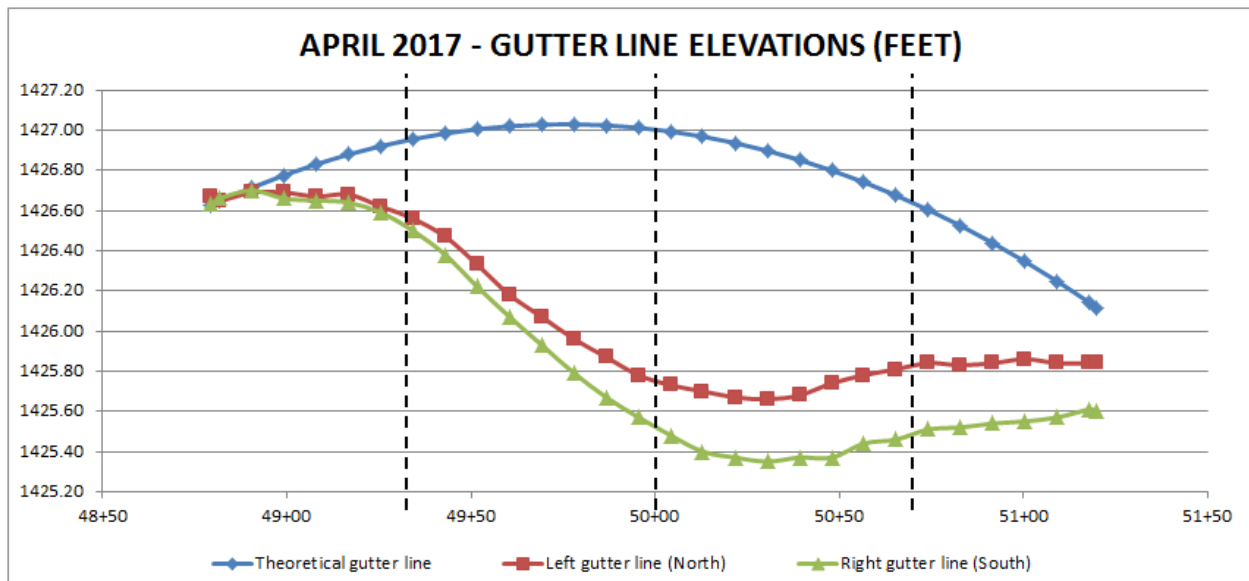


**Figure 1.2: April 2017 original and settlement profiles**

2

The profile shows the theoretical gutter line of the bridge when it was originally built, along with the actual gutter line of the bridge on the south and north side of the bridge during the April 2017 survey. The lines begin at Abutment 1 on the west side of the bridge and ends at Abutment 2 on the east side of the bridge. The three dashed lines on the graph represent the locations on the piers. Pier 1 is closest to Abutment 1, then Pier 2 in the middle, and Pier 3 is closest to Abutment 2. The south side of the bridge settles more than the north side of the bridge, which creates torsion in the box girder of the bridge along with the bending due to the settlement. The maximum settlement values occur in the middle of Pier 2 and Pier 3. The settlements at each location are shown in Table 1.1.

The values in Table 1.1 show the total settlements along the pier longitudinal line at each support location on the bridge through April 2017. These settlement values will be used later in the finite element modeling process to best approximate the settlement occurring in the bridge.

Table 1.1: Total settlements in April 2017

|  | South (in.) | North (in.) |
|---|---|---|
| **Abutment 1** | 0 | 0 |
| **Pier 1** | −5.21 | −4.65 |
| **Pier 2** | −17.80 | −15.10 |
| **Pier 3** | −14.27 | −10.21 |
| **Abutment 2** | −6.38 | −3.62 |

## 1.3 Problem Statement

Geological formations in terms of salt sinkholes exist in deep soil strata in Kansas. This problem is a challenging issue for transportation infrastructure, especially bridges. Even though deep foundations are typically implemented, super structures suffer from slow rates of settlement inducing large stresses particularly in statically indeterminate bridges. These induced stresses often build up to reach the maximum limits of member envelopes which may lead to compromising safety by promoting the attainment of strength limit states.

One such structure is bridge 059-045 Shawnee Drive over I-135 between Salina and Wichita. During routine visual inspections, the bridge showed a sign of differential settlement along the north edge barrier in 1998. From that point onward, the bridge was periodically inspected

with its profile surveyed and recorded starting October 2012. KDOT determined through preliminary analysis that the bridge pier envelopes were showing acceptable levels of induced stresses until recently. It has lately been observed that the settlement has advanced to a level that might endanger the safety of the bridge in the near future. This requires a refined and detailed analysis study to check the pier, piles, and box girder envelopes and extend the life of this bridge.

## 1.4 Objectives

As stated above, the main objectives of this project are:

1. Perform a detailed 3D finite element analysis of the bridge using Abaqus to assess the levels of stresses in the various structural components of the bridge.

2. Perform a detailed 3D finite element analysis of the bridge using RISA 3D to assess the forces and moments obtained at various structural components and to plot them against section envelope curves.

3. Propose schemes to strengthen the bridge structural components using CFRP to extend its life span, if this is found to be an effective solution.

4. Monitor the long-term settlement of the bridge for 5 years if the bridge was deemed stable and safe to be kept open to traffic.

## 1.5 Scope

This report includes six chapters in total. The first chapter includes a general introduction to the project. The second chapter presents a brief literature review relevant to the topics addressed by this report. The third chapter addresses the detailed methodology of the finite element analysis using Abaqus. Chapter 4 explains the detailed methodology of the finite element analysis using RISA 3D. Chapter 5 describes the results and discusses the finding of the analyses. Chapter 6 draws the necessary conclusions and presents the recommendations of the study to the KDOT engineers.

# Chapter 2: Literature Review

## 2.1 Overview

Differential settlement adds stress to statically indeterminate bridges after they are constructed. These settlements are typically not anticipated at the time of construction, so they are not designed for. The additional stresses that are induced in the bridge are difficult to accurately determine.

## 2.2 Effect of Differential Settlement on Bridges

In an attempt to determine the additional bending moment generated by settlement, a mathematical approximation was used for a simply supported bridge (Aggour & Aggour, 1986). It was found that there was a 13–52% increase in bending moment due to 1 centimeter of settlement depending on the skew of the bridge, with a bridge with no skew having a 13% increase of bending moment due to dead load alone. In 2014, the Delaware Department of Transportation closed a bridge on I-495 due to the bridge tilting to one side. It was determined that this tilting was caused by a large stockpile of soil that had been placed next to two of the bridge piers (O'Shea, 2015). The piles below the piers settled due to this stockpile, which resulted in the two piers being replaced in order to fix the issue. This issue could have been prevented if more accurate estimates for settlement had been available. Settlement of piles under axial load can be predicted for the type of soils present in the area (Gurbuz & Paikowsky, 2016).

## 2.3 Effect of Sinkholes on Surface Structures

Unexpected settlement is a common issue that must be dealt with across the country. Past drilling and mining can create voids in the Earth that can be unaccounted for during the initial design of a highway or bridge. The same phenomenon that caused the sinkhole, at the bridge 059-045 site, caused three separate sinkholes along I-70 in Russell County, Kansas. At these locations, KDOT has attempted to slow the settlement down by placing soil and concrete into the sinkholes, but settlement continues to occur at these locations. A county bridge at the Russell County location was forced to be torn down after it settled nearly 6 feet (Dedo & White, 2017). Many other examples of this have occurred across the country due to previous activity that was not regulated

at the turn of the 20<sup>th</sup> century. A large number of mines were not considered in the design process because their operations ended before the Bureau of Mines began to require maps of where the mines were located (Lefchik, Ruegsegger, & Henthorne, 2003). There are many techniques that are used to identify where these voids are today, but they are often only used on new construction or after settlement has been noticed around an existing structure. These methods are often nondestructive, which allows for testing around existing structures without causing any more damage to the affected area. These tests often include seismic refraction and reflection, where the wave velocity depends on the type of material the wave passes through, and ground penetrating radar which uses the reflection of radio waves to electromagnetic frequencies in materials of varying dielectric permittivity (Armstrong, Surdahl, & Armstrong, 2009). These tests are able to map voids and can generate an accurate picture of what lies beneath the surface, but have high costs that many state Departments of Transportation do not have the money to fund, which results in the use of destructive tests such as borings being used to map the affected area. The main problem that results from finding these voids is what to do after they have been identified. The most common practice is to try and pump various materials, such as concrete or grout, into the sinkhole to dry and strengthen the area. At the sinkhole in Russell County, KDOT has spent more than three million dollars in projects to attempt to fill in the sinkholes with the settlement that continues today (Dedo & White, 2017).

# Chapter 3: Detailed 3D FE Analysis Using Abaqus

## 3.1 Modeling Aspects of the Bridge

Based on the type and geometry of the various structural components comprising the bridge, the Abaqus model (presented in Figure 3.1) is made of 3D solid elements when prototyping the abutments, crossbeams, piers, and pile caps. The box girder model is made up of shell elements. The piles under the piers and under the abutments are made of frame elements. In total, the model is made of 745 beam elements, 56,544 shell elements, 130,968 solid elements, and 767,909 nodes.
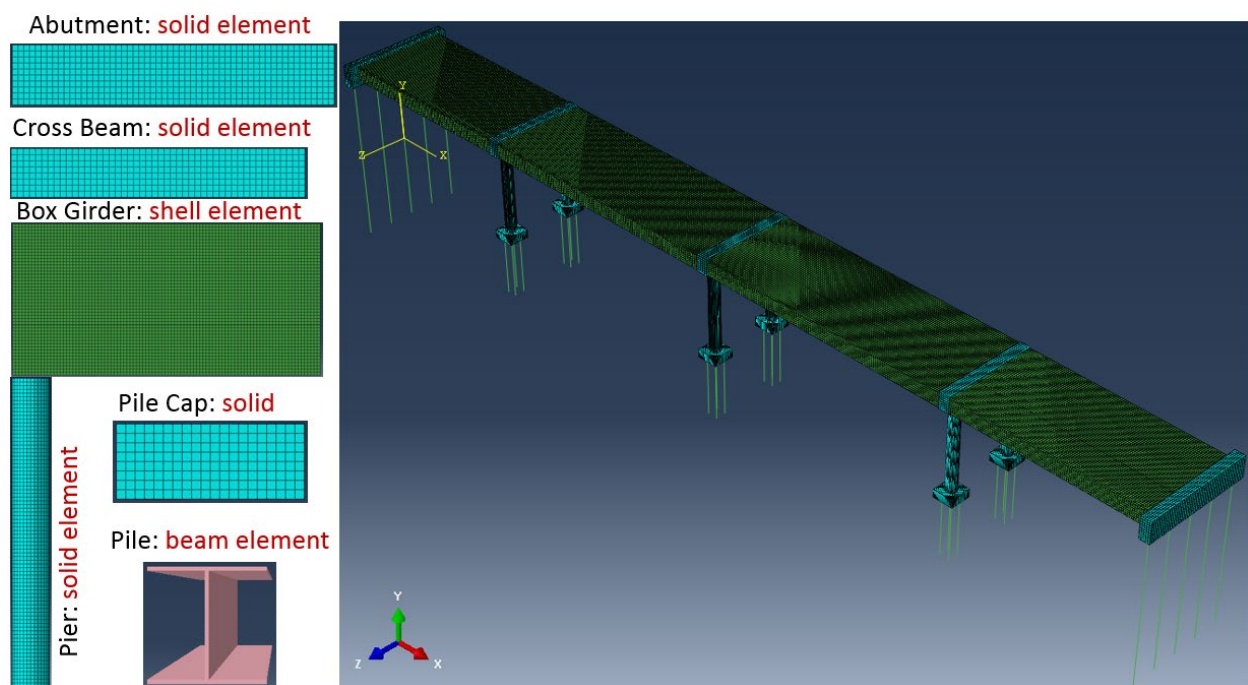


**Figure 3.1: Bridge model using Abaqus and the element types used for each part**

In order to restrain the parts in the assembly, different types of restraining elements were used. Tie elements were used to restrain solid mesh parts to each other in the assembly. The shell-to-solid coupling was used to restrain contacts between shell and solid elements. Meshes of the same kind were merged in the box girders in order to reduce recurring nodes in the contact. Linear springs were modeled in the piles to connect the piles to the surrounding soil and calculate the soil stiffness. The types of restraints are shown in Figure 3.2.
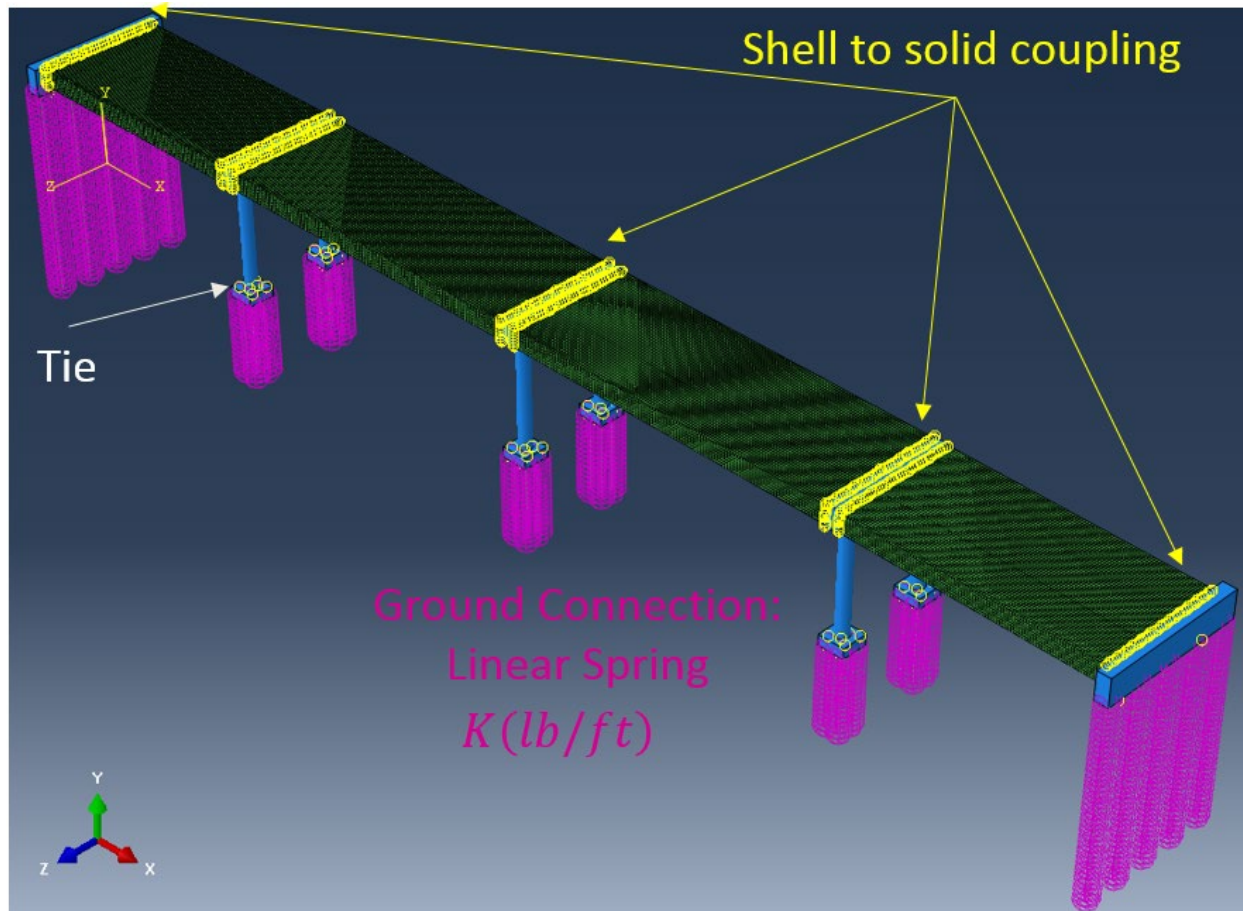
**Figure 3.2: Types of restraining elements used in the bridge model in Abaqus**

### 3.1.1 Material Properties

When creating each model, the elastic modulus of concrete was taken to be 33% of the original modulus of concrete for a concrete with a compressive strength of 4,000 psi. This was done to account for the cracking in the concrete as well as the creep that the concrete has experienced since it was placed in situ. The moment of inertia of cracked concrete is approximately half that of the gross moment of inertia. Flexural cracking was observed during the site inspection and through calculations of the effective tensile stresses in the elements exceeding the modulus of rupture of concrete. Since the geometry considered was the original unchanged dimensions, the stiffness (EI) accounted for in the program is the gross stiffness. On the other hand, cracking needs to be accounted for accurately, which was done by reducing the modulus of elasticity to 50% of its initial value. This is equivalent to reducing the moment of inertia by such a reduction factor. Then to account for the long-term creep of the concrete, the elastic modulus was further reduced

8

to 33% of the original value, as per the practice of KDOT bridge design engineers. This value is important when the finite element models determine the stiffness in each element while running the analysis. By lowering the stiffness values of the elements, the bridge is able to have more flexibility and is able to deform similar to the bridge's current conditions. Since the lower stiffness allows the model to deform similarly to how the bridge is deforming on site, the forces and stresses experienced in the elements are anticipated to be similar to those experienced in the bridge. Furthermore, the Poisson ratio of the cracked concrete is assumed to be 0.2.

### 3.1.2 Lateral Stiffness of Soil Springs

The lateral spring constants were calculated using Equation. 3.1 to Equation 3.4, while the spring model is shown in Figure 3.3 (Bowles, 1996).

$$K_S(kcf) = 250 + 125\sqrt{Y(ft)}$$ **Equation 3.1**

$$K_1(kpf) = H * B * \frac{2K_{s1} + K_{s2}}{6}$$ **Equation 3.2**

$$K_2(kpf) = \begin{cases} K'_{21} = H * B * \frac{2*K_{s2} + K_{s1}}{6} \\ K'_{22} = H * B * \frac{2*K_{s2} + K_{s3}}{6} \end{cases} = K'_{21} + K'_{22}$$ **Equation 3.3**

$$K_N(kpf) = H * B * \frac{2K_{SN} + K_{SN-1}}{6}$$ **Equation 3.4**

Where:

$K^{s1}$ and $K^{s2}$ are spring constants at Node 1 and 2 along the pile,

$K_1$ and $K_2$ are the corresponding lumped spring constants,

$K_N$ is spring constant in X and Z direction at each node along pile length,

H is the vertical distance between two nodes, and

B is the width of pile cross-section (1 ft. at pier piles and 0.83 ft. at abutment piles),

as seen in Figure 3.3 and Table 3.1.

All piles are assumed as bearing piles, hence skin friction along piles under pier and abutment is ignored in this study.

**Table 3.1: Lateral spring constants along the piles**

**Vertical springs constants and the vertical distance of springs from piles top**

**Abutment 1 — Piles: 1, 2, 3, 4, and 5**

| Y-distance (ft.) | 0 | 1 | 2 | 3 | 4 | 5 | 6 | 7 | 8 | 9 | 10 | 11 | 12 | 13 | 14 | 15 | 16 | 17 | 18 | 19 | 20 |
|---|---|---|---|---|---|---|---|---|---|---|---|---|---|---|---|---|---|---|---|---|---|
| $K_x$ (kips/ft.) | 121 | 302 | 354 | 388 | 416 | 441 | 463 | 484 | 503 | 520 | 537 | 553 | 569 | 584 | 598 | 611 | 625 | 638 | 650 | 662 | 674 |
| $K_z$ (kips/ft.) | 121 | 302 | 354 | 388 | 416 | 441 | 463 | 484 | 503 | 520 | 537 | 553 | 569 | 584 | 598 | 611 | 625 | 638 | 650 | 662 | 674 |
| Y-distance (ft.) | 21 | 22 | 23 | 24 | 25 | 26 | 27 | 28 | 29 | 30 | 31 | 32 | 33 | 34 | 35 | 36 | 37 | 38 | 39 | 40 | 41 |
| $K_x$ (kips/ft.) | 685 | 697 | 708 | 718 | 729 | 739 | 749 | 759 | 769 | 779 | 788 | 797 | 806 | 815 | 824 | 833 | 842 | 850 | 858 | 867 | 436 |
| $K_z$ (kips/ft.) | 685 | 697 | 708 | 718 | 729 | 739 | 749 | 759 | 769 | 779 | 788 | 797 | 806 | 815 | 824 | 833 | 842 | 850 | 858 | 867 | 436 |

**Piers: 1, 2, and 3 — Piles: 1, 2, 3, and 4**

| Y-distance (ft.) | 0 | 1 | 2 | 3 | 4 | 5 | 6 | 7 | 8 | 9 | 10 | 11 | 12 | 13 | 14 | 15 |
|---|---|---|---|---|---|---|---|---|---|---|---|---|---|---|---|---|
| $K_x$ (kips/ft.) | 146 | 363 | 425 | 465 | 499 | 529 | 556 | 580 | 603 | 625 | 645 | 664 | 683 | 701 | 718 | 364 |
| $K_z$ (kips/ft.) | 146 | 363 | 425 | 465 | 499 | 529 | 556 | 580 | 603 | 625 | 645 | 664 | 683 | 701 | 718 | 364 |

**Abutment 2 — Piles: 1, 2, 3, 4, and 5**

| Y-distance (ft.) | 0 | 1 | 2 | 3 | 4 | 5 | 6 | 7 | 8 | 9 | 10 | 11 | 12 | 13 | 14 | 15 | 16 | 17 | 18 | 19 | 20 |
|---|---|---|---|---|---|---|---|---|---|---|---|---|---|---|---|---|---|---|---|---|---|
| $K_x$ (kips/ft.) | 121 | 302 | 354 | 388 | 416 | 441 | 463 | 484 | 503 | 520 | 537 | 553 | 569 | 584 | 598 | 611 | 625 | 638 | 650 | 662 | 674 |
| $K_z$ (kips/ft.) | 121 | 302 | 354 | 388 | 416 | 441 | 463 | 484 | 503 | 520 | 537 | 553 | 569 | 584 | 598 | 611 | 625 | 638 | 650 | 662 | 674 |
| Y-distance (ft.) | 21 | 22 | 23 | 24 | 25 | 26 | 27 | 28 | 29 | 30 | 31 | 32 | 33 | 34 | 35 | 36 | | | | | |
| $K_x$ (kips/ft.) | 685 | 697 | 708 | 718 | 729 | 739 | 749 | 759 | 769 | 779 | 788 | 797 | 806 | 815 | 824 | 415 | | | | | |
| $K_z$ (kips/ft.) | 685 | 697 | 708 | 718 | 729 | 739 | 749 | 759 | 769 | 779 | 788 | 797 | 806 | 815 | 824 | 415 | | | | | |
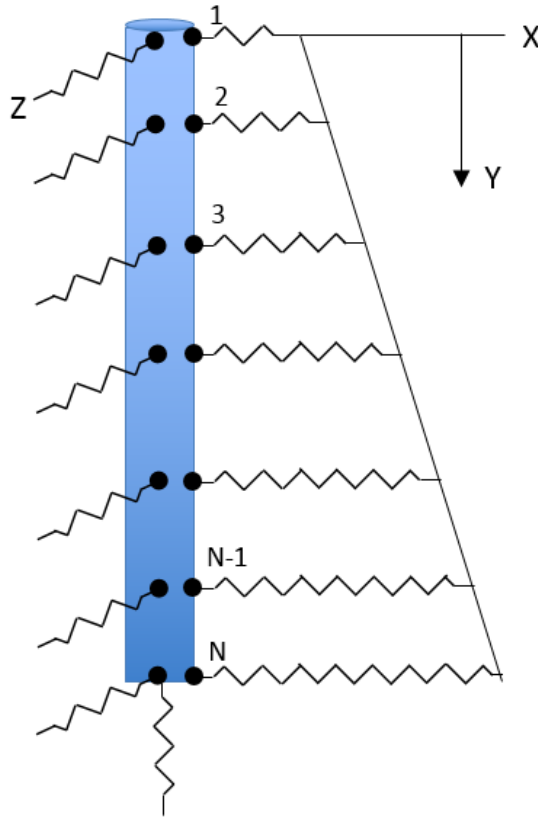
**Figure 3.3: Linear spring model between piles and surrounding soil**

## 3.2 Why Abaqus?

Differential settlements are known to add stresses to statically indeterminate bridges after they are imposed. Accordingly, it is important to analyze the bridge using a refined stress-based finite element analysis to identify locations of over-stress. Abaqus was chosen since it is one of the top-rated multi-physics finite element analysis packages and the most widely used in research and practice worldwide. Therefore, it has been implemented to perform a refined and detailed finite element stress analysis.

## 3.3 Finite Elements Used in Analysis

The commercial finite element software, Abaqus, was used to model the bridge in this part. Three element types were used: solid elements, shell elements, and frame elements. A 20-node, quadratic brick, reduced integration (C3D20R) element was used for the solid meshes in the abutments, pier crossbeams, pier columns, and pile caps. An 8-node doubly curved thick shell

element, with reduced integration scheme (S8R), was used for box girders. A 3-node quadratic beam in 3D space (B32) elements was used for the piles under the piers and abutments. A refined element size of 0.25 ft was used for the regions where stress concentration occurs such as pier columns and abutments. An element size of 0.5 ft was used for box girders, and an element size of 1.0 ft was used for the beam elements in piles. Figure 3.1 shows the complete bridge assembly and detailed element type used in the model.

## 3.4 Analysis Stages or Analysis Time Steps

The model was run in two general static loading stages. In Step 1, the self-weight of the bridge was applied to obtain the settlement of the piles up to April 2013 by iteratively changing the vertical spring constants under each pile until the said settlement is nearly achieved. The results of these tests are listed in Table 3.2 through Table 3.4.

**Table 3.2: Total settlements in April 2013**

|  | South (in.) | North (in.) |
|---|---|---|
| **Abutment 1** | 0 | 0 |
| **Pier 1** | −4.57 | −4.06 |
| **Pier 2** | −16.23 | −13.94 |
| **Pier 3** | −13.70 | −9.93 |
| **Abutment 2** | −6.42 | −4.03 |

**Table 3.3: Settlements in April 2013 under self-weight/springs**

|  | South (in.) | | | North (in.) | |
|---|---|---|---|---|---|
| **Abutment 1** | Pile 1: 0 | Pile 2: 0 | Pile 3: 0 | Pile 4: 0 | Pile 5: 0 |
| **Pier 1** | Pile 1: −4.68 | Pile 2: −4.48 | | Pile 1: −4.12 | Pile 2: −3.95 |
|  | −4.58 | | | −4.06 | |
|  | Pile 3: −4.69 | Pile 4: −4.49 | | Pile 3: −4.16 | Pile 4: −4.00 |
| **Pier 2** | Pile 1: −16.27 | Pile 2: −16.14 | | Pile 1: −14.01 | Pile 2: −13.91 |
|  | −16.19 | | | −13.94 | |
|  | Pile 3: −16.24 | Pile 4: −16.12 | | Pile 3: −13.99 | Pile 4: −13.89 |
| **Pier 3** | Pile 1: −13.67 | Pile 2: −13.81 | | Pile 1: −10.87 | Pile 2: −11.00 |
|  | −13.70 | | | −10.91 | |
|  | Pile 3: −13.60 | Pile 4: −13.73 | | Pile 3: −10.82 | Pile 4: −10.95 |
| **Abutment 2** | Pile 1: −3.46 | Pile 2: −4.33 | Pile 3: −5.20 | Pile 4: −6.10 | Pile 5: −7.00 |

**Table 3.4: Vertical spring constants under the piles**

| | South (kips/ft.) | | | North (kips/ft.) | |
|---|---|---|---|---|---|
| **Abutment 1** | Pile 1: ∞ | Pile 2: ∞ | Pile 3: ∞ | Pile 4: ∞ | Pile 5: ∞ |
| **Pier 1** | Pile 1: 233 | Pile 2: 233 | Pile 1: 175 | | Pile 2: 175 |
| | Pile 3: 233 | Pile 4: 233 | Pile 3: 175 | | Pile 4: 175 |
| **Pier 2** | Pile 1: 0.20 | Pile 2: 0.20 | Pile 1: 51 | | Pile 2: 51 |
| | Pile 3: 0.20 | Pile 4: 0.20 | Pile 3: 51 | | Pile 4: 51 |
| **Pier 3** | Pile 1: 18 | Pile 2: 18 | Pile 1: 90 | | Pile 2: 90 |
| | Pile 3: 18 | Pile 4: 18 | Pile 3: 90 | | Pile 4:90 |
| **Abutment 2** | Pile 1: 86 | Pile 2: 89 | Pile 3: 94 | Pile 4: 98 | Pile 5: 102.5 |

In Step 2, the settlement difference between the values in Table 1.1 for April 2017 and those in Table 3.2 generated from the self-weight, as of April 2013, were superimposed on top of the displacements of Step 1 (Table 3.2) using the prescribed displacement option in Abaqus to yield the total settlements given in Table 1.1 for the entire two-step analysis. This is believed to be a reasonable representation of the actual settlement mechanism which is expected to be a combination of both natural settlements, under self-weight, and imposed settlements (Figure 3.4).
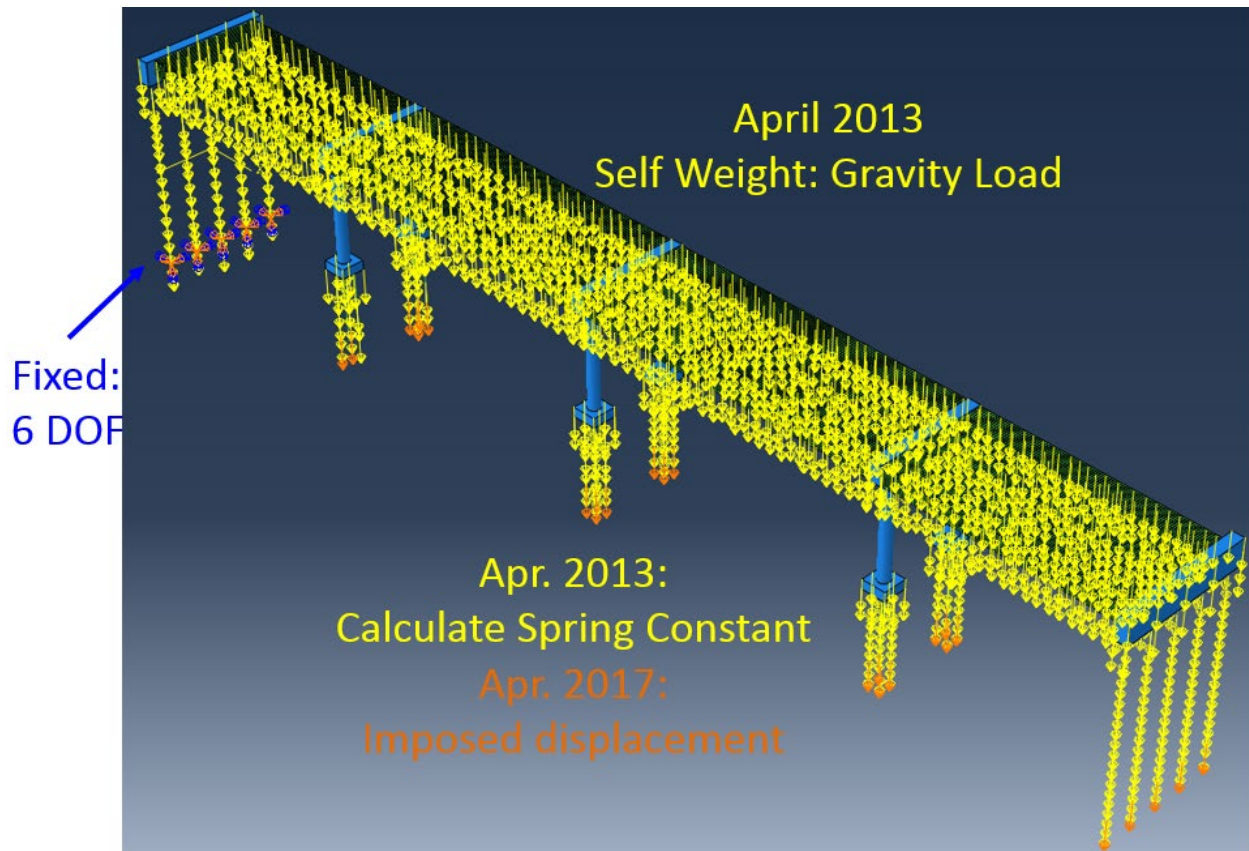


**Figure 3.4: Boundary conditions, applied self-weight, calculation of spring constant, and imposed displacements**

## 3.5 Projected Settlement

Based on the settlement data available through April 2017, the research team projected additional settlements through May 2022 by summing up the total incremental settlement of April 2014 to April 2017 and the average is determined by dividing by 4. This average is used as a constant settlement increment for each year starting April 2018 to May 2022. This was applied the same way to the north and south sides of the bridge.

$$Ave = \frac{Apr14 + Apr15 + Apr16 + Apr17}{4}$$

## 3.6 Superimposed Live Load

In order to study the effect of live load superimposed with April 2017 settlements, a truck load (HS20-44) of 72 kips total load was applied. The live load was applied at eight different locations. Four of those locations followed the truck's movement from west to east on the bridge, and the other four locations were placed along the truck's path from east to west. Figure 3.5 shows the magnitude and distance of applied live load from the edges at Location 1 (box girder Span 1) while the truck is moving from west to east. Figure 3.6 shows the application of live load (truck load) at the eight different locations using a top view. Figure 3.7 to Figure 3.10 show close-ups of the different load locations per bridge span. This is deemed to be a critical analysis to perform to guarantee the safety of the bridge to crossing traffic.
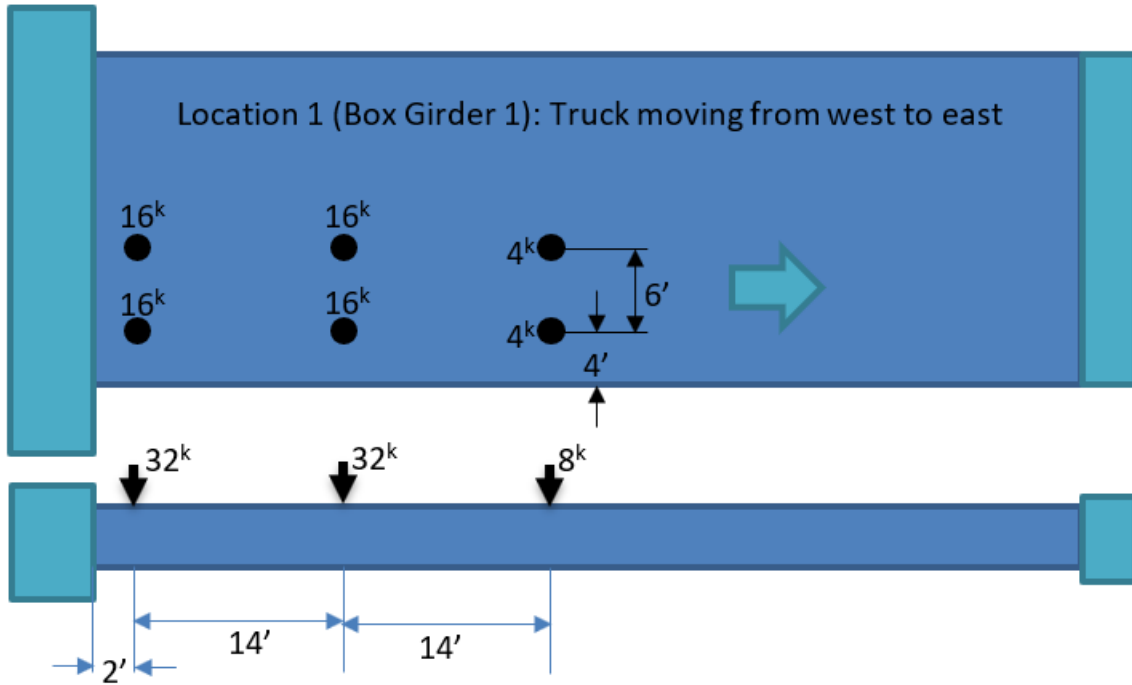
**Figure 3.5: Distance of live load from edges and magnitude of live load at Location 1 (box girder Span 1); truck moving from west to east**
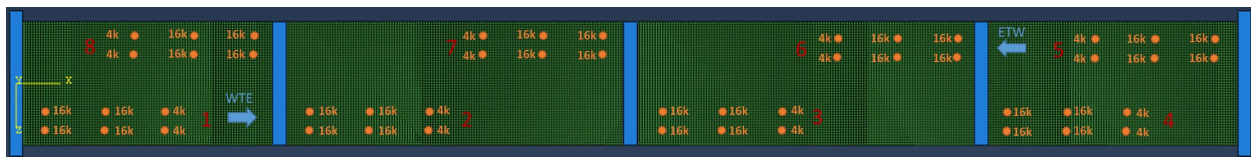


**Figure 3.6: Eight locations of live load (truck load) application**
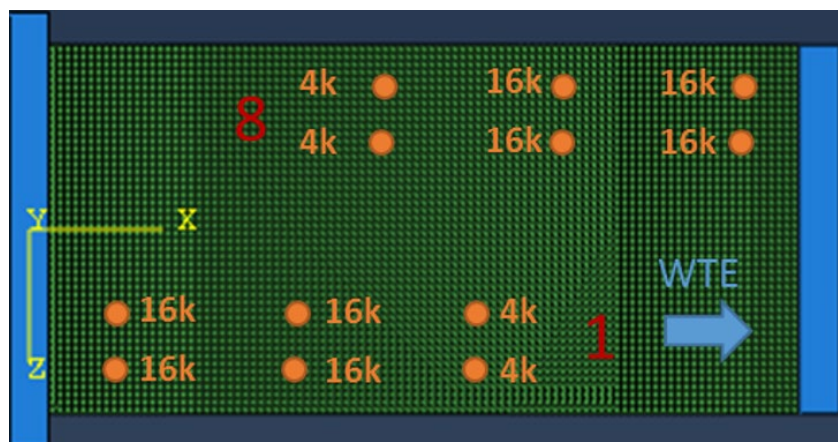


**Figure 3.7: Live load applied at Box Girder 1 (Location 1 and 8)**
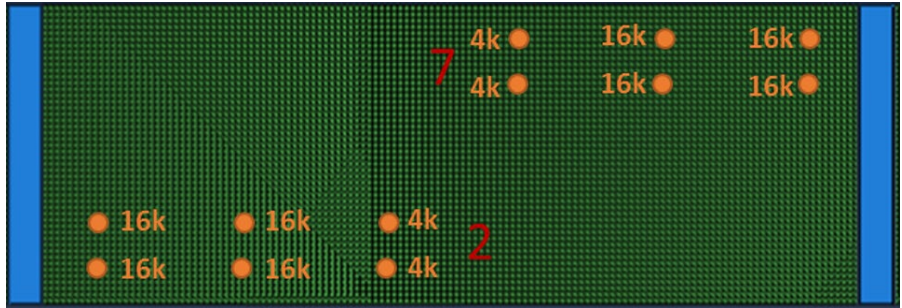
**Figure 3.8: Live load applied at Box Girder 2 (Location 2 and 7)**
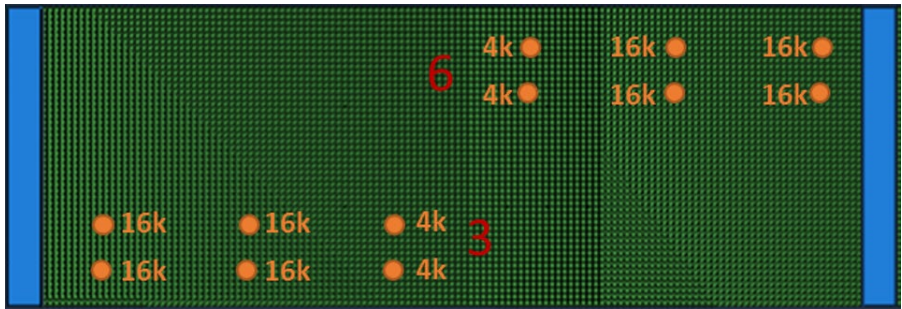


**Figure 3.9: Live load applied at Box Girder 3 (Location 3 and 6)**
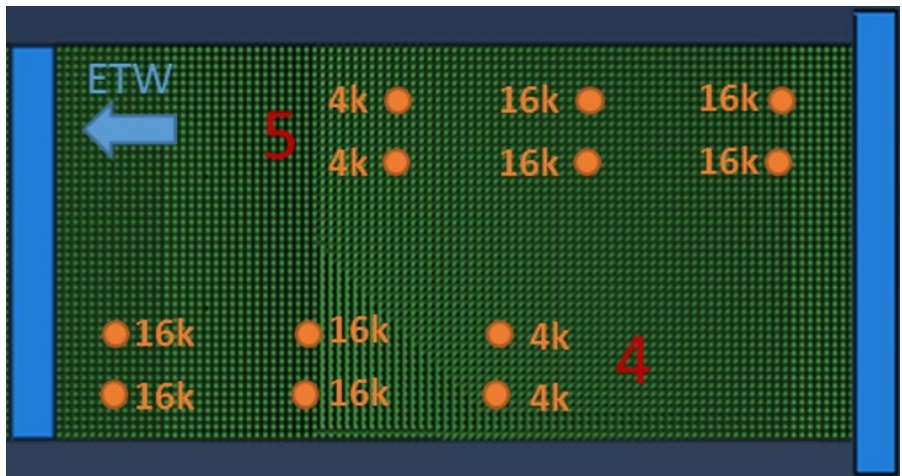


**Figure 3.10: Live load applied at Box Girder 4 (Location 4 and 5)**

# Chapter 4: Detailed 3D FE Analysis Using RISA 3D

## 4.1 Modeling Aspects of the Bridge

Due to their geometric proportions, the RISA 3D model components, shown in Figure 4.1, are made of 3D solid elements when prototyping the abutments, crossbeams, and pile caps. The box girder model is made up of plate elements, while the six piers and their piles as well as the abutment piles are made of frame elements. In total, the model is made of 516 frame elements, 33,600 plate elements, 6,784 solid elements, and 43,044 nodes.
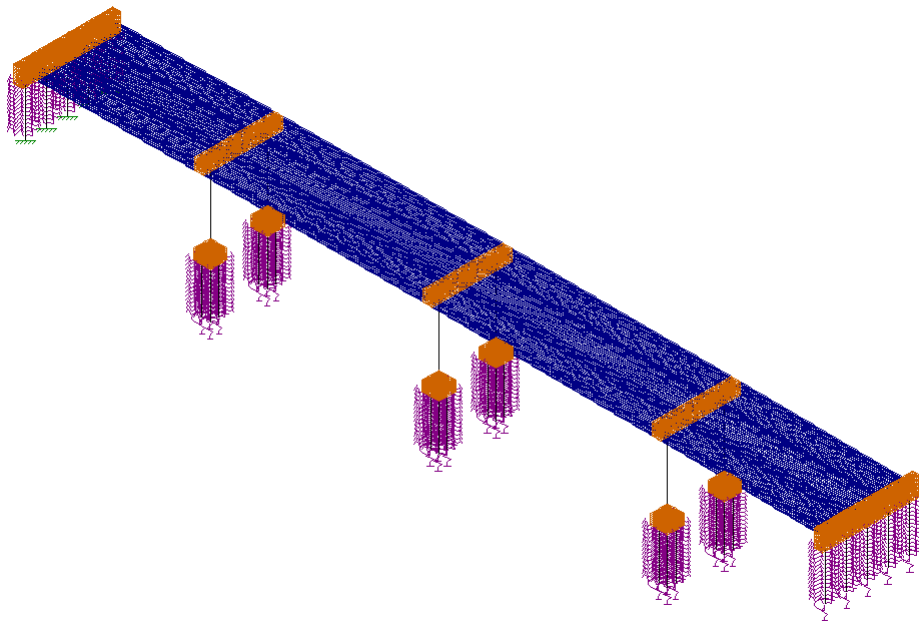


**Figure 4.1: RISA 3D model with plates modeling all spans**

### 4.1.1 Material Properties

Material properties for the RISA 3D model are identical to those used in the Abaqus model. Refer to Section 3.1.1 for details.

### 4.1.2 Lateral Stiffness of Soil Springs

The piles that support the bridge were modeled with lateral springs acting in the x and z directions, to brace the piles like the soils that surround them. The coefficients of the springs were determined by the following equations:

$$K_s(kcf) = 250 + 125\sqrt{Y(ft)}$$ 

**Equation 4.1**

$$K_1(kpf) = H * B * \frac{2K_{S1} + K_{S2}}{6}$$ 

**Equation 4.2**

$$K_2(kpf) = \begin{cases} K'_{21} = H * B * \frac{2*K_{S2} + K_{S1}}{6} \\ K'_{22} = H * B * \frac{2*K_{S2} + K_{S3}}{6} \end{cases} = K'_{21} + K'_{22}$$ 

**Equation 4.3**

$$K_N(kpf) = H * B * \frac{2K_{SN} + K_{SN-1}}{6}$$ 

**Equation 4.4**

Where:

$K_{s1}$ and $K_{s2}$ are spring constants at Node 1 and 2 along the pile,

$K_1$ and $K_2$ are the corresponding lumped spring constants,

$K_N$ is spring constant in X and Z direction at each node along pile length,

H is the vertical distance between two nodes, and

B is the width of pile cross-section (1 ft. at pier piles and 0.83 ft. at abutment piles), as seen in Figure 3.3 and Table 3.1.

In Equation 4.1 the lateral stiffness in kips per cubic foot is found by taking the square root of the depth of the soil, multiplying it by 125 and adding 250 to the result. In Equation 4.2, Equation 4.3, and Equation 4.4, the lateral stiffness in kips per linear foot is calculated by multiplying the depth between the two points (H), the width of the pile (B), by twice the coefficient at that depth, plus the coefficient at the depth at the point above divided by 6 (Bowles, 1996). The coefficients in the x and z directions were always equal at the same depth in order to ensure that soil resistance was uniform around the pile. All piles are assumed to be bearing piles, hence skin friction is ignored in this study.

## 4.2 Why RISA 3D?

The Abaqus model, explained in Chapter 3, gives its results in terms of element stresses, which is valuable because the results show how the local stress changes throughout the element or throughout a full component. However, there is no direct way to know the resultant forces and moments acting on the component section to establish an interaction diagram. For the most part, RISA 3D presents the results as separate bending and twisting moments as well as axial and shear forces acting on the member or component, which allows the forces/moments to be mapped onto the limit state interaction diagrams. This feature is available for the frame, plate, and solid

elements. After the different interaction curves are developed, the forces can be extracted and plotted to see if a component hits a limit state. This will be explained more in the results section.

## 4.3 Finite Elements Used in Analysis

The commercial finite element software, RISA 3D, was used to model the bridge in this part. Three element types were used: linear solid elements, linear plate elements, and beam elements. An 8-node linear brick element was used for the solid meshes in the abutments, pier crossbeams, and pile caps. A 4-node linear plate element was used for box girders. A 2-node cubic beam element in 3D space was used for the piles under the piers and abutments, as well as the piers themselves. The mesh used was made as fine as possible without exceeding the number of plate elements the program allows or without making the element aspect ratio closer to a solid element rather than a thin plate element (Figure 4.1). Accordingly, this model is expected to yield stiffer results compared to the Abaqus model described in Chapter 3. Modeling the bridge using RISA 3D requires a careful and sequential construction of the mesh where nodes cannot be duplicated. Figure 4.2 shows the progression of building the model.

## 4.4 Analysis Stages or Analysis Time Steps

Each of the models were analyzed using the same process. The analysis was broken into two steps. First, each pile in the model, with the exception of the piles under Abutment 1, were placed on vertical springs and were allowed to naturally settle under self-weight until the settlement was as close to the settlement measured in April 2013 as possible. The piles under Abutment 1 remained fixed at their base since Abutment 1 has not effectively settled. This process was accomplished by adjusting the vertical spring coefficients in an iterative process until the settlements were as close as possible to the final settlement without any of the points exceeding the settlement at that specific location. After the vertical coefficients were finalized, the model generated the forces and stresses within each element. Table 4.1 shows the vertical spring coefficients used in step one of the analysis.
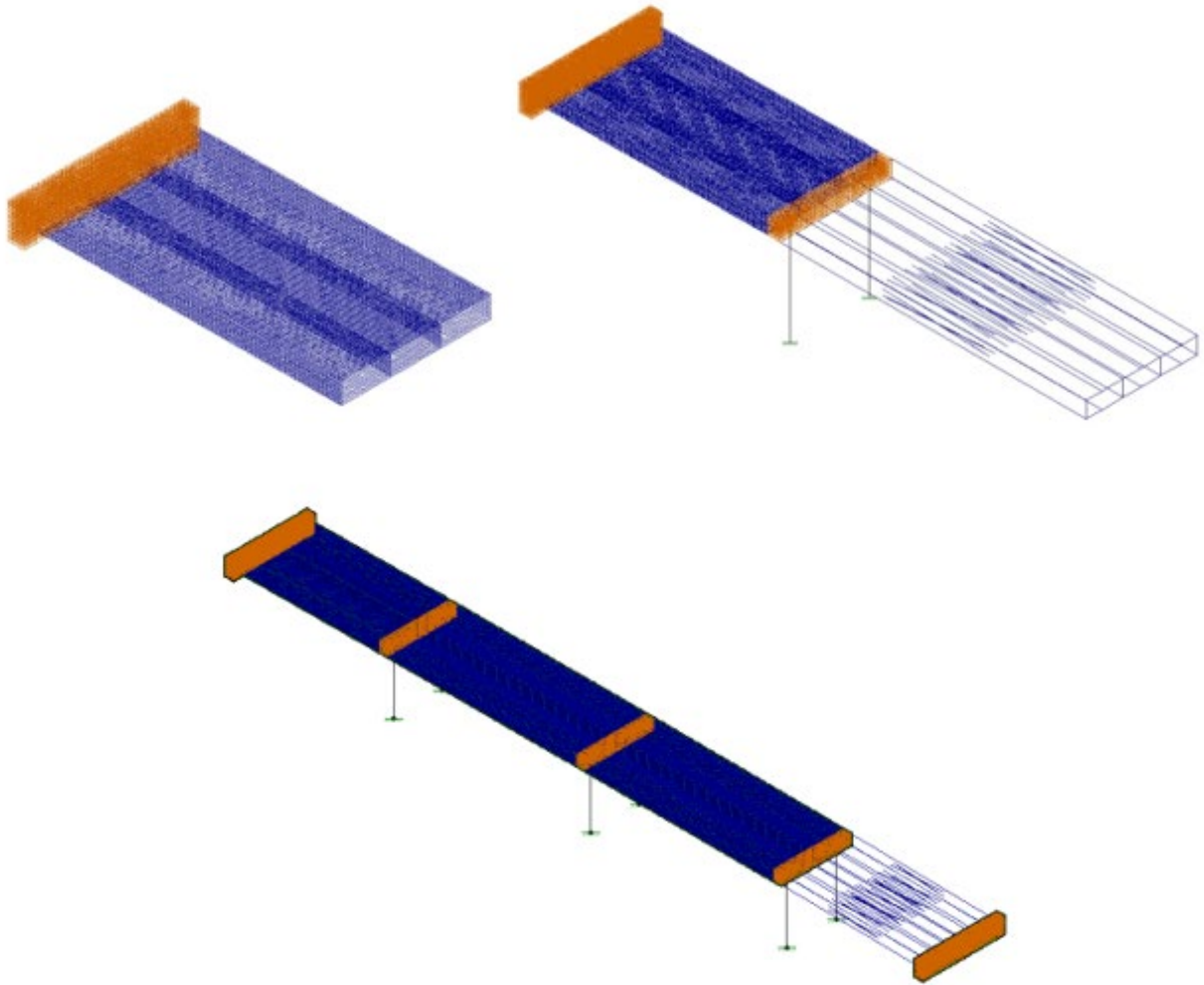
**Figure 4.2: Stages of building the RISA 3D model with plates modeling all spans**

**Table 4.1: Vertical spring coefficients at the bottom of piles in RISA3D Model**

| | Vertical Spring Coefficients | | | | | |
|---|---|---|---|---|---|---|
| | South (Kip/in.) | | | | North (kip/in.) | |
| **Pier 1** | 22.9 | 23.9 | | | 25.5 | 26.5 |
| | 22.9 | 23.9 | | | 25.5 | 26.5 |
| | | | | | | |
| **Pier 2** | 0.01 | 0.01 | | | 0.01 | 0.01 |
| | 0.01 | 0.01 | | | 0.01 | 0.01 |
| | | | | | | |
| **Pier 3** | 0.01 | 0.01 | | | 11.4 | 12.4 |
| | 0.01 | 0.01 | | | 11.4 | 12.4 |
| | | | | | | |
| **Abutment 2** | 13.2 | 10.738 | 8.275 | 5.813 | 3.35 | |

At the locations where the vertical spring coefficients are 0.01, the model was not able to match the total settlement. The total settlement was possible to be matched at Pier 1 north, Pier 3 north and Abutment 2. The decision to make the settlements so close to the total settlement was based on the next step of the analysis. In Step 2 of the analysis, displacements were imposed on the bottom of the piles to match the incremental settlement in the bridge from April 2013 to April 2017. However, extra displacement was imposed on Pier 2 north, Pier 2 south and Pier 3 south where the settlement did not match in Step 1 to compensate for the difference between the desired and achieved settlement. After the displacements were imposed, the models generated the forces and moments within each element. The forces and moment from each step were then added together to determine the total forces and moments that were acting on the bridge. These forces and moments represent the current state of the bridge, based on the benchmarking survey data in April 2017. By imposing the settlements at the bottom of the piles, the bridge would be pulled down, creating some tension in the piles and piers, until the total settlement was reached. The settlements from Step 1 could not exceed the total settlement of April 2013, because if they did, the imposed displacement added would force the pile up, creating extra compressive forces within the piles and piers that would not occur in the bridge. Table 4.2 gives the imposed displacements that were placed on the model, which represent the differences between the settlements shown in Table 1.1 and those generated by analysis Step 1 (Table 4.3).

**Table 4.2: Imposed displacements in analysis Step 2**

| Imposed Displacements | | |
|---|---|---|
| | South (in.) | North (in.) |
| Pier 1 | −0.709 | −0.656 |
| Pier 2 | −4.134 | −2.598 |
| Pier 3 | −2.437 | −0.373 |
| Abutment 2 | −0.279 | 0.685 |

**Table 4.3: Self weight settlements in analysis Step 1**

| Imposed Displacements | | |
|---|---|---|
| | South (in.) | North (in.) |
| Pier 1 | −4.501 | −3.994 |
| Pier 2 | −13.666 | −12.502 |
| Pier 3 | −11.833 | −9.837 |
| Abutment 2 | −6.101 | −4.305 |

## 4.5 Projected Settlement

After the current state of the bridge was established, the next step in the analysis was to determine how future settlements could affect the bridge. As discussed in Section 3.5, based on the settlement data available through April 2017, the research team projected additional settlements through May 2022 by summing up the total incremental settlement of April 2014 to April 2017. The average was determined by dividing the total incremental settlement by four. This average was used as a constant settlement increment for each year starting April 2018 to May 2022.

The projected settlements were then added to the model as imposed displacements at the bottom of the piles, just as the imposed displacements were added in Stage 2 of the original analysis of the bridge. The imposed displacements were added on a yearly basis, and the forces and stresses from each imposed displacement year were then superimposed to the forces and stresses from the self-weight model on vertical springs, and the imposed displacements that match April 2017 to determine the state of the bridge in whichever future year was being analyzed. Figure 4.3 shows the profile of the deflected shape of the bridge. The deflected shape in RISA 3D matches the true deflected shape of the bridge.
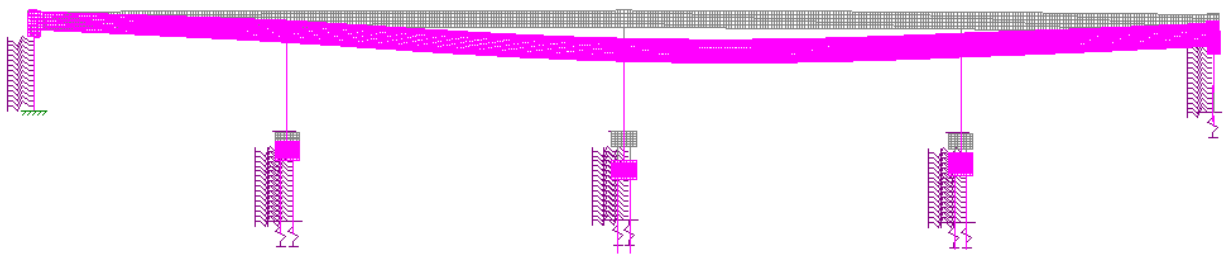


**Figure 4.3: Profile of projected deflected shape in RISA 3D in April 2017**

**Table 4.4: Total projected settlements in May 2022**

|            | South (in.) | North (in.) |
|------------|-------------|-------------|
| Abutment 1 | 0           | 0           |
| Pier 1     | −6.290      | −6.109      |
| Pier 2     | −20.34      | −16.719     |
| Pier 3     | −14.84      | −10.221     |
| Abutment 2 | −6.846      | −3.996      |

**Table 4.5: Imposed displacements in analysis Step 2 for the projected settlement in May 2022**

|  | South (in.) | North (in.) |
|---|---|---|
| Pier 1 | −1.789 | −2.115 |
| Pier 2 | −6.683 | −4.217 |
| Pier 3 | −3.01 | −0.38475 |
| Abutment 2 | −0.745 | 0.308 |
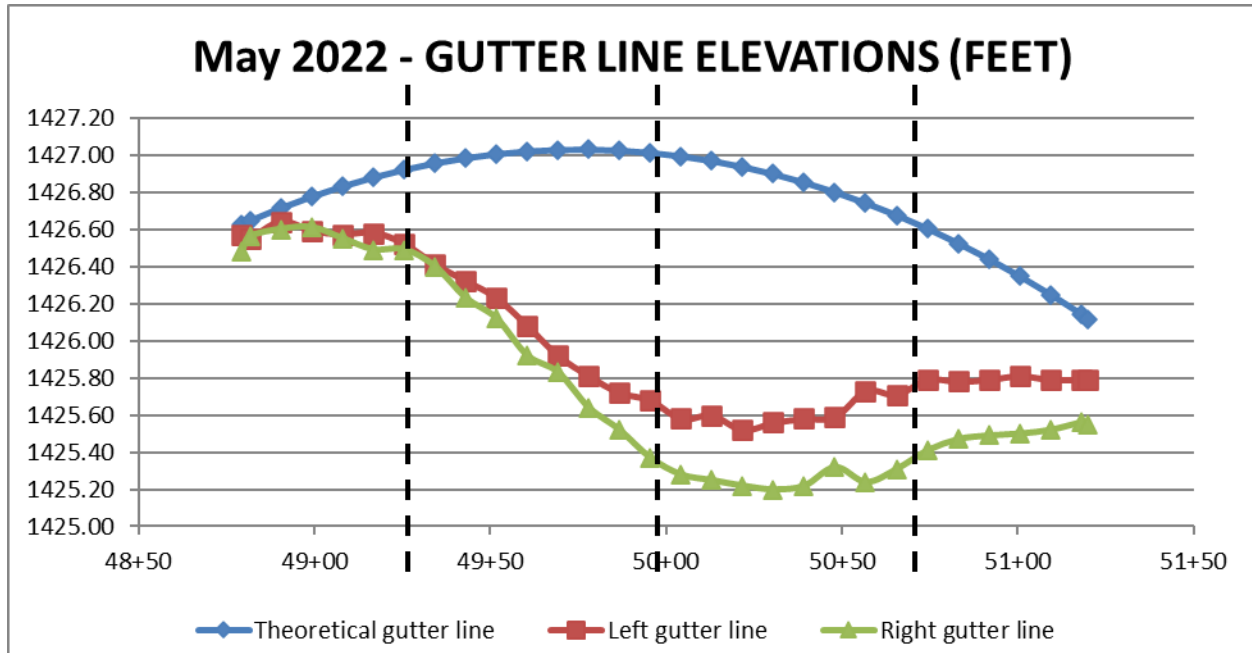


**Figure 4.4: May 2022 original and settlement profiles**

## 4.6 Superimposed Live Load

The bridge was loaded with a HS20-44 truck. The truck is 28 ft long between the frontmost and the rearmost axles and it is 6 ft wide between the two wheels of each axle. The front axle was 8 kips in total while the other two axle loads were 32 kips each. Only one truck was placed on the bridge at a time, based on the low traffic count that is experienced on that bridge. One truck was moved across the bridge at a time in both the eastbound and westbound lanes. In order to move the truck across the bridge in RISA 3D, each wheel was a point load that was loaded on the bridge at a node. In RISA 3D, moving loads are not allowed to be placed on plates, so a new loading case had to be established to move the truck across the bridge, much like what was done in Section 3.6 of Chapter 3. Since the wheel loads from the truck had to be placed on nodes, the actual distance

between the axles changed from the original 14 feet to 14.242 feet. Similarly, the width of the truck was adjusted from the original 6 feet to 5.85 feet. The truck was moved to three different locations on each span of the bridge. For example, the locations of the truck on Span 1 were such that the rear 32 kip-axle load was placed on the node nearest Abutment 1, the center 32 kip axle at the mid-span node, and the 8 kip axle load at the node nearest Pier 1. This resulted in a total of 12 locations that were used for each lane, and a grand total of 24 locations. Results for each of these locations were generated and processed for each part of the bridge.
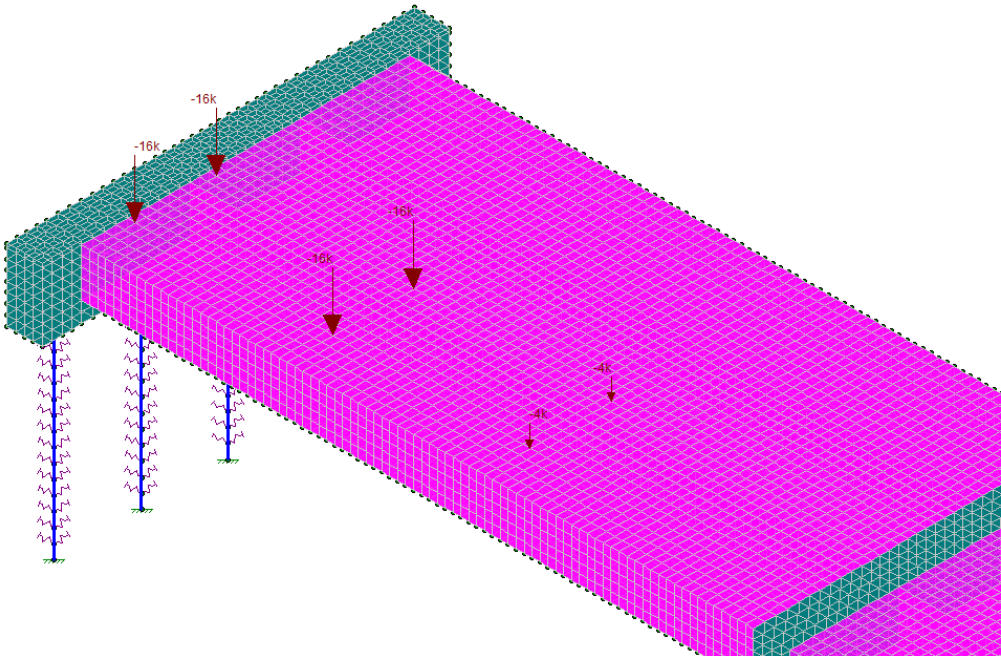


**Figure 4.5: Isometric view of the truck loading on Span 1 in the west to east direction**
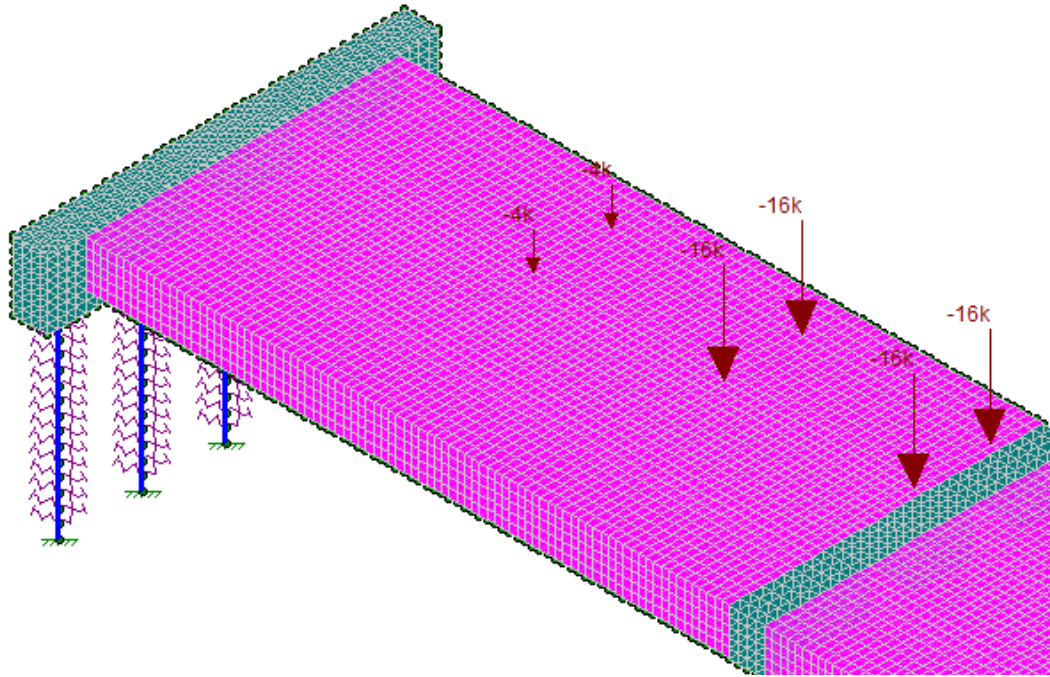
**Figure 4.6: Isometric view of the truck loading on Span 1 in the east to west direction**

# Chapter 5: Results and Discussions

## 5.1 Abaqus Model Results

The Abaqus results are mainly presented in terms of color-coded stress contour drawings for the various components of the bridge. It is important to indicate here that the threshold of concrete compressive strength (4,000 psi) is set at the boundary of the red and orange color. This means that any red color showing up in the contour of colors indicates an exceedance of the concrete compressive strength. However, the red color in Figure 5.1 is irrelevant since it only happens in the steel piles that have a yield strength of 36 kilopounds (ksi).
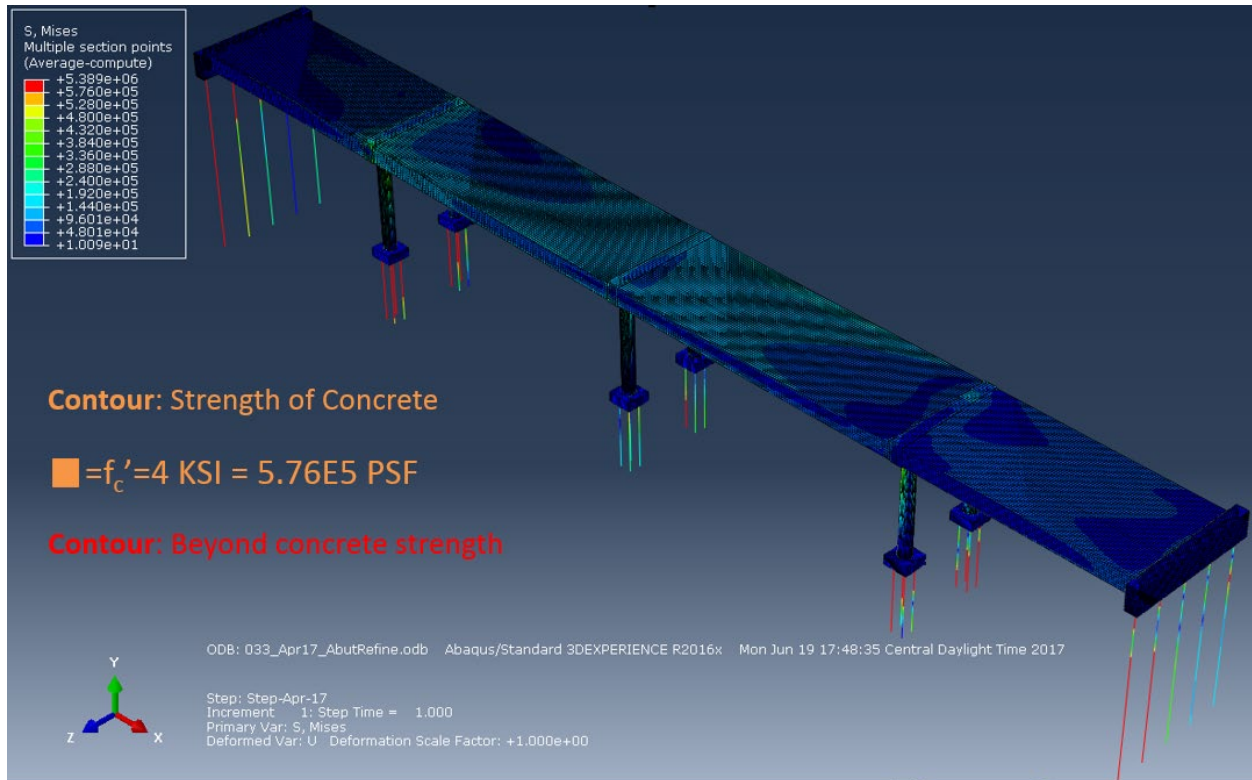


**Figure 5.1: Von Mises stress distribution along the bridge (April 2017)**

## 5.1.1 Settlement Analysis

### 5.1.1.1 Box Girder Results

The first two-step analysis performed is that of the settlements alone up to April 2017. The von Mises stress distribution on the box girders is shown in Figure 5.2. The stresses in the box girder are not critical where they are much lower than the strength of concrete (4 ksi).
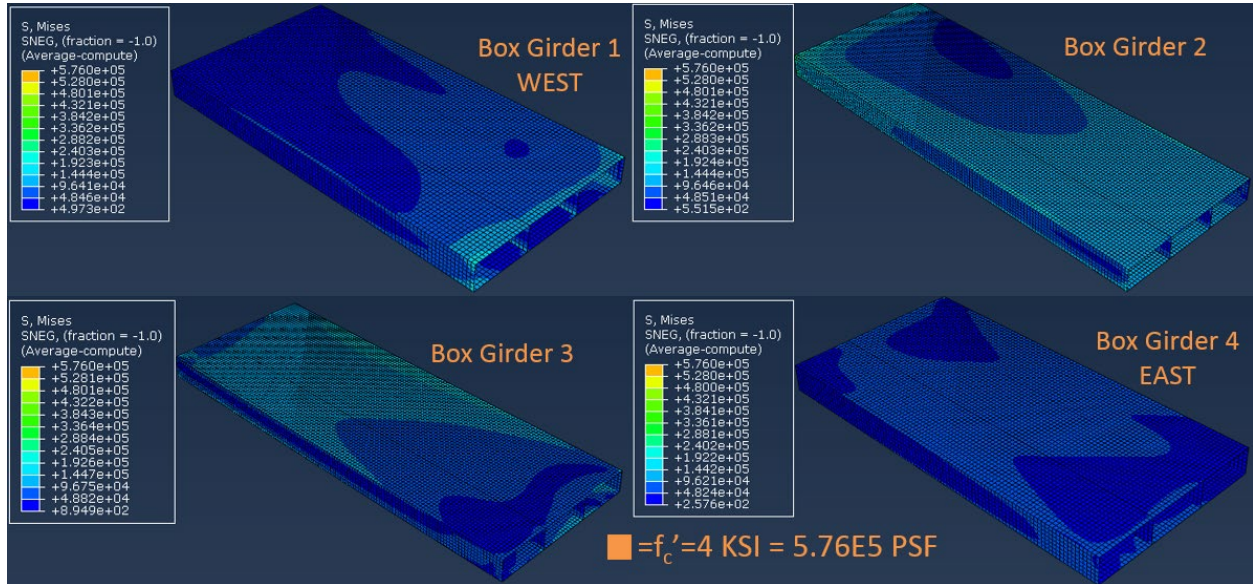


**Figure 5.2: Von Mises stress distribution on the box girders (April 2017)**

In order to confirm the stress distribution results, the strain contours for the box girders were plotted. Figure 5.3 shows the strain results in the X-direction, longitudinally along the bridge. Figure 5.4 shows the strain results in the Y-direction, transverse to the bridge deck. All strain values are below the expected concrete cracking value of 0.003.
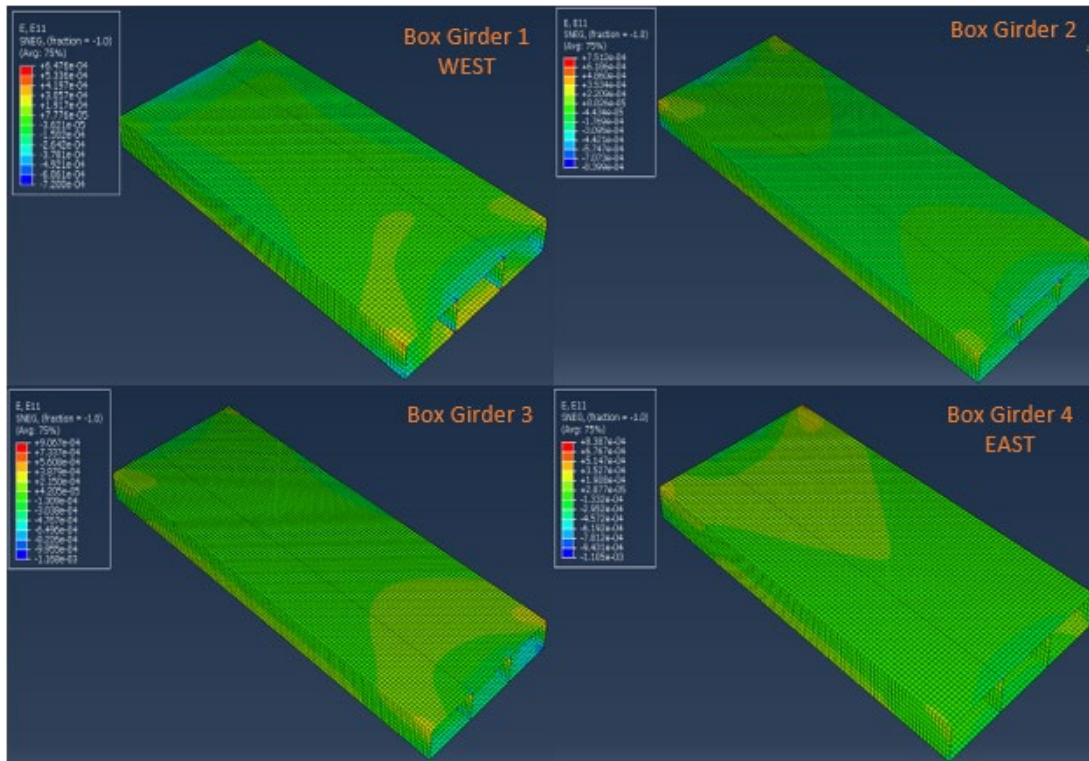
**Figure 5.3: Strain distribution on the box girders longitudinally along the bridge (April 2017)**
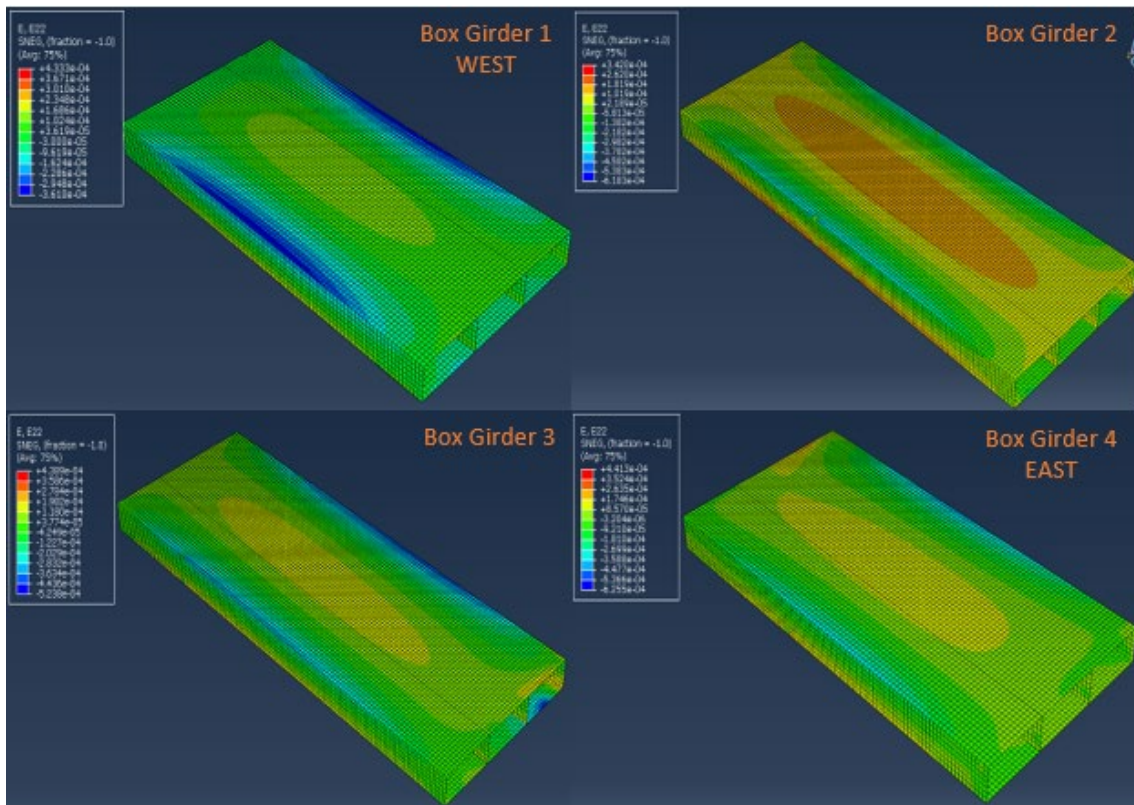


**Figure 5.4: Strain distribution on the box girders transverse to the bridge deck (April 2017)**

28

## 5.1.1.2 Pier Results

Figure 5.5 shows the von Mises stress contours of the crossbeams at piers. The maximum von Mises stress of crossbeams is much lower than the strength of concrete (4 ksi). Therefore, crossbeams are not considered to be critical. In order to confirm the stress distribution results, the strain contours for the crossbeams were plotted. Figure 5.6 shows the strain results in the X-direction, longitudinal along the bridge. Figure 5.7 shows the strain results in the Y-direction, transverse to the bridge deck. Figure 5.8 shows the strain results in the Z-direction, along the width of the bridge. All strain values are below the expected concrete cracking value of 0.003.
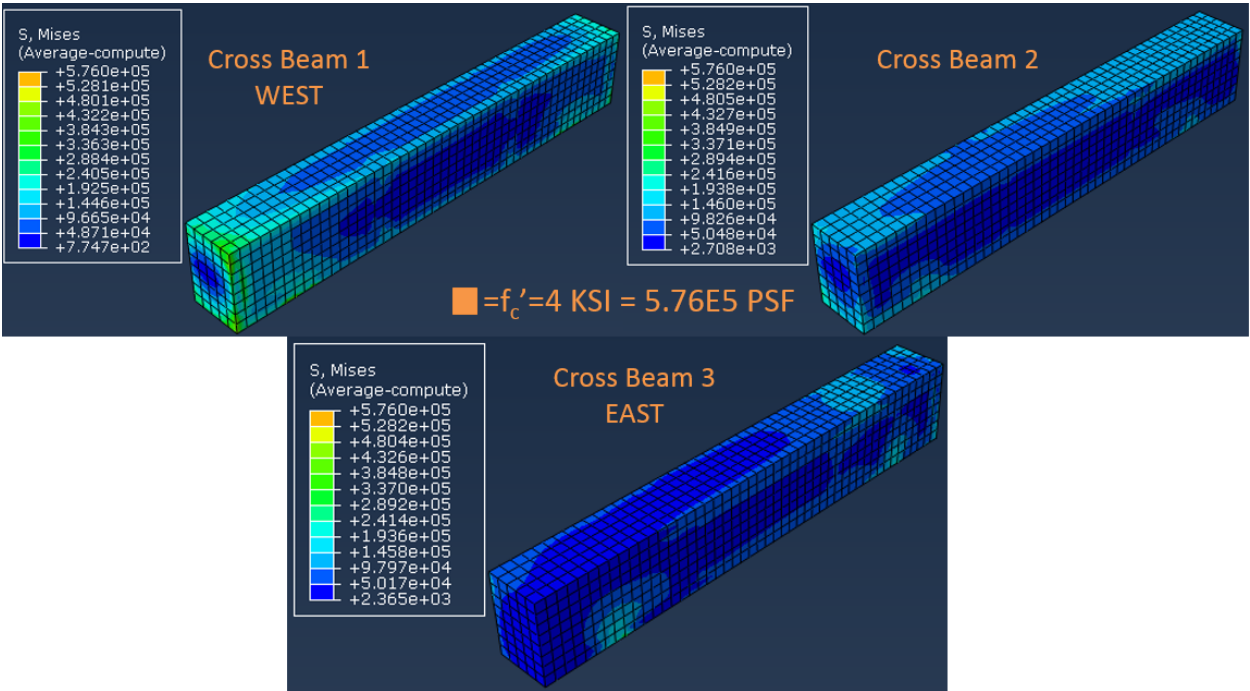


**Figure 5.5: Von Mises stress on the crossbeams at piers (April 2017)**

29
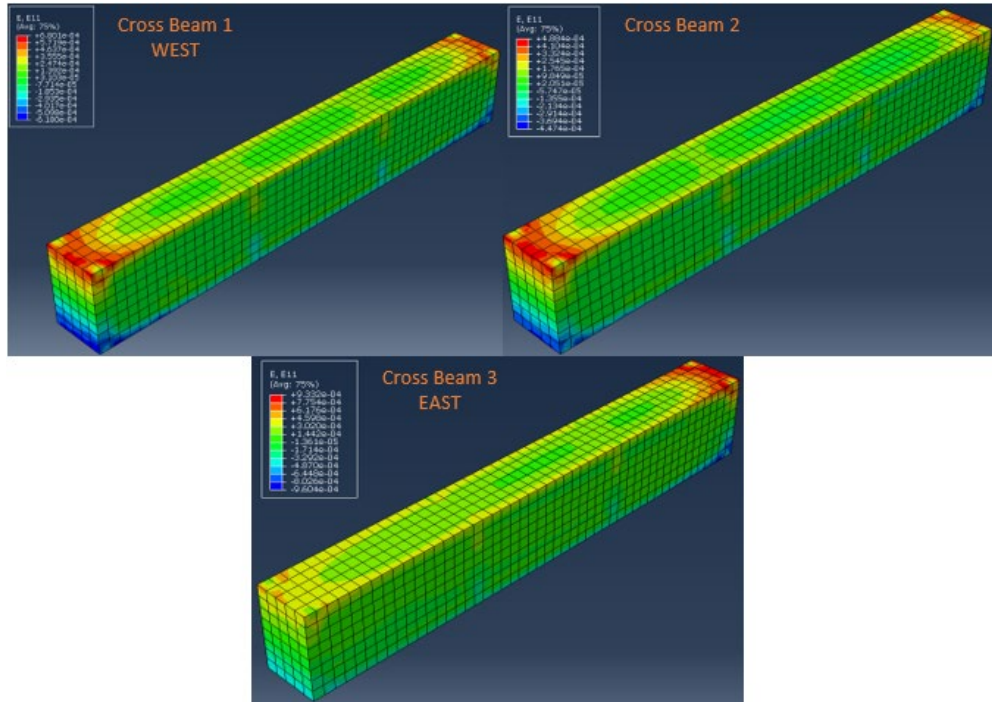
**Figure 5.6: Strain distribution on the crossbeams longitudinally along the bridge (April 2017)**
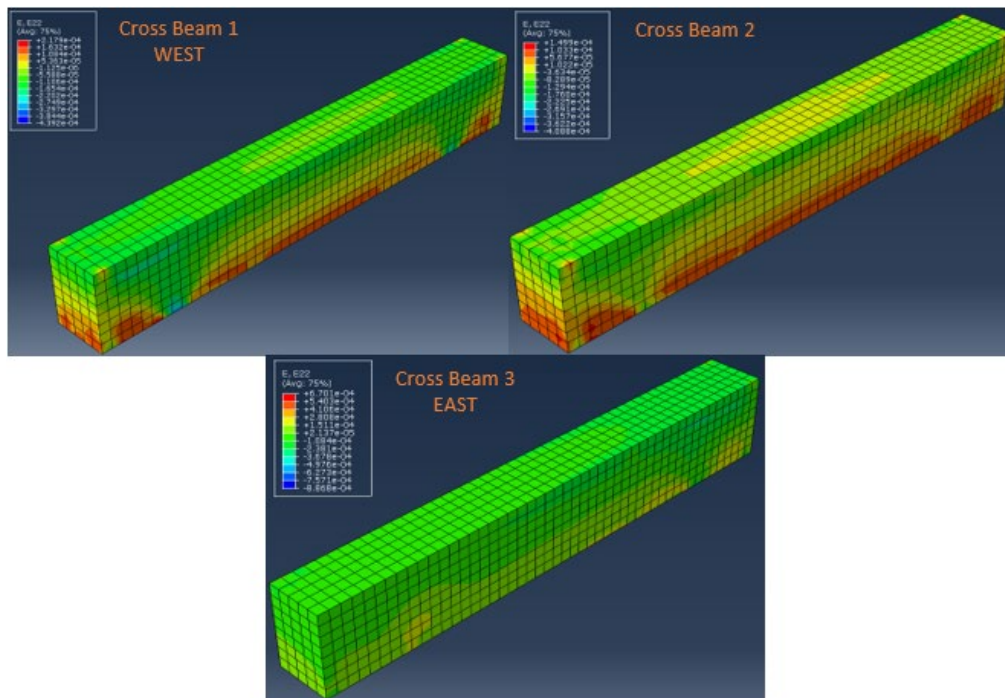


**Figure 5.7: Strain distribution on the crossbeams transverse to the bridge deck (April 2017)**
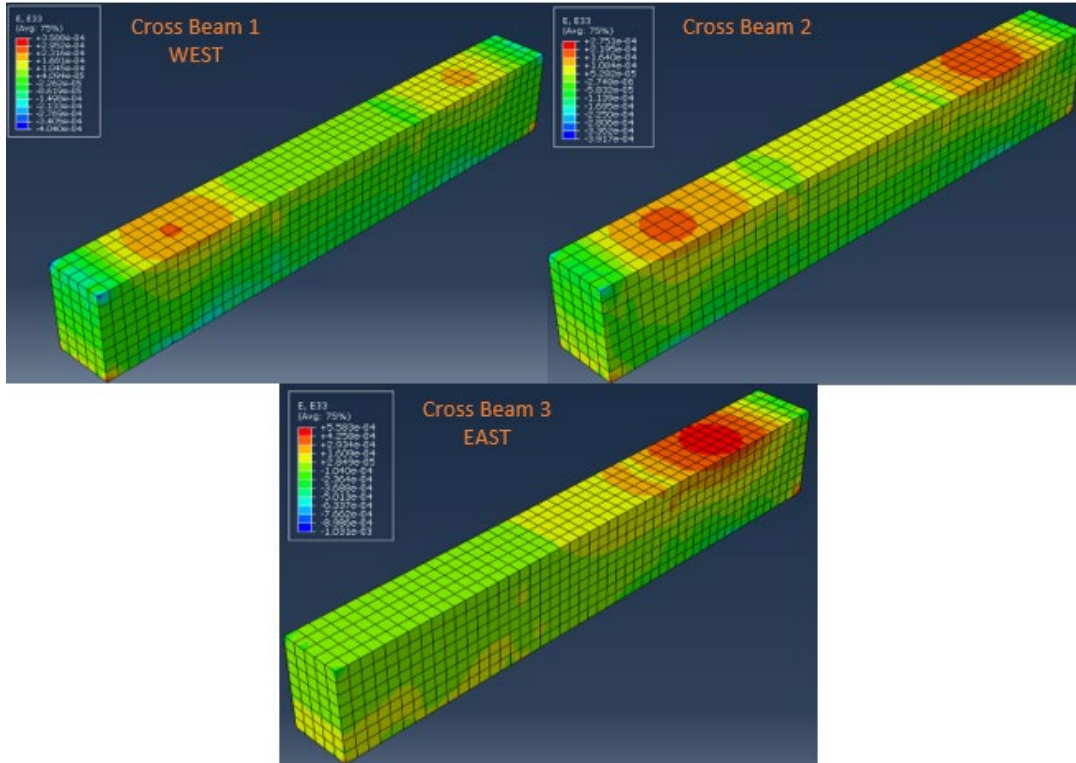
**Figure 5.8: Strain distribution on the crossbeams along the width of the bridge (April 2017)**

The stresses of pier columns are shown in Figure 5.9 where a higher stress, larger than the strength of concrete, is observed at the top edge of the columns. These higher stresses are expected to be due to the stress concentration of the connection between the crossbeams and pier columns.
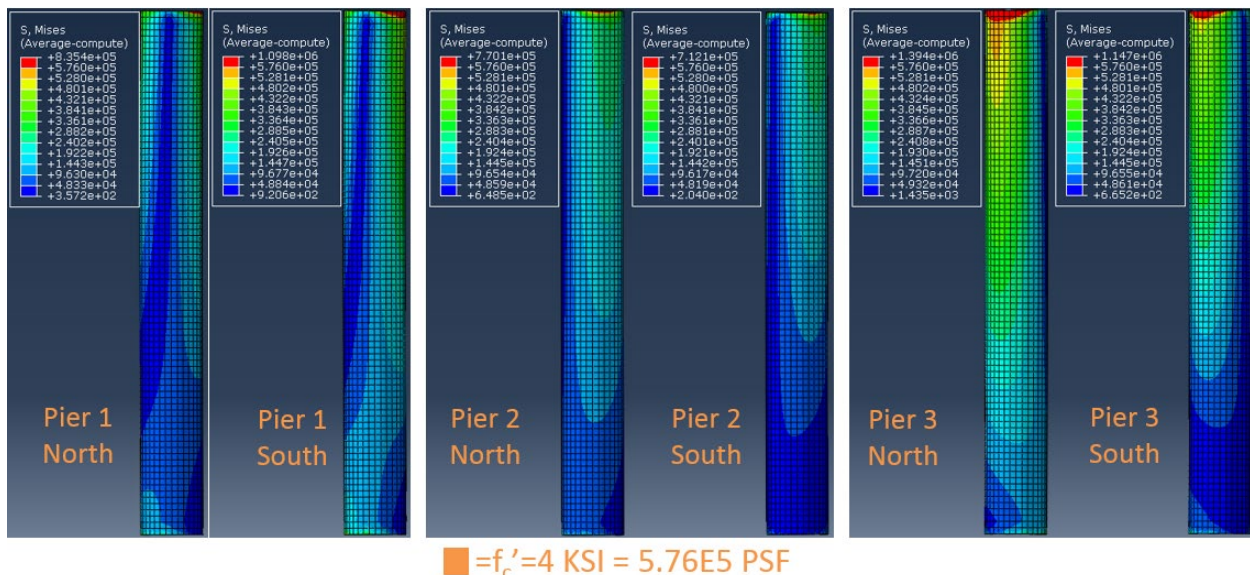


**Figure 5.9: Von Mises stress at pier columns (April 2017)**

**Figure 5.10: Concrete distress at top of the pier**

The results from April 2017 show the same stress concentration beyond the concrete strength, which matches the current condition at the top of the pier, as seen in Figure 5.10. It is also important to mention that the model doesn't consider the reinforcement embedded in the piers. The steel will take some of the load and lower the concrete's share of the stresses induced on the section.
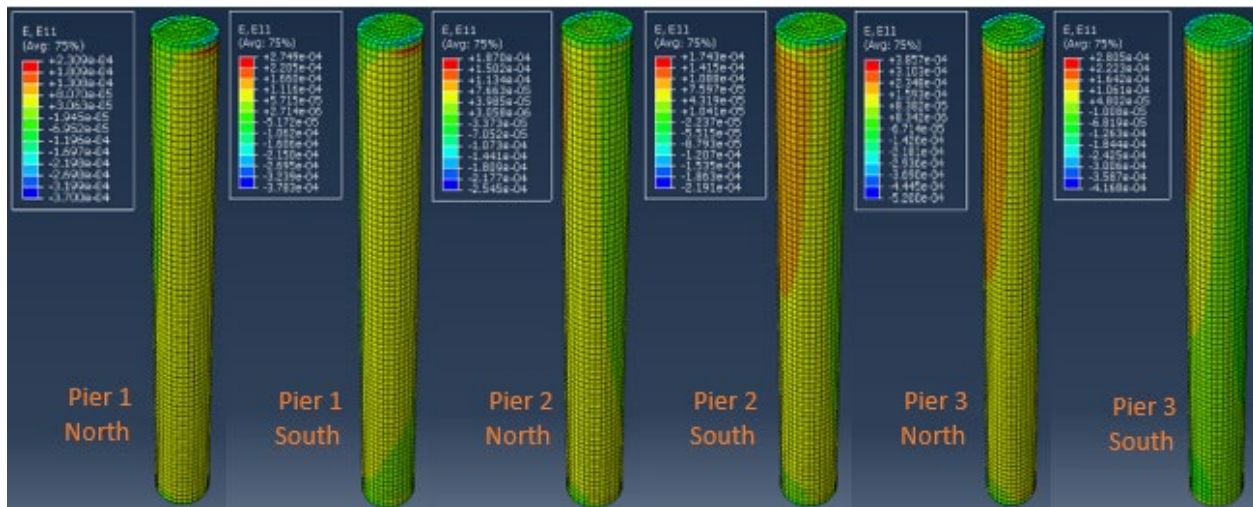


**Figure 5.11: Strain distribution on the piers longitudinally along the bridge (April 2017)**

In order to confirm the stress distribution results, the strain contours for the crossbeams were plotted. Figure 5.11 shows the strain results in the X-direction, longitudinal along the bridge. Figure 5.12 shows the strain results in the Y-direction, transverse to the bridge deck. Figure 5.13 shows the strain results in the Z-direction, along the width of the bridge. Strain values in each individual direction are slightly below the expected concrete cracking value of 0.003.
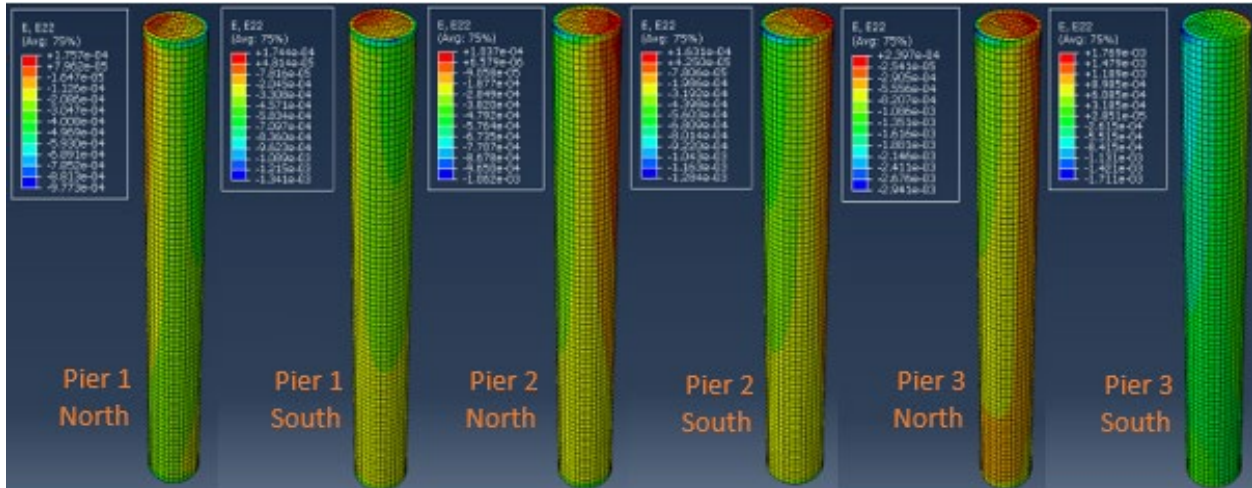


**Figure 5.12: Strain distribution on the piers transverse to the bridge deck (April 2017)**
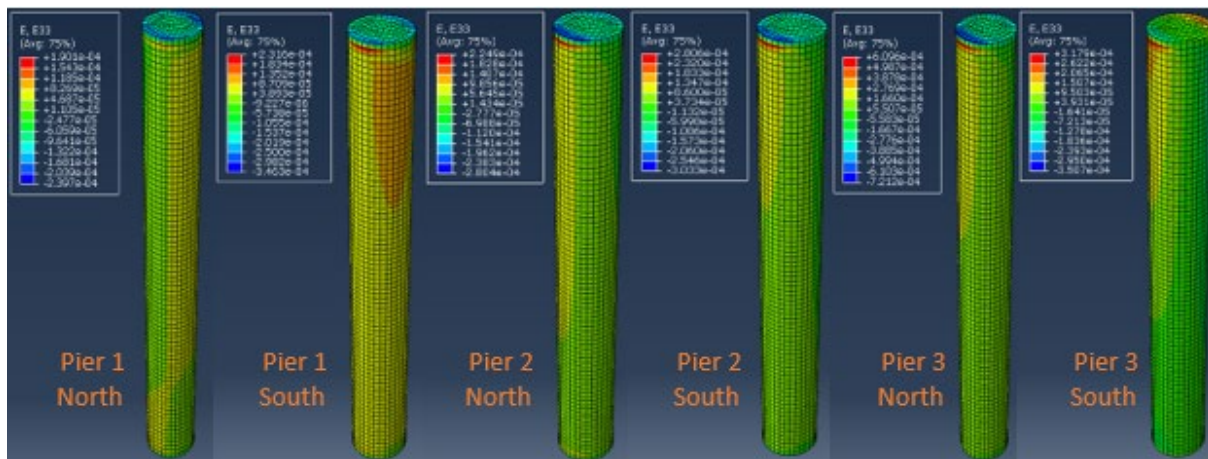


**Figure 5.13: Strain distribution on the piers along the bridge width (April 2017)**

### 5.1.1.3 Abutment Results

Abutments are considered not to be critical at all. Figure 5.14 shows the von Mises stress distribution at the abutments. The only critical stress higher than strength of concrete is observed at the top of piles. This is due to stress concentration from piles where the piles were modeled as one-dimensional beam elements.
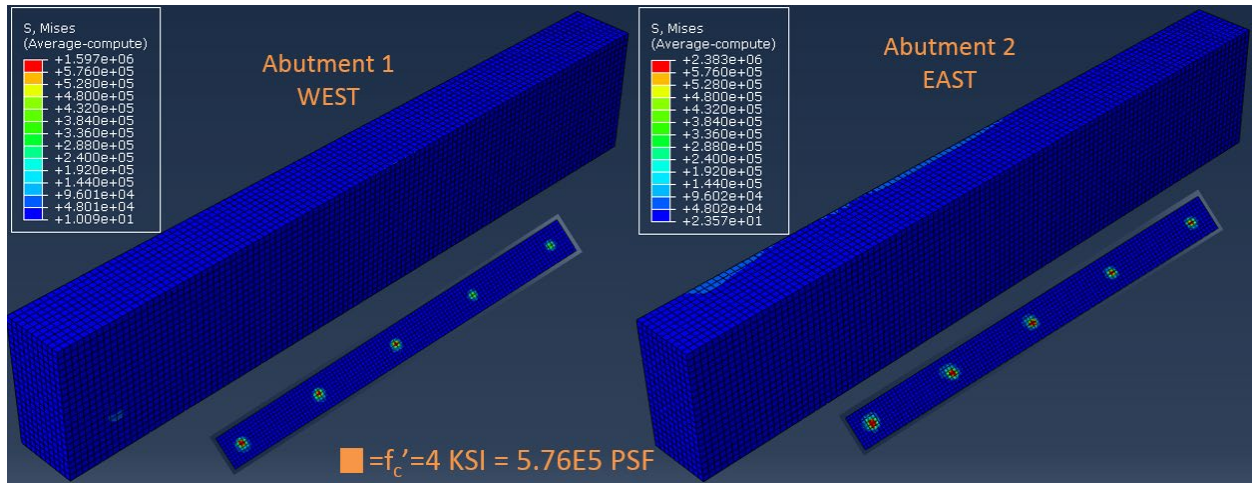


**Figure 5.14: Von Mises stresses at the abutments (April 2017)**

### 5.1.1.4 Pier and Abutment Pile Results

Figure 5.15 shows the von Mises stresses at the piles of abutments and piers. The maximum stress is observed at Pile 1 (south) of Abutment 1 (west). The highest stress value is about two-thirds of the ultimate strength of steel (36 ksi) which doesn't fail. The nodal forces of the piles at the top, which may cause de-bonding (shear) stress at the embedded area between piles and pile caps, are also calculated. Based on Rabbat and Russell (1985) an average bonding strength between steel and concrete is calculated to be 97 psi (57 psi bond strength and 40 psi shear strength), which is slightly on the conservative side. Whenever the shear stress increases beyond the limit of 97 psi at the embedded area, de-bonding is likely to occur. Figure 5.16 and Figure 5.17 show the cross-section and dimensions of the H-piles used at the piers and abutments, respectively. Based on the perimeters of the piles section, the embedment depth, and bonding strength from Rabbat and Russell (1985), the maximum tensile nodal force should not be more than 82.5 kips at pier piles and 102.87 kips at abutment piles.

34
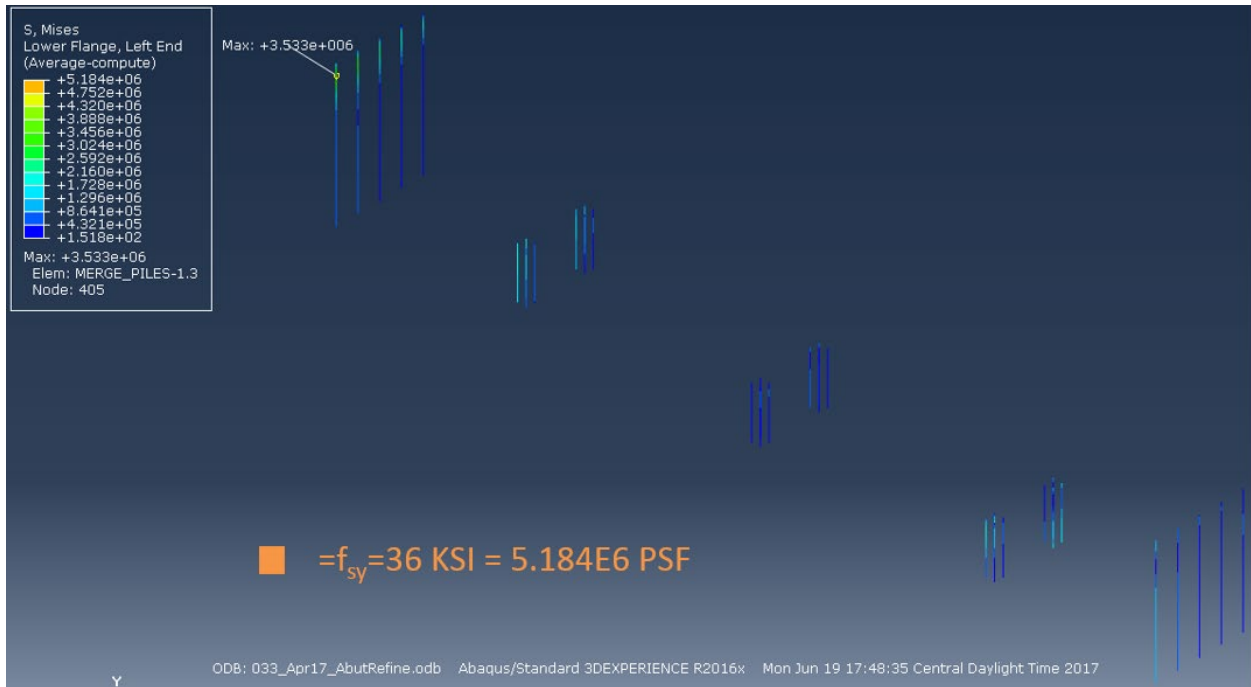
**Figure 5.15: Von Mises stress at piles of abutments and piers (April 2017)**
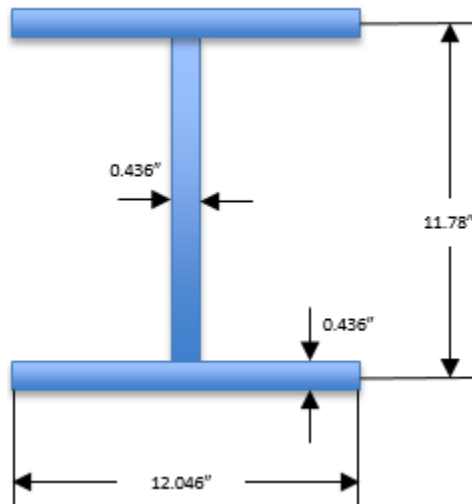


**Figure 5.16: Cross-section and dimension of H-piles used at piers with embedded length of 12 inches into the pile cap**
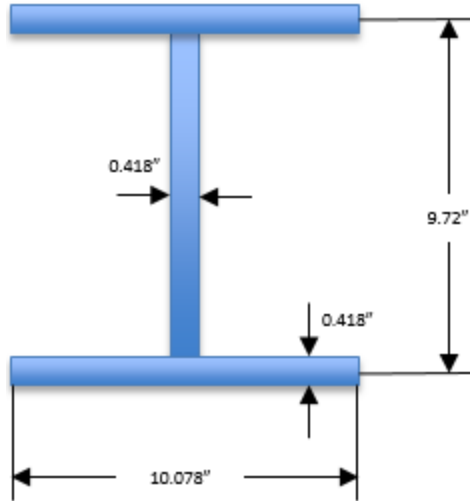
**Figure 5.17: Cross-section and dimension of H-piles used at abutments with embedded length of 18 inches into the abutment**

In case of tensile forces in the piles, it is important to evaluate the forces at the pile cap–pile intersection and compare it to the critical forces due to bond between the concrete and steel section. The calculation of the section perimeter, embedded surface area, and the critical nodal tensile force on top of the pile is presented in Equations 5.1, Equation 5.2, and Equation 5.3, respectively.

$$Perimeter\ (in) = 2 * b_f + 2 * (b_f - t_w) + 2 * d_w \qquad \textbf{Equation 5.1}$$

$$Perimeter\ (in)_{pier} = 2 * 12.046 + 2 * (12.046 - 0.436) + 2 * 11.78 = 70.87\ in.$$

$$Perimeter\ (in)_{abutment} = 2 * 10.078 + 2 * (10.078 - 0.418) + 2 * 9.72 = 58.916\ in.$$

$$Embedded\ Area\ (in^2) = Embedded\ Lenght(L) * Perimeter \qquad \textbf{Equation 5.2}$$

$$Embedded\ Area\ (in^2)_{piers} = 12 * 70.87 = 850.46\ in.^2$$

$$Embedded\ Area\ (in^2)_{abutments} = 18 * 58.916 = 1060.48\ in.^2$$

$$T_{max}\ (tensile) = Embedded\ Area * Bonding\ Strength \qquad \textbf{Equation 5.3}$$

$$T_{max}\ (tensile)_{piers} = 850.46 * 97 = 82494\ lb = 82.5\ kips$$

$$T_{max}\ (tensile)_{abutments} = 1060.48 * 97 = 102866\ lb = 102.87\ kips$$

Figure 5.18 shows the location of piles at piers and abutments from top view. The numbering is shown as a reference to correctly read the magnitude of nodal forces from related tables. Figure 5.19 through Figure 5.23 show the deformation at the pile top–bottom of the pile cap junction to visually indicate a tension or compression force at each pile top by pulling out of or pushing into the pile cap. Table 5.1 and Table 5.2 show the compressive and tensile nodal forces of piles at the piers and abutments, respectively. The positive value is tensile force while the negative value is compressive force. The tables show that de-bonding will not occur when E=0.33E is used, but de-bonding likely occurs at Pile 1 of Pier 3 south column and if E=0.5E is used.
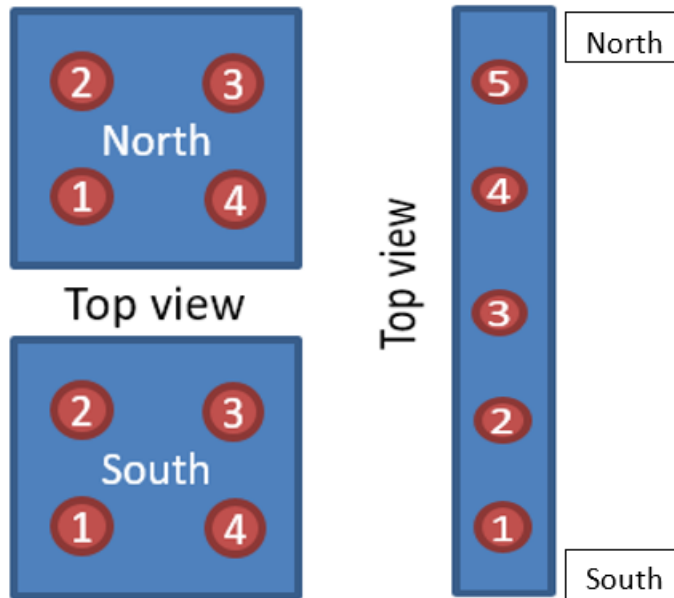


**Figure 5.18: Location of piles at piers and abutments: Pier (left) and Abutment (right)**

North        South
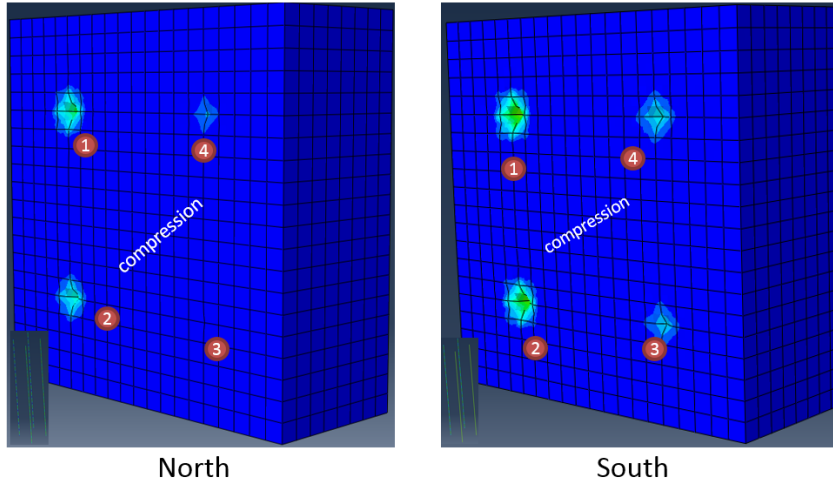
**Figure 5.19: Pier 1 piles–pile cap junctions with pulling out or pushing in deformation**



North        South
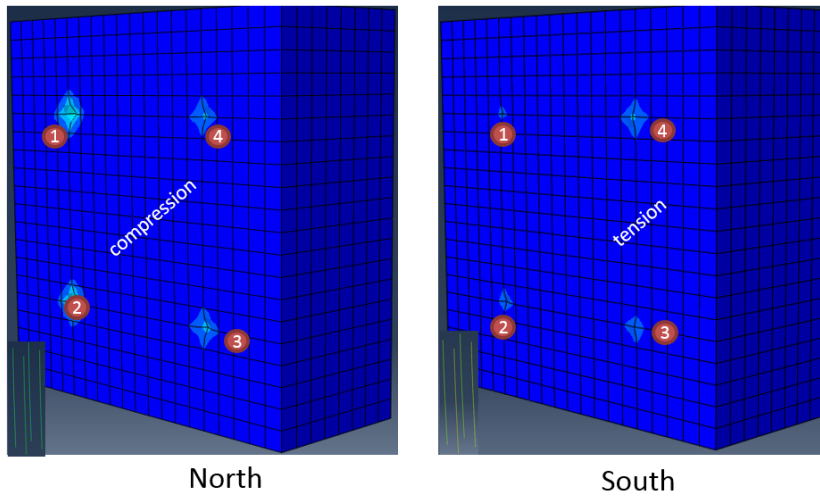
**Figure 5.20: Pier 2 piles–pile cap junctions with pulling-out or pushing-in deformation**



North        South
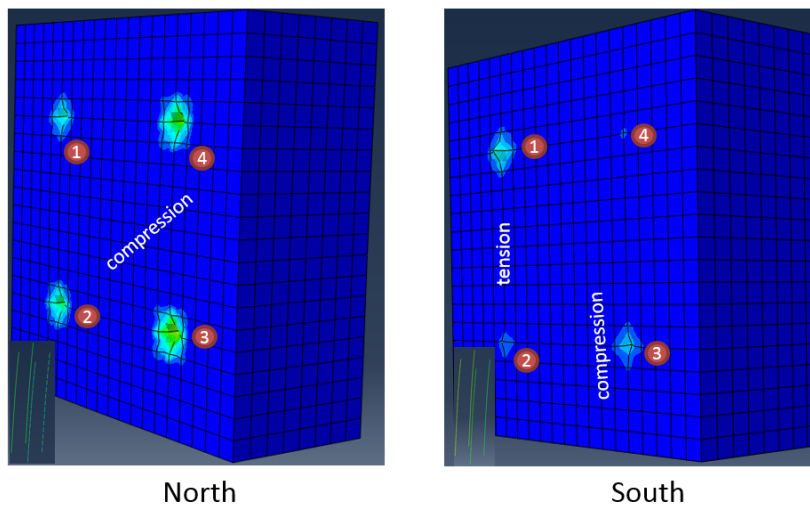
**Figure 5.21: Pier 3 piles–pile cap junctions with pulling-out or pushing-in deformation**
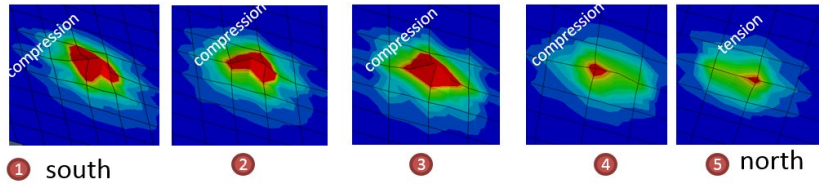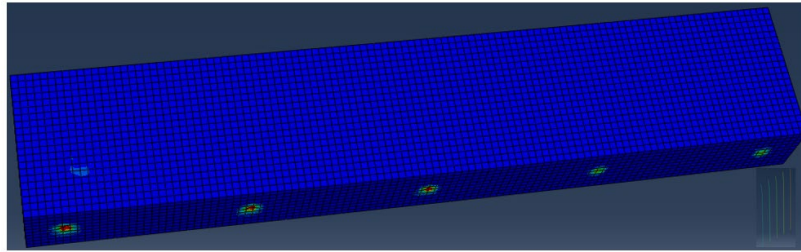
**Figure 5.22: Abutment 1 piles–abutment junctions with pulling-out or pushing-in deformation**
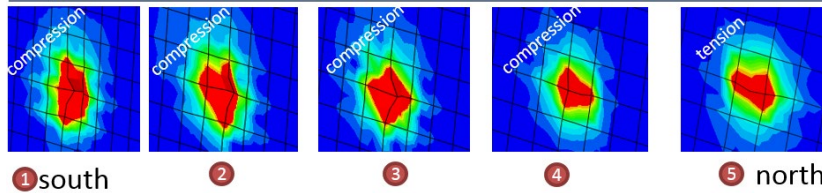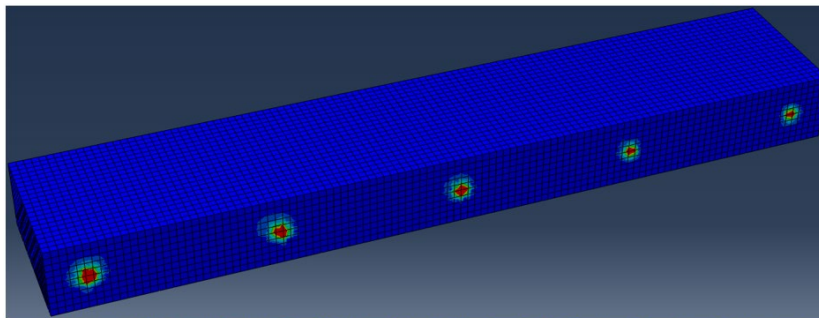


**Figure 5.23: Abutment 2 piles–abutment junctions with pulling-out or pushing-in deformation**

**Table 5.1: Piles nodal forces at the pile cap of the piers (April 2017)**

| Pier 1 Pile (Nodal force at piles top) Pullout starts at 82.5 kips | | | | |
|---|---|---|---|---|
| **North** | | | | |
| | **Pile 1** | **Pile 2** | **Pile 3** | **Pile 4** |
| Forces | NFORCSO1 | NFORCSO1 | NFORCSO1 | NFORCSO1 |
| E=0.5E | −123.123 | −85.566 | 11.728 | −25.819 |
| E=0.33E | −104.16 | −77.925 | −2.702 | −28.927 |
| **South** | | | | |
| | **Pile 1** | **Pile 2** | **Pile 3** | **Pile 4** |
| Forces | NFORCSO1 | NFORCSO1 | NFORCSO1 | NFORCSO1 |
| E=0.5E | −198.11 | −173.679 | −51.652 | −76.068 |
| E=0.33E | −152.871 | −138.641 | −44.715 | −58.93 |
| Pier 2 Pile cap (Nodal force at piles top) | | | | |
| **North** | | | | |
| | **Pile 1** | **Pile 2** | **Pile 3** | **Pile 4** |
| Forces | NFORCSO1 | NFORCSO1 | NFORCSO1 | NFORCSO1 |
| E=0.5E | −67.912 | −68.189 | −26.888 | −26.609 |
| E=0.33E | −64.208 | −67.921 | −35.222 | −31.509 |
| **South** | | | | |
| | **Pile 1** | **Pile 2** | **Pile 3** | **Pile 4** |
| Forces | NFORCSO1 | NFORCSO1 | NFORCSO1 | NFORCSO1 |
| E=0.5E | 1.065 | −0.189 | 60.832 | 62.095 |
| E=0.33E | −16.218 | −23.007 | 24.317 | 31.112 |
| Pier 3 Pile cap (Nodal force at piles top) | | | | |
| **North** | | | | |
| | **Pile 1** | **Pile 2** | **Pile 3** | **Pile 4** |
| Forces | NFORCSO1 | NFORCSO1 | NFORCSO1 | NFORCSO1 |
| E=0.5E | −92.723 | −133.064 | −220.856 | −180.503 |
| E=0.33E | −72.406 | −108.639 | −173.3 | −137.058 |
| **South** | | | | |
| | **Pile 1** | **Pile 2** | **Pile 3** | **Pile 4** |
| Forces | NFORCSO1 | NFORCSO1 | NFORCSO1 | NFORCSO1 |
| E=0.5E | <u>108.583</u> | 58.319 | −32.217 | 18.048 |
| E=0.33E | 68.941 | 23.189 | −44.378 | 1.376 |

**Table 5.2: Piles nodal forces at the abutments (April 2017)**

| Abutment 1 (Nodal force at piles top) Pullout starts at 102.87 kips | | | | | |
|---|---|---|---|---|---|
| | **Pile 1** | **Pile 2** | **Pile 3** | **Pile 4** | **Pile 5** |
| Forces | NFORCSO1 | NFORCSO1 | NFORCSO1 | NFORCSO1 | NFORCSO1 |
| E=0.5E | −70.156 | −45.612 | −17.658 | 10.612 | 44.888 |
| E=0.33E | −58.342 | −40.915 | −19.686 | −2.035 | 21.862 |
| Abutment 2 (Nodal force at piles top) | | | | | |
| | **Pile 1** | **Pile 2** | **Pile 3** | **Pile 4** | **Pile 5** |
| Forces | NFORCSO1 | NFORCSO1 | NFORCSO1 | NFORCSO1 | NFORCSO1 |
| E=0.5E | −126.789 | −82.376 | −32.273 | −3.947 | 33.641 |
| E=0.33E | −99.502 | −66.291 | −27.297 | −10.792 | 14.905 |

### 5.1.2 Superimposing Live Load

The truck loading and locations described in Section 3.5 of Chapter 3 are used in this analysis. Since it is very cumbersome to present the results of all truck locations graphically, the most critical case is found to be that of Location 6, which is presented in this report below. Figure 5.24 shows the whole bridge in von Mises stress-contour drawing with the red color indicating stress exceeding 4 ksi.
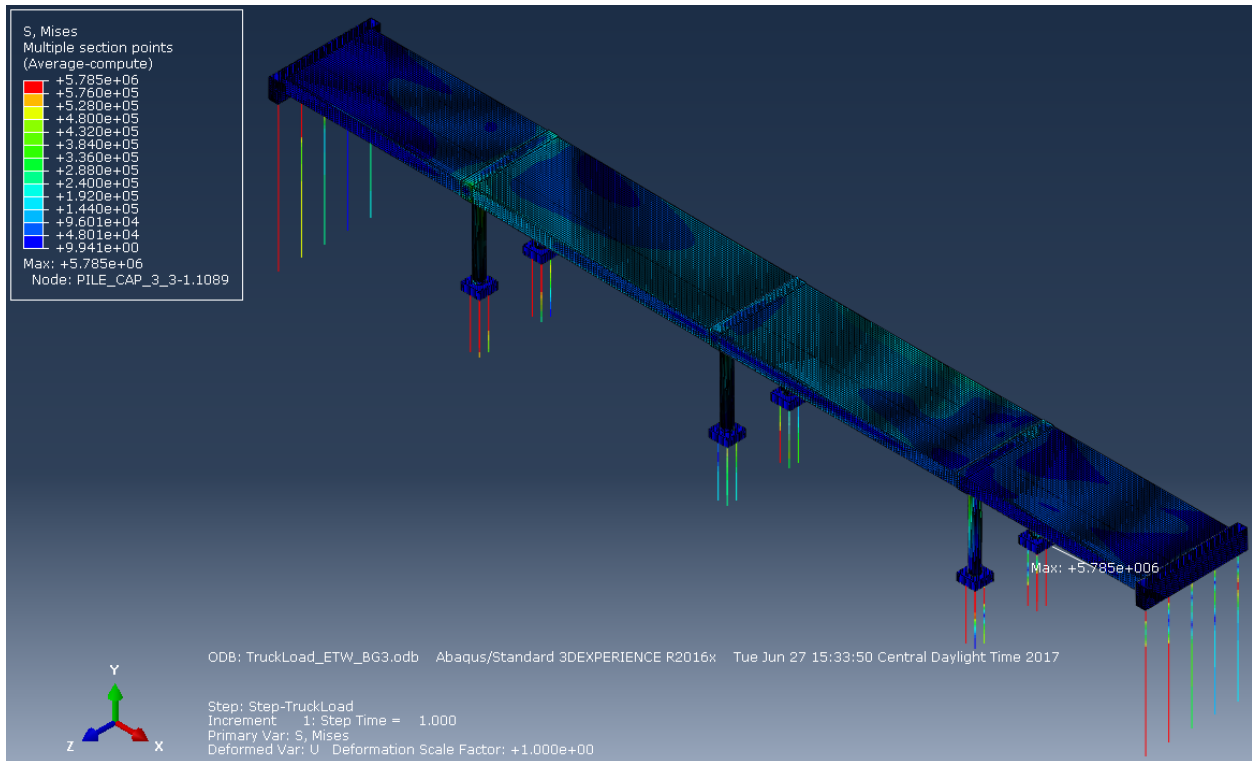


**Figure 5.24: Von Mises stress distribution along the bridge (April 2017 settlement + truck loading)**

Figure 5.25 presents the von Mises stress variation in the abutments. It is evident that the stresses are very low except for the junctions with piles which represent numerical stress concentration points due to joining beam to solid elements.

=f$_c$'=4 KSI = 5.76E5 PSF
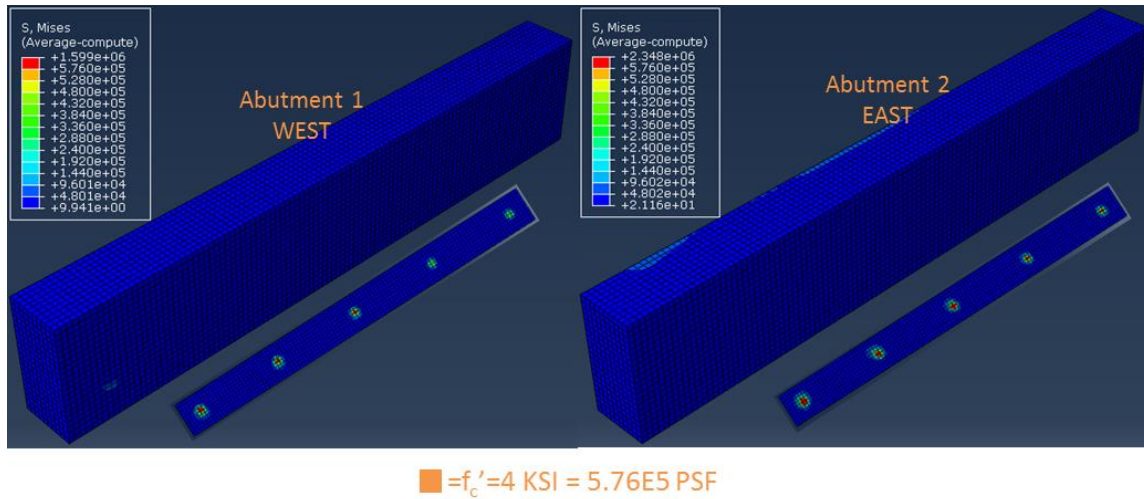
**Figure 5.25: Von Mises stress distribution along the abutments (April 2017 settlement + truck loading)**



=f$_c$'=4 KSI = 5.76E5 PSF
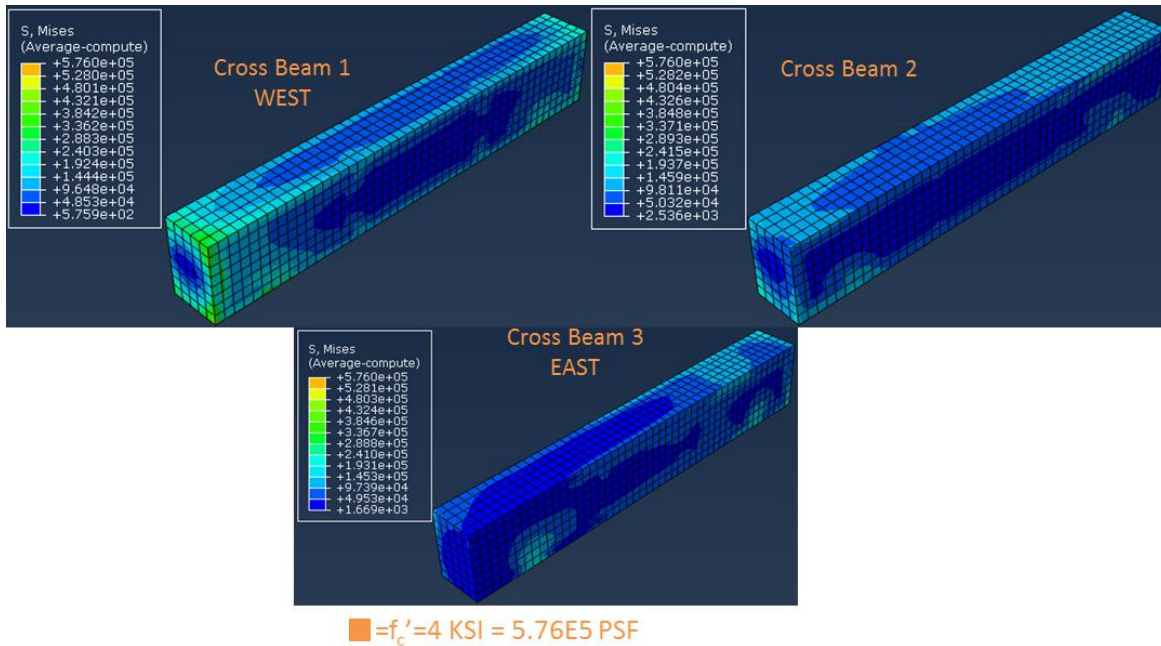
**Figure 5.26: Von Mises stress distribution along crossbeams (April 2017 settlement + truck loading)**

**=f$_c$'=4 KSI = 5.76E5 PSF**
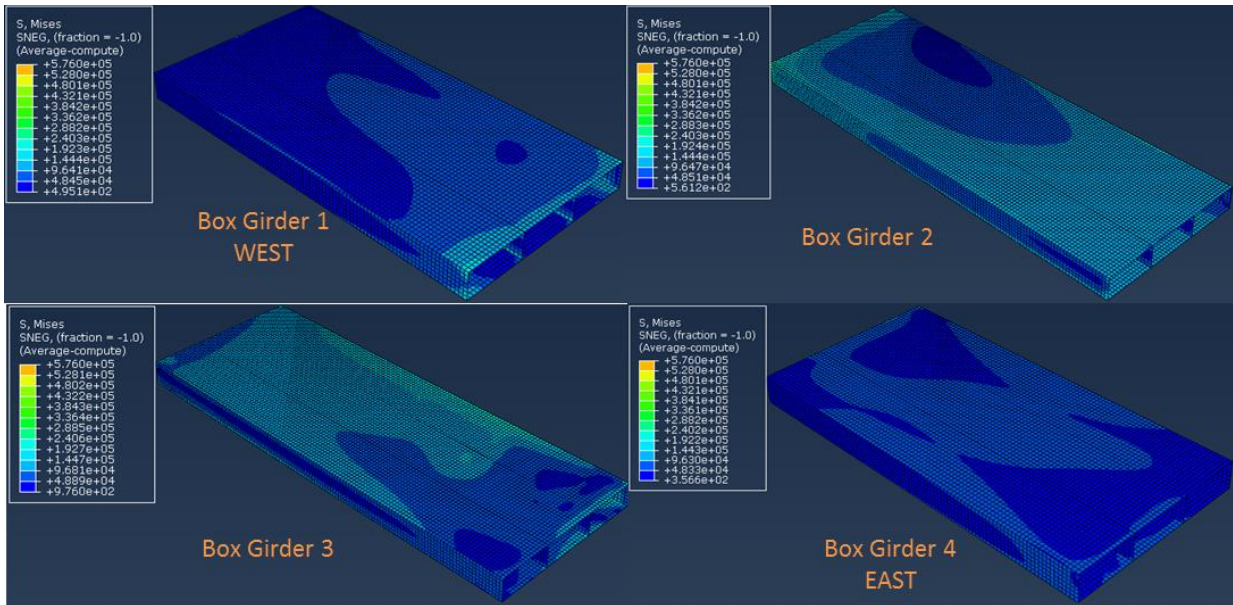
**Figure 5.27: Von Mises stress distribution along box girders (April 2017 settlement + truck loading)**



**=f$_c$'=4 KSI = 5.76E5 PSF**

**Figure 5.28: Von Mises stress distribution along piers (April 2017 settlement + truck loading)**

**Figure 5.29: Von Mises stress distribution along the piles (April 2017 settlement + truck loading)**

Figure 5.26 presents the von Mises stress variation in the crossbeams. It is evident that the stresses are comparable to those of Figure 5.5, so they do not represent a critical stage. Figure 5.27 shows the von Mises stress variation in the box girders. It is clear from this figure that the stress-contours do not represent any critical stage of exceeding the concrete strength of 4 ksi. Figure 5.28 shows the von Mises stress variation in the piers. Clearly the stress concentration spots at the pier tops are similar to those of Figure 5.9. Figure 5.29 illustrates the fact that the yield strength of the piles was not reached when the truck loading was added.

In addition to the contour drawings, tables are provided below to report the pile forces at the junctions, with pile caps or abutments for all eight locations of the truck, with its effects added to the settlement up to April 2017. Tables 5.3 through Table 5.6 lists all the pile forces under all load locations for the three piers and Abutment 1. None of the pile forces exceed the critical de-bonding tensile forces calculated earlier.

**Table 5.3: Piles nodal force of Pier 1, loads applied at eight different locations respectively**

| Pier 1 Pile (Nodal force at piles top) (Kips) Pullout states at 82.5 kips | | | | |
|---|---|---|---|---|
| **North** | | | | |
| | **Pile 1** | **Pile 2** | **Pile 3** | **Pile 4** |
| Location | NFORCSO1 | NFORCSO1 | NFORCSO1 | NFORCSO1 |
| 1 | −105.043 | −78.477 | −4.474 | −31.029 |
| 2 | −109.097 | −82.795 | −6.237 | −32.528 |
| 3 | −103.234 | −76.895 | −2.119 | −28.448 |
| 4 | −104.371 | −78.06 | −2.544 | −28.845 |
| 5 | −104.436 | −78.209 | −2.536 | −28.753 |
| 6 | −103.595 | −77.547 | −2.561 | −28.599 |
| 7 | −108.748 | −82.172 | −4.822 | −31.388 |
| 8 | −113.57 | −86.532 | −14.604 | −41.631 |
| **South** | | | | |
| | **Pile 1** | **Pile 2** | **Pile 3** | **Pile 4** |
| Location | NFORCSO1 | NFORCSO1 | NFORCSO1 | NFORCSO1 |
| 1 | −155.706 | −142.085 | −50.644 | −64.251 |
| 2 | −165.674 | −152.356 | −54.929 | −68.232 |
| 3 | −152.362 | −137.858 | −44.405 | −58.894 |
| 4 | −153.147 | −138.856 | −44.605 | −58.881 |
| 5 | −153.11 | −138.9 | −44.541 | −58.735 |
| 6 | −152.261 | −138.103 | −44.417 | −58.56 |
| 7 | −154.352 | −140.457 | −45.316 | −59.196 |
| 8 | −156.097 | −141.879 | −49.278 | −63.481 |

**Table 5.4: Piles nodal force of Pier 2, loads applied at eight different locations respectively**

| Pier 2 Pile cap (Nodal force at piles top) | | | | |
|---|---|---|---|---|
| **North** | | | | |
| | **Pile 1** | **Pile 2** | **Pile 3** | **Pile 4** |
| Location | NFORCSO1 | NFORCSO1 | NFORCSO1 | NFORCSO1 |
| 1 | −63.753 | −67.444 | −34.911 | −31.219 |
| 2 | −64.701 | −68.071 | −36.554 | −33.184 |
| 3 | −68.98 | −72.549 | −38.499 | −34.929 |
| 4 | −63.67 | −67.312 | −34.58 | −30.937 |
| 5 | −63.904 | −67.733 | −34.885 | −31.055 |
| 6 | −68.632 | −72.037 | −37.269 | −33.864 |
| 7 | −74.24 | −77.147 | −47.961 | −45.055 |
| 8 | −63.845 | −67.759 | −35.044 | −31.129 |
| **South** | | | | |
| | **Pile 1** | **Pile 2** | **Pile 3** | **Pile 4** |
| Location | NFORCSO1 | NFORCSO1 | NFORCSO1 | NFORCSO1 |
| 1 | −15.931 | −22.602 | 24.588 | 31.266 |
| 2 | −18.265 | −25.363 | 19.891 | 26.995 |
| 3 | −28.96 | −36.548 | 14.289 | 21.884 |
| 4 | −16.037 | −22.626 | 24.68 | 31.276 |
| 5 | −15.891 | −22.689 | 24.826 | 31.631 |
| 6 | −17.549 | −24.682 | 23.823 | 30.963 |
| 7 | −19.499 | −26.425 | 19.547 | 26.48 |
| 8 | −15.573 | −22.434 | 24.857 | 31.724 |

**Table 5.5: Piles nodal force of Pier 3, loads applied at eight different locations respectively**

| Pier 3 Pile cap (Nodal force at piles top) | | | |
|---|---|---|---|
| **North** | | | |
| | **Pile 1** | **Pile 2** | **Pile 3** | **Pile 4** |
| Location | NFORCSO1 | NFORCSO1 | NFORCSO1 | NFORCSO1 |
| 1 | −72.253 | −108.464 | −173.51 | −137.289 |
| 2 | −72.107 | −108.269 | −172.691 | −136.52 |
| 3 | −73.008 | −108.904 | −174.782 | −138.876 |
| 4 | −76.982 | −113.202 | −176.54 | −140.31 |
| 5 | −79.089 | −114.608 | −176.476 | −140.947 |
| 6 | −82.622 | −117.934 | −186.1 | −150.776 |
| 7 | −72.096 | −108.602 | −172.789 | −136.274 |
| 8 | −72.295 | −108.59 | −173.577 | −137.272 |
| **South** | | | |
| | **Pile 1** | **Pile 2** | **Pile 3** | **Pile 4** |
| Location | NFORCSO1 | NFORCSO1 | NFORCSO1 | NFORCSO1 |
| 1 | 69.085 | 23.344 | −44.623 | 1.119 |
| 2 | 69.083 | 23.517 | −43.813 | 1.754 |
| 3 | 66.824 | 20.728 | −48.968 | −2.871 |
| 4 | 57.056 | 10.499 | −53.771 | −7.213 |
| 5 | 66.808 | 20.696 | −45.508 | 0.605 |
| 6 | 65.401 | 19.586 | −49.315 | −3.499 |
| 7 | 69.523 | 23.668 | −43.451 | 2.405 |
| 8 | 69.1 | 23.27 | −44.589 | 1.242 |

**Table 5.6: Piles nodal force of Abutments, loads applied at eight different locations respectively**

| | Pile 1 | Pile 2 | Pile 3 | Pile 4 | Pile 5 |
|---|---|---|---|---|---|
| **Abutment 1 (Nodal force at piles top) Pullout starts at 102.87 kips** | | | | | |
| Location | NFORCSO1 | NFORCSO1 | NFORCSO1 | NFORCSO1 | NFORCSO1 |
| 1 | −77.025 | −55.41 | −28.347 | −8.172 | 18.424 |
| 2 | −57.534 | −40.351 | −19.179 | −0.955 | 23.788 |
| 3 | −58.629 | −41.076 | −19.755 | −2.1 | 21.77 |
| 4 | −58.353 | −40.926 | −19.693 | −2.038 | 21.869 |
| 5 | −58.36 | −40.934 | −19.702 | −2.053 | 21.846 |
| 6 | −58.457 | −40.99 | −19.743 | −2.144 | 21.676 |
| 7 | −57.274 | −40.297 | −19.349 | −1.564 | 22.603 |
| 8 | −59.772 | −41.974 | −21.294 | −6.482 | 13.619 |
| **Abutment 2 (Nodal force at piles top) Pullout starts at 102.87 kips** | | | | | |
| Location | NFORCSO1 | NFORCSO1 | NFORCSO1 | NFORCSO1 | NFORCSO1 |
| 1 | −99.517 | −66.308 | −27.312 | −10.81 | 14.889 |
| 2 | −99.692 | −66.399 | −27.351 | −10.865 | 14.788 |
| 3 | −98.744 | −65.824 | −26.981 | −10.181 | 15.994 |
| 4 | −107.898 | −70.708 | −28.785 | −11.785 | 13.4 |
| 5 | −103.024 | −71.776 | −34.852 | −24.175 | −3.425 |
| 6 | −97.541 | −65.223 | −26.822 | −10.24 | 15.738 |
| 7 | −99.596 | −66.353 | −27.361 | −10.951 | 14.613 |
| 8 | −99.496 | −66.295 | −27.305 | −10.804 | 14.894 |

### 5.1.3 Applying Projected Settlements

Because settlement data was available only for April 2013 to April 2017 when modeling in Abaqus, projected settlement was calculated using the six schemes described below. Based on the settlement data available through April 2017, the research team projected additional settlements through May 2022 under six different schemes according to specific criteria to study the possibility of de-bonding between the piles and pile caps, as well as the likelihood of failure in any of the other bridge components. The analysis will continue for each scheme until May 2022 or until failure is indicated in the specific component under investigation. The following criteria show how the projected settlements for the different schemes are established.

**Scheme I:** The total incremental settlements of April 2014 to April 2017 are summed up and the average is determined by dividing by 4. This average is used as a constant settlement increment for each year starting April 2018 to May 2022. This was applied the same way to the North and South sides of the bridge.

$$Ave = \frac{Apr14 + Apr15 + Apr16 + Apr17}{4}$$

$$Apr18 = Ave, Apr19 = Ave, Apr20 = Ave, Apr21 = Ave, Apr22 = Ave$$

**Scheme II:** The total incremental settlements of April 2014 to April 2017 are summed up. This sum is used as a constant settlement increment for each year starting April 2018 to May 2022 multiplied by a modifying fraction such that the total four-year increment is kept the same. This was applied the same way to the North and South sides of the bridge.

$$Sum = Apr14 + Apr15 + Apr16 + Apr17$$

$$Apr18 = Sum \times \frac{5}{16}, Apr19 = Sum \times \frac{3}{16}, Apr20 = Sum \times \frac{5}{16}$$

$$Apr21 = Sum \times \frac{3}{16}, Apr22 = Sum \times \frac{5}{16}$$

**Scheme III:** The total incremental settlements of April 2014 to April 2017 are summed up and the average is determined by dividing by 4 and multiplying by 1.25. This augmented average is used as a constant settlement increment for each year starting April 2018 to May 2022. This was applied the same way to the North and South sides of the bridge.

$$Ave_m = \frac{Apr14 + Apr15 + Apr16 + Apr17}{4} \times 1.25$$

$$Apr18 = Ave_m, Apr19 = Ave_m, Apr20 = Ave_m, Apr21 = Ave_m, Apr22 = Ave_m$$

**Scheme IV:** The total incremental settlements of April 2014 to April 2017 are summed up and multiplied by 1.25. This augmented sum is used as a constant settlement increment for each year starting April 2018 to May 2022 multiplied by a modifying fraction such that the total four-year increment is kept the same. This was applied the same way to the North and South sides of the bridge.

$$Sum_m = (Apr14 + Apr15 + Apr16 + Apr17) \times 1.25$$

$$Apr18 = Sum_m \times \frac{6}{16}, Apr19 = Sum_m \times \frac{2}{16}, Apr20 = Sum_m \times \frac{6}{16}$$

$$Apr21 = Sum_m \times \frac{2}{16}, Apr22 = Sum_m \times \frac{6}{16}$$

**Scheme V:** The total incremental settlements of April 2014 to April 2017 are summed up and the average is determined by dividing by 4 and multiplying by 1.5. This augmented average is used as a constant settlement increment for each year starting April 2018 to May 2022. This was applied the same way to the North and South sides of the bridge.

$$Ave_n = \frac{Apr14 + Apr15 + Apr16 + Apr17}{4} \times 1.5$$

$$Apr18 = Ave_n, Apr19 = Ave_n, Apr20 = Ave_n, Apr21 = Ave_n, Apr22 = Ave_n$$

**Scheme VI:** The total incremental settlements of April 2014 to April 2017 are summed up and multiplied by 1.5. This augmented sum is used as a constant settlement increment for each year starting April 2018 to May 2022, multiplied by a modifying fraction such that the total four-year increment is kept the same. This was applied the same way to the North and South sides of the bridge.

$$Sum_n = (Apr14 + Apr15 + Apr16 + Apr17) \times 1.5$$

$$Apr18 = Sum_n \times \frac{5}{16}, Apr19 = Sum_n \times \frac{3}{16}, Apr20 = Sum_n \times \frac{5}{16}$$

$$Apr21 = Sum_n \times \frac{3}{16}, Apr22 = Sum_n \times \frac{5}{16}$$

The application of the six different schemes of projected settlements was made on top of the settlements of April 2017 without considering any truck loading to determine the year in which the settlement represents a threat of failure to the different bridge components for the various settlement schemes at hand. Because there are 5 years' worth of incremental settlements within six schemes, the data produced a large amount of results. For the sake of this report, the worst settlement scheme (Scheme VI) was selected, with the very last year of 2022, for presentation and discussion in this chapter for the stress-contour of the different bridge components. Furthermore, the forces on the top of all piles for all years of Scheme VI are presented in Table 5.7 and Table 5.8.

Figure 5.30 presents the von Mises stress distribution for the entire bridge subjected to the total settlement of May 2022 using the critical Scheme VI. It is evident from this figure that the stresses show more overall increase compared to those of April 2017 (Figure 5.1). However, the stresses in compression are still lower than the concrete strength of 4 ksi. Similar observations apply to Figure 5.31 for abutment stresses, Figure 5.32 for crossbeam stresses, and Figure 5.33 for box girder stresses. However, Figure 5.34 shows more critical stress exceedance especially at the Pier 3 on the north side. On the other hand, Figure 5.35 for piles show that their stresses are below 36 ksi.
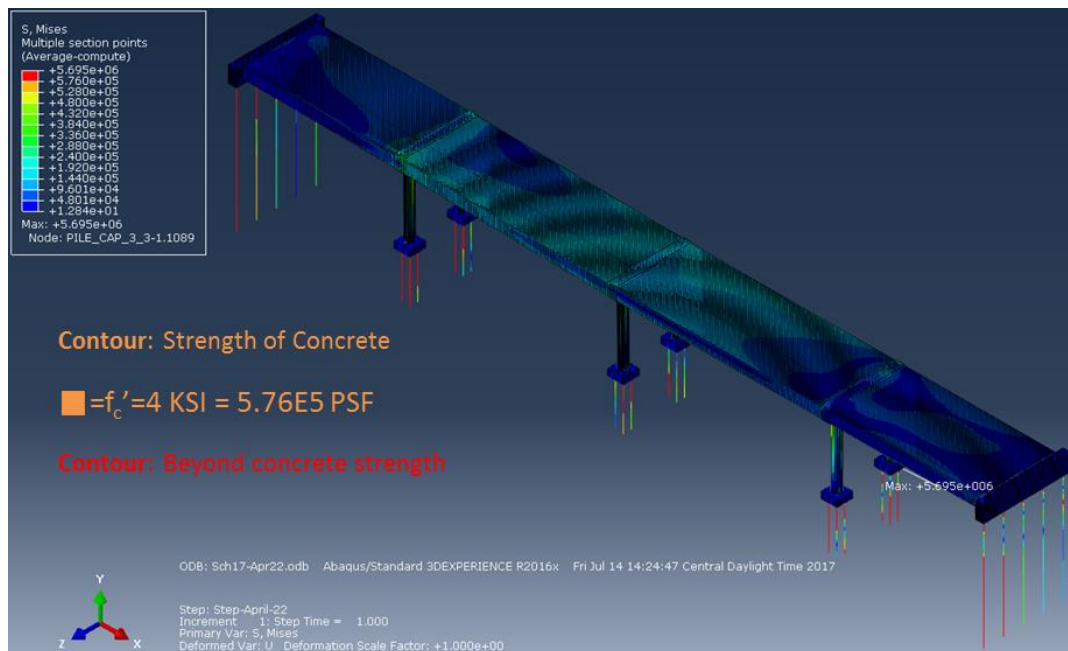


**Figure 5.30: Von Mises stress distribution along the bridge (May 2022 settlement)**
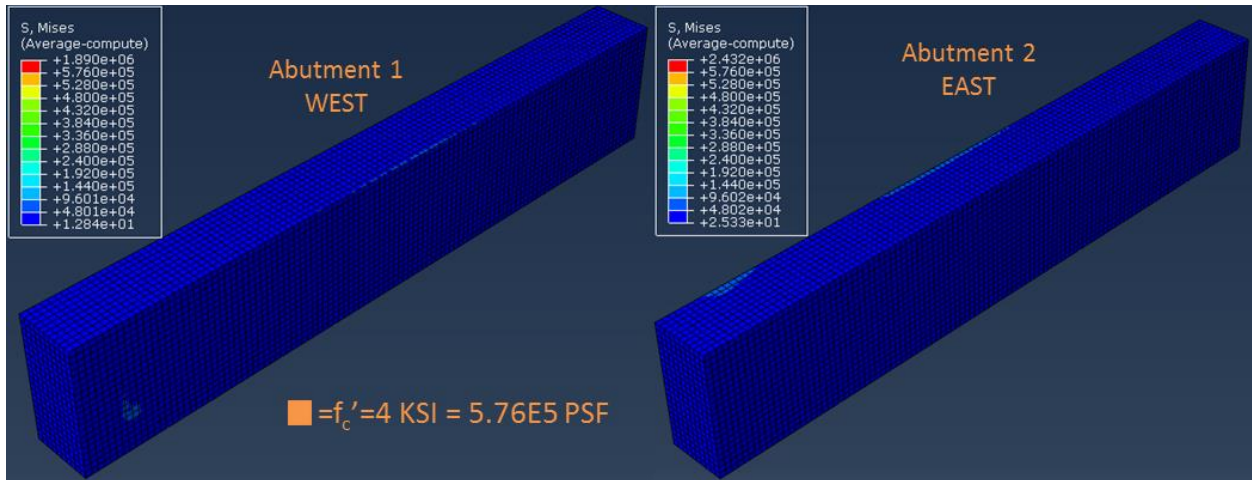
**Figure 5.31: Von Mises stress distribution along the abutments (May 2022 settlement)**
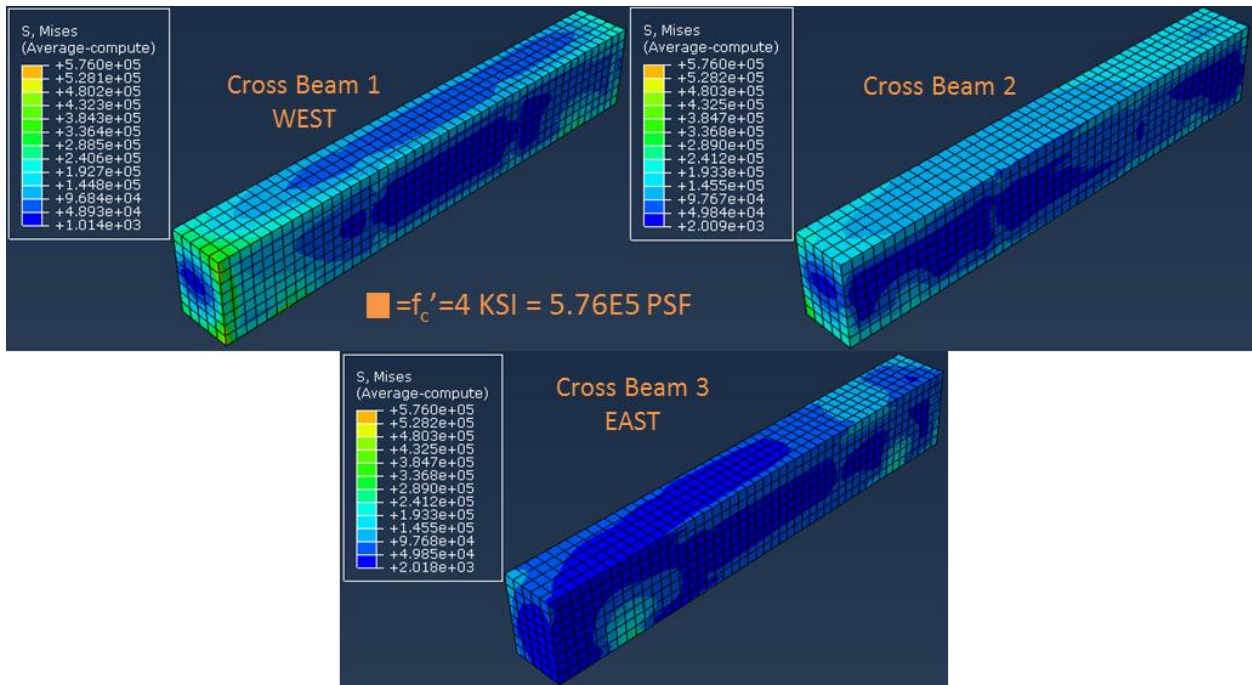


**Figure 5.32: Von Mises stress distribution along the crossbeams (May 2022 settlement)**

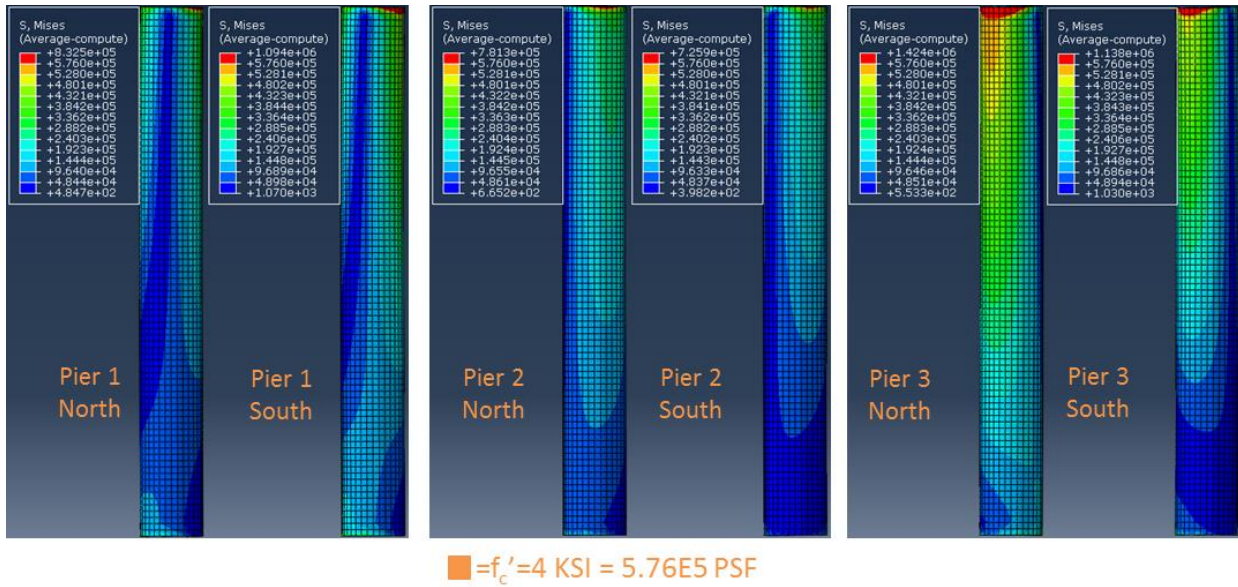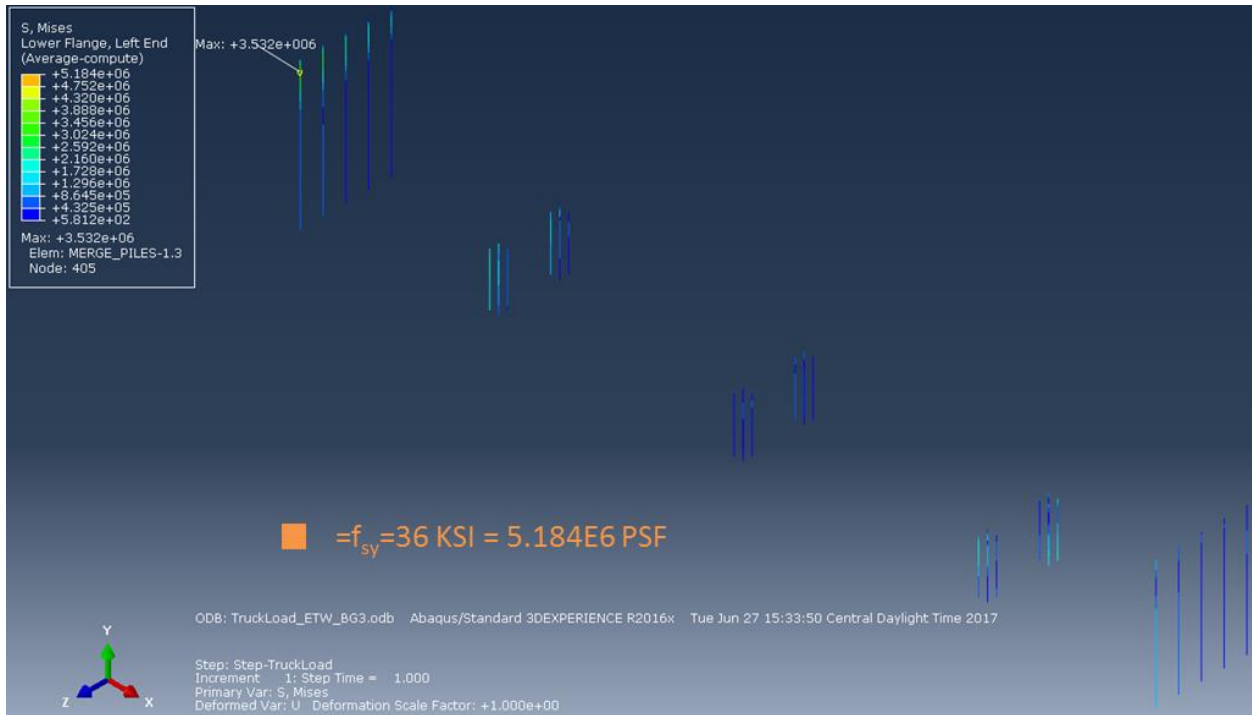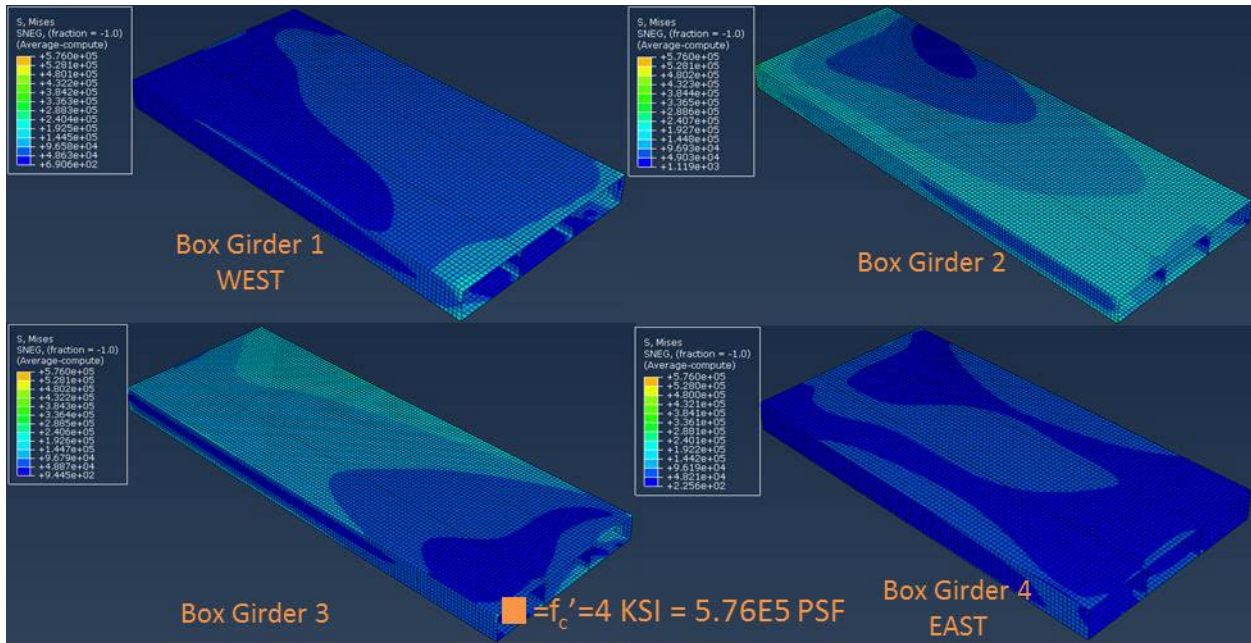**Figure 5.33: Von Mises stress distribution along the box girders (May 2022 settlement)**
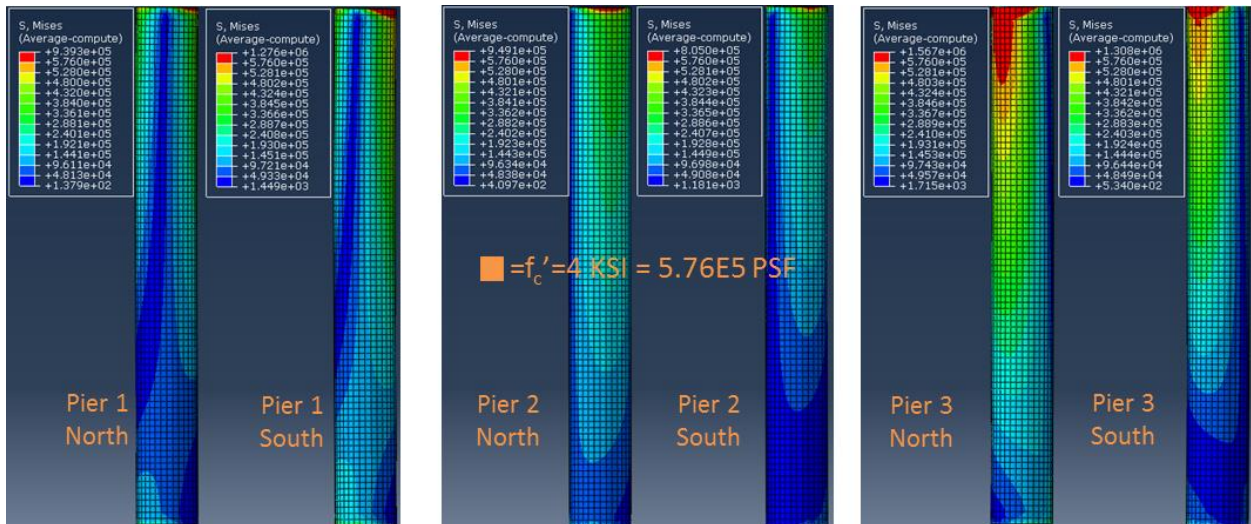


**Figure 5.34: Von Mises stress distribution along the piers (May 2022 settlement)**
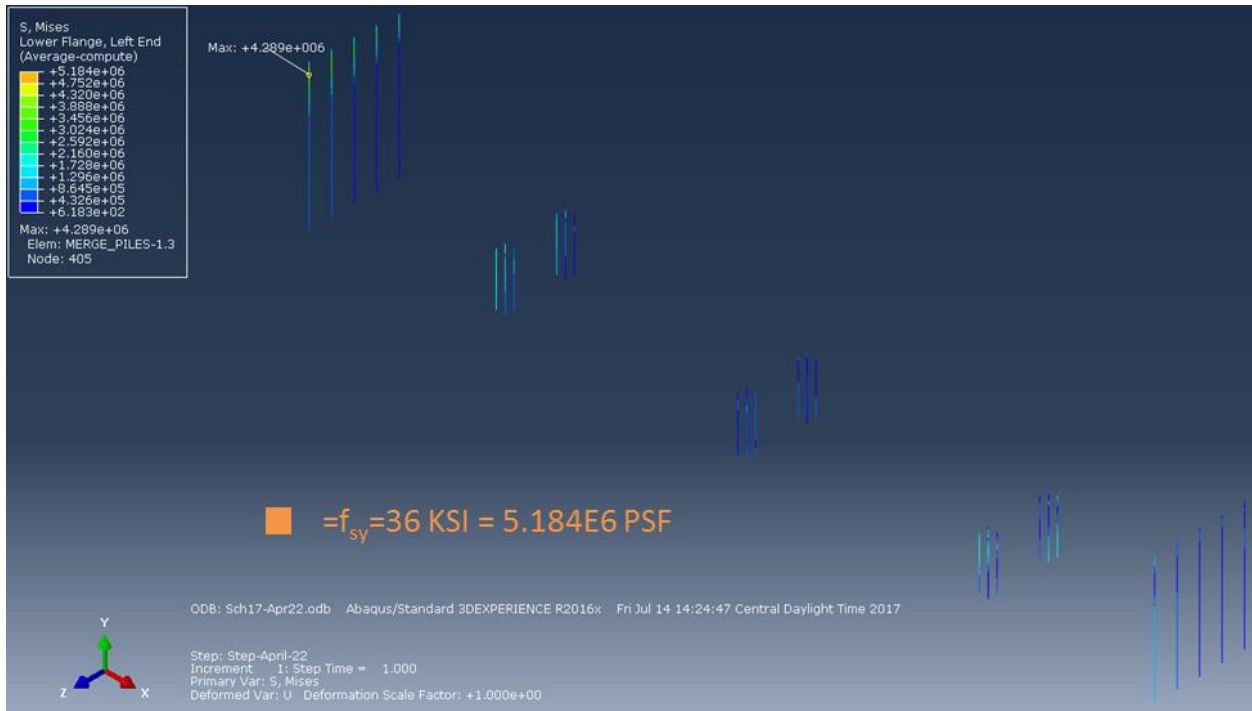
**Figure 5.35: Von Mises stress distribution along the piles (May 2022 settlement)**

In addition to the contour drawings, tables are provided below to report the pile forces at the junctions with pile caps or abutments for all 5 years of projected settlements under the six schemes analyzed. Table 5.7 through Table 5.10 list all the pile forces of all 5 years for the three piers and two abutments under Scheme VI. None of the pile forces exceed the critical de-bonding tensile forces calculated earlier.

**Table 5.7: Scheme VI projected piles nodal forces at Pier 1**

| Pier 1 Pile (Nodal force at piles top) (Kips) Pullout states at 82.5 kips | | | |
|---|---|---|---|
| North | | | |
| Pile 1 | Pile 2 | Pile 3 | Pile 4 |
| Forces | | | |
| NFORCSO1 | NFORCSO1 | NFORCSO1 | NFORCSO1 |
| Apr. 2013 | −59.91 | −59.26 | −56.81 | −57.45 |
| Apr. 2017 | −104.16 | −77.93 | −2.70 | −28.93 |
| Apr. 2018 | −104.90 | −77.34 | 0.88 | −26.67 |
| Apr. 2019 | −105.39 | −77.07 | 2.94 | −25.37 |
| Apr. 2020 | −106.18 | −76.61 | 6.41 | −23.16 |
| Apr. 2021 | −106.73 | −76.40 | 8.40 | −21.92 |
| Apr. 2022 | −107.56 | −75.99 | 11.81 | −19.75 |
| South | | | |
| Pile 1 | Pile 2 | Pile 3 | Pile 4 |
| Forces | NFORCSO1 | NFORCSO1 | NFORCSO1 | NFORCSO1 |
| Apr. 2013 | −90.49 | −90.14 | −86.26 | −86.61 |
| Apr. 2017 | −152.87 | −138.64 | −44.72 | −58.93 |
| Apr. 2018 | −158.42 | −143.08 | −45.04 | −60.36 |
| Apr. 2019 | −161.65 | −145.69 | −45.18 | −61.12 |
| Apr. 2020 | −167.07 | −150.07 | −45.44 | −62.42 |
| Apr. 2021 | −170.24 | −152.62 | −45.52 | −63.12 |
| Apr. 2022 | −175.62 | −156.97 | −45.74 | −64.37 |

**Table 5.8: Scheme VI projected piles nodal forces at Pier 2**

| Pier 2 Pile cap (Nodal force at piles top) | | | |
|---|---|---|---|
| North | | | |
| Pile 1 | Pile 2 | Pile 3 | Pile 4 |
| Forces | NFORCSO1 | NFORCSO1 | NFORCSO1 | NFORCSO1 |
| Apr. 2013 | −58.68 | −58.74 | −58.32 | −58.26 |
| Apr. 2017 | −64.21 | −67.92 | −35.22 | −31.51 |
| Apr. 2018 | −66.07 | −71.06 | −38.88 | −33.88 |
| Apr. 2019 | −67.23 | −73.01 | −41.12 | −35.34 |
| Apr. 2020 | −69.19 | −76.33 | −44.91 | −37.78 |
| Apr. 2021 | −70.29 | −78.15 | −47.02 | −39.17 |
| Apr. 2022 | −72.23 | −81.40 | −50.76 | −41.58 |
| South | | | |
| Pile 1 | Pile 2 | Pile 3 | Pile 4 |
| Forces | NFORCSO1 | NFORCSO1 | NFORCSO1 | NFORCSO1 |
| Apr. 2013 | 0.50 | 0.50 | 0.50 | 0.50 |
| Apr. 2017 | −16.22 | −23.01 | 24.32 | 31.11 |
| Apr. 2018 | −9.81 | −17.67 | 29.74 | 37.61 |
| Apr. 2019 | −5.91 | −14.43 | 33.02 | 41.55 |
| Apr. 2020 | 0.65 | −9.02 | 38.51 | 48.18 |
| Apr. 2021 | 4.40 | −5.86 | 41.73 | 52.00 |
| Apr. 2022 | 10.91 | −0.48 | 47.19 | 58.58 |

**5.2 RISA 3D Model Results**

*5.2.1 Settlement Analysis*

In Figure 5.36, bridge layout is given where shear and axial force, bending moment, and torsion due to the applied loads and imposed settlement were studied. Values for the forces and moments were obtained from RISA 3D. The internal force summation tool (IFST) was used to extract forces and moments within the plane of a cut in a section. However, since the program uses local axes for vertical and horizontal elements, the internal forces were calculated separately and summed up at the end. In the following, forces and moments due to self-weight and imposed settlement are given for each section.
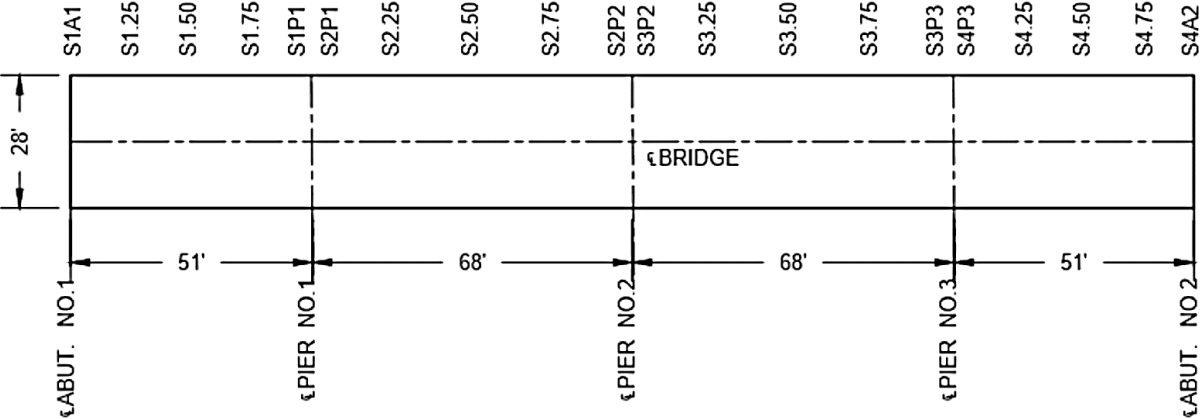


**Figure 5.36: Bridge layout and sections where shear force, axial force, bending moment, and torsion were studied**

5.2.1.1 Box Girder Results

In this section, forces and moments for each section shown in Figure 5.36 are provided. Notice that the internal forces summation tool (IFST) of RISA 3D gives forces and moments based on the element's local axes, therefore, forces and moments for web elements and top and bottom slabs were added based on their local axes shown below. The final results in the table follow the web local axes.
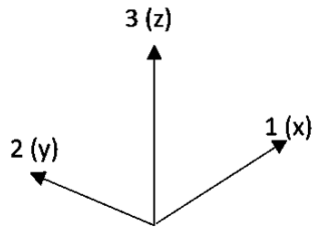
**Figure 5.37: Top and bottom slab local axes**
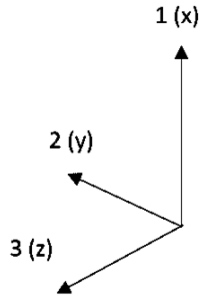


**Figure 5.38: Web element local axes**
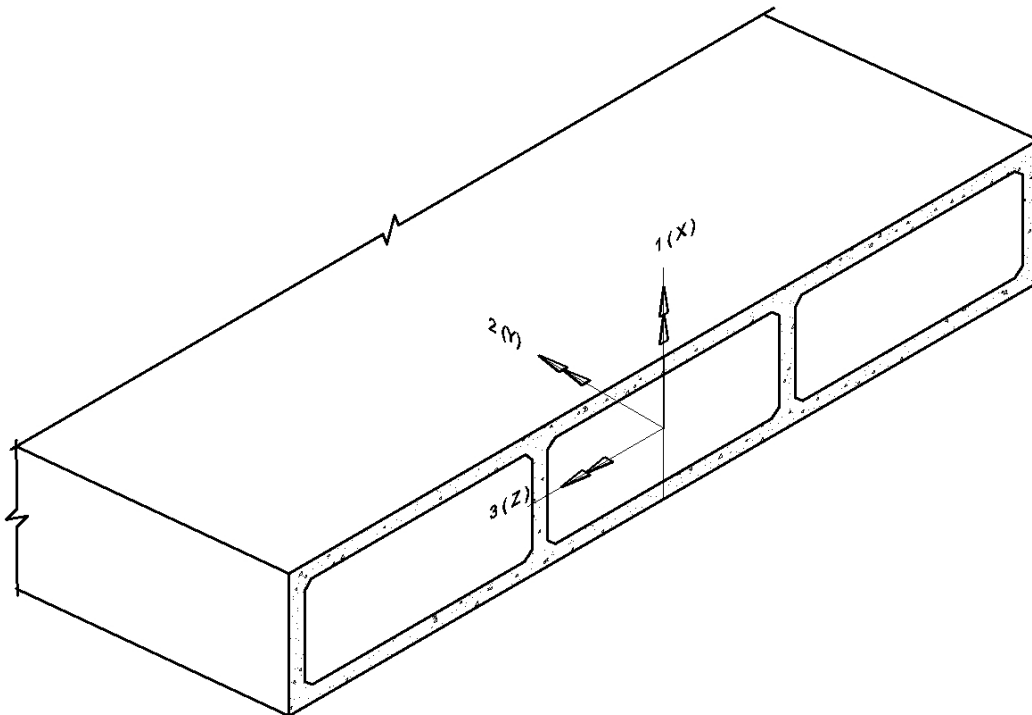


**Figure 5.39: Isometric view of the bridge section with axes and moments shown**

**Table 5.9: Forces and moments in section S1A1 in April 2017**

|  | ∑ Self wt. | ∑ Forced Displacement | Total |  |
|---|---|---|---|---|
| F1 (shear) | 42.02 | 63.43 | 105.44 | k |
| F2 (axial) | 89.65 | 18.31 | 107.95 | k |
| F3 | −2.41 | −1.28 | −3.69 | k |
| M1 | 92.44 | 44.42 | 136.86 | k-ft |
| M2 (tors.) | −2794.03 | −1402.61 | −4196.64 | k-ft |
| M3 (bend.) | −298.92 | −182.39 | −481.31 | k-ft |

*See Figure 5.36 for section locations

**Table 5.10: Predicted forces and moments in section S1A1 in May 2022**

|  | ∑ Self wt. | ∑ Forced Displacement | Total |  |
|---|---|---|---|---|
| F1 (shear) | 42.02 | 56.80 | 98.81 | k |
| F2 (axial) | 89.65 | 26.87 | 116.52 | k |
| F3 | −2.41 | −0.69 | −3.10 | k |
| M1 | 92.44 | 21.51 | 113.95 | k-ft |
| M2 (tors.) | −2794.03 | −776.91 | −3570.93 | k-ft |
| M3 (bend.) | −298.92 | −170.54 | −469.46 | k-ft |

**Table 5.11: Forces and moments in section S1.25 in April 2017**

|  | ∑ Self wt. | ∑ Forced Displacement | Total |  |
|---|---|---|---|---|
| F1 (shear) | 101.04 | 67.92 | 168.95 | k |
| F2 (axial) | 89.65 | 18.31 | 107.95 | k |
| F3 | 0.34 | 0.08 | 0.42 | k |
| M1 | 12.07 | 9.96 | 22.03 | k-ft |
| M2 (tors.) | −2794.00 | −1402.61 | −4196.61 | k-ft |
| M3 (bend.) | −957.10 | −782.34 | −1739.44 | k-ft |

**Table 5.12: Predicted forces and moments in section S1.25 in May 2022**

|  | ∑ Self wt. | ∑ Forced Displacement | Total |  |
|---|---|---|---|---|
| F1 (shear) | 101.04 | 61.10 | 162.13 | k |
| F2 (axial) | 89.65 | 26.87 | 116.52 | k |
| F3 | 0.34 | 0.04 | 0.37 | k |
| M1 | 12.07 | 11.92 | 24.00 | k-ft |
| M2 (tors.) | −2794.00 | −776.91 | −3570.91 | k-ft |
| M3 (bend.) | −957.10 | −653.19 | −1610.30 | k-ft |

**Table 5.13: Forces and moments in section S1.5 in April 2017**

|  | ∑ Self wt. | ∑ Forced Displacement | Total |  |
|---|---|---|---|---|
| F1 (shear) | 161.31 | 67.81 | 229.12 | k |
| F2 (axial) | 89.65 | 18.31 | 107.95 | k |
| F3 | 0.33 | 0.10 | 0.43 | k |
| M1 | 26.86 | 7.16 | 34.01 | k-ft |
| M2 (tors.) | −2793.98 | −1402.60 | −4196.58 | k-ft |
| M3 (bend.) | −2196.65 | −1449.86 | −3646.51 | k-ft |

**Table 5.14: Predicted forces and moments in section S1.5 in May 2022**

|  | ∑ Self wt. | ∑ Forced Displacement | Total |  |
|---|---|---|---|---|
| F1 (shear) | 161.31 | 60.99 | 222.31 | k |
| F2 (axial) | 89.65 | 26.87 | 116.52 | k |
| F3 | 0.33 | 0.09 | 0.41 | k |
| M1 | 26.86 | −2.42 | 24.44 | k-ft |
| M2 (tors.) | −2793.98 | −776.91 | −3570.88 | k-ft |
| M3 (bend.) | −2196.65 | −1255.76 | −3452.42 | k-ft |

**Table 5.15: Forces and moments in section S1.75 in April 2017**

|  | ∑ Self wt. | ∑ Forced Displacement | Total |  |
|---|---|---|---|---|
| F1 (shear) | 227.22 | 67.68 | 294.89 | k |
| F2 | 89.65 | 18.31 | 107.95 | k |
| F3 | 0.31 | 0.14 | 0.45 | k |
| M1 | 26.75 | −36.77 | −10.02 | k-ft |
| M2 (tors.) | −2793.95 | −1402.60 | −4196.55 | k-ft |
| M3 (bend.) | −4207.21 | −2118.75 | −6325.96 | k-ft |

**Table 5.16: Predicted forces and moments in section S1.75 in May 2022**

|  | ∑ Self wt. | ∑ Forced Displacement | Total |  |
|---|---|---|---|---|
| F1 (shear) | 227.22 | 60.89 | 288.11 | k |
| F2 | 89.65 | 26.87 | 116.52 | k |
| F3 | 0.31 | 0.17 | 0.48 | k |
| M1 | 26.75 | −90.56 | −63.81 | k-ft |
| M2 (tors.) | −2793.95 | −776.90 | −3570.86 | k-ft |
| M3 (bend.) | −4207.21 | −1855.37 | −6062.57 | k-ft |

**Table 5.17: Forces and moments in section S1P1 in April 2017**

|  | Σ Self wt. | Σ Forced Displacement | Total |  |
|---|---|---|---|---|
| F1 (shear) | 330.46 | 95.36 | 425.82 | k |
| F2 | 89.65 | 18.31 | 107.95 | k |
| F3 | −0.08 | −0.38 | −0.46 | k |
| M1 | 21.78 | −126.08 | −104.30 | k-ft |
| M2 (tors.) | −2793.93 | −1402.60 | −4196.53 | k-ft |
| M3 (bend.) | −6287.17 | −2688.34 | −8975.51 | k-ft |

**Table 5.18: Predicted forces and moments in section S1P1 in May 2022**

|  | Σ Self wt. | Σ Forced Displacement | Total |  |
|---|---|---|---|---|
| F1 (shear) | 330.46 | 85.38 | 415.85 | k |
| F2 | 89.65 | 26.87 | 116.52 | k |
| F3 | −0.08 | −0.64 | −0.71 | k |
| M1 | 21.78 | −299.51 | −277.73 | k-ft |
| M2 (tors.) | −2793.93 | −776.90 | −3570.83 | k-ft |
| M3 (bend.) | −6287.17 | −2414.26 | −8701.43 | k-ft |

**Table 5.19: Forces and moments in section S2P1 in April 2017**

|  | Σ Self wt. | Σ Forced Displacement | Total |  |
|---|---|---|---|---|
| F1 (shear) | −483.61 | −162.40 | −646.02 | k |
| F2 (axial) | 89.65 | 18.31 | 107.95 | k |
| F3 | 0.03 | −0.14 | −0.10 | k |
| M1 | 11.41 | −125.23 | −113.82 | k-ft |
| M2 (tors.) | −2863.75 | −4842.58 | −7706.33 | k-ft |
| M3 (bend.) | −5775.68 | −2493.91 | −8269.59 | k-ft |

**Table 5.20: Predicted forces and moments in section S2P1 in May 2022**

|  | Σ Self wt. | Σ Forced Displacement | Total |  |
|---|---|---|---|---|
| F1 (shear) | −483.61 | −200.86 | −684.47 | k |
| F2 (axial) | 89.65 | 26.87 | 116.52 | k |
| F3 | 0.03 | −0.19 | −0.16 | k |
| M1 | 11.41 | −289.09 | −277.68 | k-ft |
| M2 (tors.) | −2863.75 | −8379.24 | −11242.99 | k-ft |
| M3 (bend.) | −5775.68 | −2206.04 | −7981.72 | k-ft |

**Table 5.21: Forces and moments in section S2.25 in April 2017**

| | ∑ Self wt. | ∑ Forced Displacement | Total | |
|---|---|---|---|---|
| F1 (shear) | −365.17 | −140.62 | −505.79 | k |
| F2 (axial) | 89.65 | 18.31 | 107.95 | k |
| F3 | 0.30 | 0.08 | 0.37 | k |
| M1 | 11.22 | −15.66 | −4.44 | k-ft |
| M2 (tors.) | −2863.75 | −4842.58 | −7706.33 | k-ft |
| M3 (bend.) | −716.65 | −789.75 | −1506.40 | k-ft |

**Table 5.22: Predicted forces and moments in section S2.25 in May 2022**

| | ∑ Self wt. | ∑ Forced Displacement | Total | |
|---|---|---|---|---|
| F1 (shear) | −365.17 | −186.41 | −551.58 | k |
| F2 (axial) | 89.65 | 26.87 | 116.52 | k |
| F3 | 0.30 | 0.06 | 0.36 | k |
| M1 | 11.22 | −45.90 | −34.68 | k-ft |
| M2 (tors.) | −2863.75 | −8379.24 | −11242.99 | k-ft |
| M3 (bend.) | −716.65 | 57.92 | −658.73 | k-ft |

**Table 5.23: Forces and moments in section S2.25 in April 2017**

| | ∑ Self wt. | ∑ Forced Displacement | Total | |
|---|---|---|---|---|
| F1 (shear) | −284.67 | −140.58 | −425.25 | k |
| F2 (axial) | 89.65 | 18.31 | 107.95 | k |
| F3 | 0.30 | 0.07 | 0.37 | k |
| M1 | 8.09 | 10.17 | 18.26 | k-ft |
| M2 (tors.) | −2863.75 | −4842.58 | −7706.32 | k-ft |
| M3 (bend.) | 3320.69 | 1025.96 | 4346.65 | k-ft |

**Table 5.24: Predicted forces and moments in section S2.5 in May 2022**

| | ∑ Self wt. | ∑ Forced Displacement | Total | |
|---|---|---|---|---|
| F1 (shear) | −284.67 | −186.38 | −471.05 | k |
| F2 (axial) | 89.65 | 26.87 | 116.52 | k |
| F3 | 0.30 | 0.06 | 0.36 | k |
| M1 | 8.09 | 13.97 | 22.06 | k-ft |
| M2 (tors.) | −2863.75 | −8379.24 | −11242.99 | k-ft |
| M3 (bend.) | 3320.69 | 2463.89 | 5784.57 | k-ft |

**Table 5.25: Forces and moments in section S2.75 in April 2017**

| | ∑ Self wt. | ∑ Forced Displacement | Total | |
|---|---|---|---|---|
| F1 (shear) | −201.37 | −140.57 | −341.94 | k |
| F2 (axial) | 89.65 | 18.31 | 107.95 | k |
| F3 | 0.30 | 0.06 | 0.36 | k |
| M1 | 4.41 | 34.47 | 38.88 | k-ft |
| M2 (tors.) | −2863.74 | −4842.58 | −7706.32 | k-ft |
| M3 (bend.) | 6446.05 | 2841.47 | 9287.52 | k-ft |

**Table 5.26: Predicted forces and moments in section S2.75 in May 2022**

| | ∑ Self wt. | ∑ Forced Displacement | Total | |
|---|---|---|---|---|
| F1 (shear) | −201.37 | −186.38 | −387.75 | k |
| F2 (axial) | 89.65 | 26.87 | 116.52 | k |
| F3 | 0.30 | 0.03 | 0.33 | k |
| M1 | 4.41 | 74.06 | 78.47 | k-ft |
| M2 (tors.) | −2863.74 | −8379.24 | −11242.98 | k-ft |
| M3 (bend.) | 6446.05 | 4868.42 | 11314.47 | k-ft |

**Table 5.27: Forces and moments in section S2P2 in April 2017**

| | ∑ Self wt. | ∑ Forced Displacement | Total | |
|---|---|---|---|---|
| F1 (shear) | −225.83 | −187.14 | −412.97 | k |
| F2 (axial) | 89.65 | 18.31 | 107.95 | k |
| F3 | −0.02 | −0.22 | −0.24 | k |
| M1 | 2.22 | 137.03 | 139.25 | k-ft |
| M2 (tors.) | −2863.74 | −4842.58 | −7706.31 | k-ft |
| M3 (bend.) | 8517.58 | 4584.09 | 13101.66 | k-ft |

**Table 5.28: Predicted forces and moments in section S2P2 in May 2022**

| | ∑ Self wt. | ∑ Forced Displacement | Total | |
|---|---|---|---|---|
| F1 (shear) | −225.83 | −262.20 | −488.03 | k |
| F2 (axial) | 89.65 | 26.87 | 116.52 | k |
| F3 | −0.02 | −0.29 | −0.31 | k |
| M1 | 2.22 | 316.39 | 318.61 | k-ft |
| M2 (tors.) | −2863.74 | −8379.24 | −11242.98 | k-ft |
| M3 (bend.) | 8517.58 | 7162.61 | 15680.18 | k-ft |

**Table 5.29: Forces and moments in section S3P2 in April 2017**

|  | ∑ Self wt. | ∑ Forced Displacement | Total |  |
| --- | --- | --- | --- | --- |
| F1 (shear) | 84.20 | 154.01 | 238.21 | k |
| F2 (axial) | 89.65 | 18.31 | 107.95 | k |
| F3 | −0.05 | −0.36 | −0.41 | k |
| M1 | −10.70 | 130.65 | 119.94 | k-ft |
| M2 (tors.) | −2864.13 | −1608.62 | −4472.75 | k-ft |
| M3 (bend.) | 8685.69 | 4545.95 | 13231.64 | k-ft |

**Table 5.30: Predicted forces and moments in section S3P2 in May 2022**

|  | ∑ Self wt. | ∑ Forced Displacement | Total |  |
| --- | --- | --- | --- | --- |
| F1 (shear) | 84.20 | 276.34 | 360.54 | k |
| F2 (axial) | 89.65 | 26.87 | 116.52 | k |
| F3 | −0.05 | −0.61 | −0.66 | k |
| M1 | −10.70 | 314.98 | 304.28 | k-ft |
| M2 (tors.) | −2864.13 | −795.34 | −3659.48 | k-ft |
| M3 (bend.) | 8685.69 | 7146.26 | 15831.94 | k-ft |

**Table 5.31: Forces and moments in section S3.25 in April 2017**

|  | ∑ Self wt. | ∑ Forced Displacement | Total |  |
| --- | --- | --- | --- | --- |
| F1 (shear) | 52.56 | 104.48 | 157.05 | k |
| F2 (axial) | 89.65 | 18.31 | 107.95 | k |
| F3 | 0.31 | 0.11 | 0.42 | k |
| M1 | −19.69 | 16.07 | −3.62 | k-ft |
| M2 (tors.) | −2864.17 | −1608.62 | −4472.79 | k-ft |
| M3 (bend.) | 8448.37 | 3259.75 | 11708.13 | k-ft |

**Table 5.32: Predicted forces and moments in section S3.25 in May 2022**

|  | ∑ Self wt. | ∑ Forced Displacement | Total |  |
| --- | --- | --- | --- | --- |
| F1 (shear) | 52.56 | 201.70 | 254.26 | k |
| F2 (axial) | 89.65 | 26.87 | 116.52 | k |
| F3 | 0.31 | 0.14 | 0.45 | k |
| M1 | −19.69 | 56.83 | 37.14 | k-ft |
| M2 (tors.) | −2864.17 | −795.34 | −3659.51 | k-ft |
| M3 (bend.) | 8448.37 | 4644.44 | 13092.81 | k-ft |

**Table 5.33: Forces and moments in section S3.5 in April 2017**

|  | ∑ Self wt. | ∑ Forced Displacement | Total |  |
|---|---|---|---|---|
| F1 (shear) | 133.05 | 104.67 | 237.72 | k |
| F2 (axial) | 89.65 | 18.31 | 107.95 | k |
| F3 | 0.34 | 0.12 | 0.45 | k |
| M1 | −21.72 | −13.59 | −35.31 | k-ft |
| M2 (tors.) | −2864.19 | −1608.63 | −4472.82 | k-ft |
| M3 (bend.) | 7257.51 | 1903.38 | 9160.89 | k-ft |

**Table 5.34: Predicted forces and moments in section S3.5 in May 2022**

|  | ∑ Self wt. | ∑ Forced Displacement | Total |  |
|---|---|---|---|---|
| F1 (shear) | 133.05 | 202.08 | 335.13 | k |
| F2 (axial) | 89.65 | 26.87 | 116.52 | k |
| F3 | 0.34 | 0.10 | 0.44 | k |
| M1 | −21.72 | −10.93 | −32.65 | k-ft |
| M2 (tors.) | −2864.19 | −795.35 | −3659.54 | k-ft |
| M3 (bend.) | 7257.51 | 2043.69 | 9301.20 | k-ft |

**Table 5.35: Forces and moments in section S3.75 in April 2017**

|  | ∑ Self wt. | ∑ Forced Displacement | Total |  |
|---|---|---|---|---|
| F1 (shear) | 214.12 | 104.93 | 319.05 | k |
| F2 (axial) | 89.65 | 18.31 | 107.95 | k |
| F3 | 0.36 | 0.16 | 0.52 | k |
| M1 | 12.05 | 37.10 | 49.15 | k-ft |
| M2 (tors.) | −2864.22 | −1608.63 | −4472.85 | k-ft |
| M3 (bend.) | 5064.11 | 546.73 | 5610.84 | k-ft |

**Table 5.36: Predicted forces and moments in section S3.75 in May 2022**

|  | ∑ Self wt. | ∑ Forced Displacement | Total |  |
|---|---|---|---|---|
| F1 (shear) | 214.12 | 202.55 | 416.67 | k |
| F2 (axial) | 89.65 | 26.87 | 116.52 | k |
| F3 | 0.36 | 0.14 | 0.50 | k |
| M1 | 12.05 | 53.75 | 65.80 | k-ft |
| M2 (tors.) | −2864.22 | −795.35 | −3659.56 | k-ft |
| M3 (bend.) | 5064.11 | −678.42 | 4385.69 | k-ft |

**Table 5.37: Forces and moments in section S3P3 in April 2017**

|  | ∑ Self wt. | ∑ Forced Displacement | Total |  |
|---|---|---|---|---|
| F1 (shear) | 241.20 | 106.36 | 347.57 | k |
| F2 (axial) | 89.65 | 18.31 | 107.95 | k |
| F3 | 0.40 | 0.44 | 0.84 | k |
| M1 | 145.36 | 243.28 | 388.64 | k-ft |
| M2 (tors.) | −2864.24 | −1608.64 | −4472.88 | k-ft |
| M3 (bend.) | 2054.80 | −720.35 | 1334.45 | k-ft |

**Table 5.38: Predicted forces and moments in section S3P3 in May 2022**

|  | ∑ Self wt. | ∑ Forced Displacement | Total |  |
|---|---|---|---|---|
| F1 (shear) | 241.20 | 226.39 | 467.59 | k |
| F2 (axial) | 89.65 | 26.87 | 116.52 | k |
| F3 | 0.40 | 0.59 | 0.99 | k |
| M1 | 145.36 | 302.37 | 447.73 | k-ft |
| M2 (tors.) | −2864.24 | −795.35 | −3659.59 | k-ft |
| M3 (bend.) | 2054.80 | −3021.24 | −966.45 | k-ft |

**Table 5.39: Forces and moments in section S4P3 in April 2017**

|  | ∑ Self wt. | ∑ Forced Displacement | Total |  |
|---|---|---|---|---|
| F1 (shear) | −39.39 | −28.60 | −67.99 | k |
| F2 (axial) | 89.65 | 18.31 | 107.95 | k |
| F3 | 0.19 | 0.28 | 0.47 | k |
| M1 | 172.45 | 296.03 | 468.48 | k-ft |
| M2 (tors.) | 1104.78 | 4412.87 | 5517.65 | k-ft |
| M3 (bend.) | 1767.41 | −823.02 | 944.39 | k-ft |

**Table 5.40: Predicted forces and moments in section S4P3 in May 2022**

|  | ∑ Self wt. | ∑ Forced Displacement | Total |  |
|---|---|---|---|---|
| F1 (shear) | −39.39 | −115.42 | −154.81 | k |
| F2 (axial) | 89.65 | 26.87 | 116.52 | k |
| F3 | 0.19 | 0.45 | 0.64 | k |
| M1 | 172.45 | 371.57 | 544.02 | k-ft |
| M2 (tors.) | 1104.78 | 6517.64 | 7622.42 | k-ft |
| M3 (bend.) | 1767.41 | −3239.47 | −1472.06 | k-ft |

**Table 5.41: Forces and moments in section S4.25 in April 2017**

|            | ∑ Self wt. | ∑ Forced Displacement | Total    |      |
|------------|-----------|----------------------|----------|------|
| F1 (shear) | −18.67    | −20.51               | −39.18   | k    |
| F2 (axial) | 89.65     | 18.31                | 107.95   | k    |
| F3         | 0.44      | 0.25                 | 0.69     | k    |
| M1         | 69.60     | 151.33               | 220.93   | k-ft |
| M2 (tors.) | 1104.75   | 4412.86              | 5517.61  | k-ft |
| M3 (bend.) | 2096.82   | −660.47              | 1436.35  | k-ft |


**Table 5.42: Predicted forces and moments at section S4.25 in May 2022**

|            | ∑ Self wt. | ∑ Forced Displacement | Total     |      |
|------------|-----------|----------------------|-----------|------|
| F1 (shear) | −18.67    | −81.96               | −100.63   | k    |
| F2 (axial) | 89.65     | 26.87                | 116.52    | k    |
| F3         | 0.44      | 0.23                 | 0.67      | k    |
| M1         | 69.60     | 184.97               | 254.57    | k-ft |
| M2 (tors.) | 1104.75   | 6517.63              | 7622.38   | k-ft |
| M3 (bend.) | 2096.82   | −2482.12             | −385.30   | k-ft |


**Table 5.43: Forces and moments in section S4.5 in April 2017**

|            | ∑ Self wt. | ∑ Forced Displacement | Total    |      |
|------------|-----------|----------------------|----------|------|
| F1 (shear) | 41.88     | −20.57               | 21.31    | k    |
| F2 (axial) | 89.65     | 18.31                | 107.95   | k    |
| F3         | 0.36      | 0.11                 | 0.47     | k    |
| M1         | 19.87     | 70.33                | 90.19    | k-ft |
| M2 (tors.) | 1104.71   | 4412.85              | 5517.56  | k-ft |
| M3 (bend.) | 1964.40   | −457.91              | 1506.49  | k-ft |


**Table 5.44: Predicted forces and moments at section S4.5 in May 2022**

|            | ∑ Self wt. | ∑ Forced Displacement | Total    |      |
|------------|-----------|----------------------|----------|------|
| F1 (shear) | 41.88     | −82.18               | −40.31   | k    |
| F2 (axial) | 89.65     | 26.87                | 116.52   | k    |
| F3         | 0.36      | 0.05                 | 0.41     | k    |
| M1         | 19.87     | 96.79                | 116.66   | k-ft |
| M2 (tors.) | 1104.71   | 6517.63              | 7622.34  | k-ft |
| M3 (bend.) | 1964.40   | −1703.70             | 260.70   | k-ft |

**Table 5.45: Forces and moments in section S4.75 in April 2017**

|  | ∑ Self wt. | ∑ Forced Displacement | Total |  |
|---|---|---|---|---|
| F1 (shear) | 102.54 | −20.63 | 81.91 | k |
| F2 (axial) | 89.65 | 18.31 | 107.95 | k |
| F3 | 0.30 | −0.01 | 0.29 | k |
| M1 | 1.19 | 26.45 | 27.63 | k-ft |
| M2 (tors.) | 1104.67 | 4412.85 | 5517.52 | k-ft |
| M3 (bend.) | 1266.61 | −246.67 | 1019.94 | k-ft |

**Table 5.46: Predicted forces and moments at section S4.75 in May 2022**

|  | ∑ Self wt. | ∑ Forced Displacement | Total |  |
|---|---|---|---|---|
| F1 (shear) | 102.54 | −82.40 | 20.15 | k |
| F2 (axial) | 89.65 | 26.87 | 116.52 | k |
| F3 | 0.30 | −0.08 | 0.22 | k |
| M1 | 1.19 | 45.03 | 46.22 | k-ft |
| M2 (tors.) | 1104.67 | 6517.63 | 7622.30 | k-ft |
| M3 (bend.) | 1266.61 | −972.55 | 294.06 | k-ft |

**Table 5.47: Forces and moments in section S4A2 in April 2017**

|  | ∑ Self wt. | ∑ Forced Displacement | Total |  |
|---|---|---|---|---|
| F1 (shear) | 152.49 | −18.98 | 133.51 | k |
| F2 (axial) | 89.65 | 18.31 | 107.95 | k |
| F3 | 1.37 | 4.39 | 5.76 | k |
| M1 | 42.79 | 170.25 | 213.04 | k-ft |
| M2 (tors.) | 1104.63 | 4412.84 | 5517.47 | k-ft |
| M3 (bend.) | 37.06 | −74.20 | −37.14 | k-ft |

**Table 5.48: Predicted forces and moments at section S4A2 in May 2022**

|  | ∑ Self wt. | ∑ Forced Displacement | Total |  |
|---|---|---|---|---|
| F1 (shear) | 152.49 | −82.87 | 69.62 | k |
| F2 (axial) | 89.65 | 26.87 | 116.52 | k |
| F3 | 1.37 | −1.31 | 0.06 | k |
| M1 | 42.79 | 51.96 | 94.75 | k-ft |
| M2 (tors.) | 1104.63 | 6517.63 | 7622.26 | k-ft |
| M3 (bend.) | 37.06 | −263.20 | −226.13 | k-ft |

### 5.2.1.2 Shear-Torsion Interaction Diagrams

Combined shear, torsion, and bending capacity for each section is determined using the corresponding AASHTO-LRFD 2014 equations. Equation 5.8, Equation 5.9A, and Equation 5.10 are used to plot shear-torsion (T-V) relations for a given bending moment at a specific section. To do so, Equation 5.8 and Equation 5.10 relates shear and torsion strengths to transverse and longitudinal reinforcement respectively while Equation 5.9A gives an upper bound for the nominal shear strength of a section. For a given bending moment and shear force, corresponding torsion was determined using the Excel Goal Seek function for each of the equations. Minimum torsion value was selected to plot T-V curves.

In the following, T-V interaction curves for both un-strengthened and strengthened sections are given for each section.

For Sections S2.75, S2P2, S3P2, S3.25, and S3.75 combined shear and torsion capacity is assumed zero for the un-strengthened case. This is because the obtained torsion value did not satisfy after substituting it back in Equation 5.10. In addition, increasing transverse and longitudinal reinforcement lead to lower torsion values while greater torsion was obtained for lower values of the reinforcement. This instability in the behavior shows that the section has already reached its maximum capacity due to the current loading and settlement conditions. Due to settlement, positive moment was observed in some sections near piers and negative moment at the mid span. Positive moment is defined here as a moment producing tensile stress at the bottom and compressive stress at the top of the section. Because the box-girder was originally designed for gravity loads rather than settlement and gravity loads combined, it does not have enough negative reinforcement at mid span and positive reinforcement near the support/pier. These sections become critical under continuous settlements of the piers and have already reached their maximum capacity. Different options were investigated to strengthen the box girder to resist the loads induced by the settlement depending on the efficiency and applicability of the strengthening method. These include the application of CFRP sheets along the longitudinal axis at the bottom, U-Wraps along the sides, and No. 8 CFRP bars at the top. Table 5.51 through Table 5.54 give strengthening details for all four spans. S2.75 and S2P2 were found to be the most critical sections along the box girder. For S2.75 the proposed CFRP sheets and U-Wraps are barely enough for the

predicted loads till May 2022. However, four layers of CFRP sheets applied longitudinally at the bottom are required at S2P2 for the predicted loads in May 2022. This is one layer more than the proposed amount for April 2017. In addition, to avoid cover delamination or deboning failure, CFRP anchors will be needed.

U-Wraps will be applied at the bottom and two sides of the box girder to increase shear strength as shown in Figure 5.95. However, since the induced shear stress due to torsion acts around the perimeter of the section, a brief calculation is presented below to determine shear capacity of the top slab. The effect on the box girder is illustrated in Figure 5.40.

As stated above, Sections S2.75 and S2P2 are the most critical sections along the box girder. In addition to the large bending moment (Table 5.25 and Table 5.27), a torsion of 11,243 k-ft is also present at each section which produces considerably high shear stress around the section. For a box section, shear stress due to torsion can be approximated using the following equation.
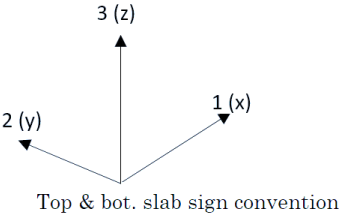
$$\tau = \frac{T}{2A_o t} = \frac{11,243 \; k-ft}{2*(3.46ft*23.62 \; ft)*(0.58ft)} = 117.92 \; ksf \; or \; 818.87 \; psi$$

The corresponding shear force equals $\tau * top \; slab \; thick.* width = 117.92 \; ksf * 0.58ft * 24ft = 1650 \; k$
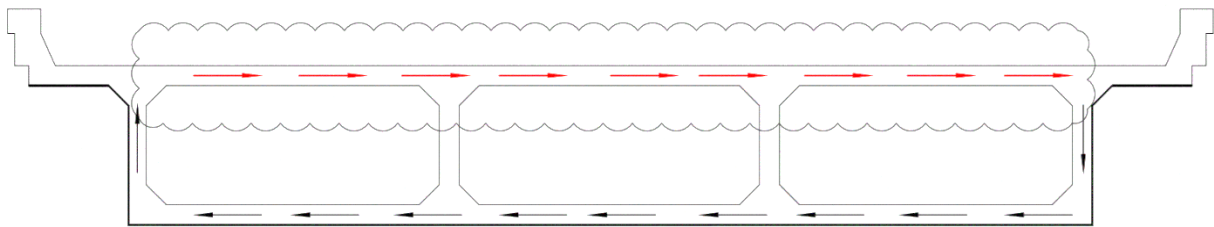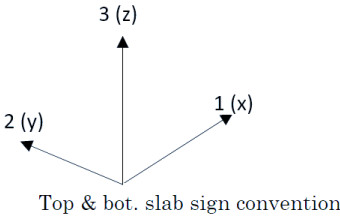


**Figure 5.40: Box girder section under torsional shear forces and top slab clouded**

**Table 5.49: Induced forces and moments due to self-weight from RISA 3D**

| | |
|---|---|
| F1 | −409.09 k |
| F2 | 2,180.47 k |
| F3 | 2.69 k |
| M1 | −38.13 k-ft |
| M2 | −15.94 k-ft |
| M3 | −9.52 k-ft |

3 (z)

1 (x)

2 (y)

Top & bot. slab sign convention

**Table 5.50: Induced forces and moments due to imposed displacement of May 2022 from RISA 3D**

| | |
|---|---|
| F1 | −1,156.67 k |
| F2 | 1,645.92 k |
| F3 | 2.14 k |
| M1 | −28.45 k-ft |
| M2 | −48.75 k-ft |
| M3 | 498.20 k-ft |

3 (z)

1 (x)

2 (y)

Top & bot. slab sign convention

Axial load (F2) = 2,180.47+1,645.95=3,826.39 k

[1]Horizontal shear (F1) = -409.09 -1,156.67 = -1,565.76 k

Bending moment (M3) = -9.52+498.2 = 488.68 k-ft.

The AASHTO LRFD procedure for computing the effects of combined loading on the shear capacity of the top slab, as adapted from the Simplified Modified Compression Field Theory (SMCFT) may be summarized in the example calculations shown below. The actual equations,

---

[1] The horizontal shear force calculated from torsion matches that of RISA 3D value (1650 k) for the top slab with an error of 5.15%. The error is due to the assumptions the equation $\tau = \dfrac{T}{2A_o t}$ is based on.

taken directly from the AASHTO LRFD Specifications, are listed after the given calculations with references to the AASHTO equation numbers provided.

| | | |
|---|---|---|
| Mn | 488.68 | k-ft |
| Dv | 24 | ft |
| Nn | -3826.39 | k (comp. to be taken as negative) |
| Vn | -1565.76 | k |
| Es | 29000 | ksi |
| f'c | 4000 | psi |
| Ec | 3605 | ksi (based on f'c =4,000 psi) |
| Bv or t | 7 | in |
| Ac | 672 | in² |
| # bar | 5 | |
| Total no. bar | 32 | |
| Total bar area | 9.82 | in² |

Equation 5.4 is used to calculate strain in the longitudinal reinforcement at the top slab. Since the strain is negative, it is assumed zero according to Section 5.8.3.4.2 of AASHTO LRFD Bridge Design Specification.

| | | |
|---|---|---|
| Eps_s | -0.0011 | |
| Assumed Eps_s zero according to Section 5.8.3.4.2 of AASHTO-LRFD | 0 | |
| Sxe | 5.25 | |
| Betha | 5.53 | (AASHTO-LRFD 5.8.3.4.2-2) |
| Theta | 29.00 deg | (AASHTO-LRFD 5.8.3.4.2-3) |
| Vc | 704.86 k | (AASHTO-LRFD 5.8.3.3-3) |
| Av | 0.88 in² | |
| Fy | 60 ksi | |
| S | 12 in | |
| Vs | 2295.37 k | (AASHTO-LRFD 5.8.3.3-4) |
| Vn=Vc+Vs | 3000.24 k | |
| Vn_limit | 2016 k | Controls! |

The above calculations show that the top slab has enough shear strength as the applied shear force (1,565.76 k) is smaller than the Vn_limit.

List of AASHTO equations used in the sample calculations above:

$$\beta = \frac{4.8}{(1 + 750 * \varepsilon_s)}$$

**Equation 5.1**
(AASHTO-LRFD 5.8.3.4.2-1)

If Av < Av,min

$$\beta = \frac{4.8}{(1 + 750 * \varepsilon_s)} * \frac{51}{(39 + s_{xe})}$$

**Equation 5.2**
(AASHTO-LRFD 5.8.3.4.2-2)

$$s_{xe} = s_x \frac{1.38}{a_g + 0.63}$$

(AASHTO-LRFD 5.8.3.4.2-5)

$$\theta = 29 + 3500 * \varepsilon_s$$

**Equation 5.3**
(AASHTO-LRFD 5.8.3.4.2-3)

$$\varepsilon_s = \frac{\left(\frac{|Mu|}{d_v} + 0.5N_u + |V_u|\right)}{(E_s A_s)}$$

**Equation 5.4**
(AASHTO-LRFD 5.8.3.4.2-4)

$$V_c = 0.0316\beta\sqrt{f'_c}b_v d_v$$

**Equation 5.5**
(AASHTO-LRFD 5.8.3.3-3)

$$V_s = \frac{A_v f_y d_v(\cot\theta + \cot\alpha) * \sin\alpha}{s}$$

**Equation 5.6**
(AASHTO-LRFD 5.8.3.3-4)

$$V_n = V_c + V_s$$

**Equation 5.7**
(AASHTO-LRFD 5.8.3.3-1)

$$\frac{A_t f_y}{s} = \frac{T_n}{4A_o \cot\theta} + \frac{V_s}{2d_v \cot\theta}$$

**Equation 5.8**
(COMBINED AASHTO-LRFD
[5.8.3.6.2-1] & [5.8.3.3.-4])

$$\frac{A_t f_y}{s} + \frac{A_f f_{fe}}{s_f} = \frac{T_n}{4A_o \cot\theta} + \frac{V_s}{2d_v \cot\theta}$$

**Equation 5.8A**

$$V_{n,limit} = 0.25f'_c b_v d_v$$

**Equation 5.9**
(AASHTO-LRFD 5.8.3.3-2)

$$0.25f'_c \geq \frac{\left|V_n + \frac{T_n d_s}{2A_o}\right|}{b_v d_v}$$

**Equation 5.9A**
(Combined AASHTO-LRFD
[5.8.3.3-1] & [5.8.2.1-7])

**Equation 5.10**
(AASHTO-LRFD 5.8.3.6.3-1)

$$A_s f_y - \left[ \frac{M_u}{\phi d_v} + \frac{0.5 N_u}{\phi} + \cot\theta \right.$$

$$\left. * \sqrt{\left( \left| \frac{V_u}{\phi} \right| - 0.5 V_s \right)^2 + \left( \frac{0.45 P_h T_u}{2 A_o \phi} \right)^2} \right] = 0$$

**Equation 5.10A**

$$A_s f_y + 0.7 A_f f_{fu}$$

$$- \left[ \frac{M_u}{\phi d_v} + \frac{0.5 N_u}{\phi} + \cot\theta \right.$$

$$\left. * \sqrt{\left( \left| \frac{V_u}{\phi} \right| - 0.5 V_s \right)^2 + \left( \frac{0.45 P_h T_u}{2 A_o \phi} \right)^2} \right] = 0$$

**Table 5.51: Span 1 strengthening details**

| | Details / stations | S1A1 | S1.25 | S1.5 | S1.75 | S1P1 |
|---|---|---|---|---|---|---|
| **CFRP BAR** | Location | - | - | top | - | - |
| | CFRP bar size | - | - | #8 | - | - |
| | No. of bars | - | - | 28.00 | - | - |
| | $f_{fu}$ (ksi) | - | - | 80.00 | - | - |
| | $0.7A_f*f_{fu}$ (kip) | - | - | 1,231.50 | - | - |
| | | | | | | |
| **U-WRAPS** | $\varepsilon_{fe}$ | - | - | 0.004 | - | - |
| | $E_f$ (ksi) | - | - | 10,700.00 | - | - |
| | $t_f$ (in) | - | - | 0.04 | - | - |
| | $S_f$ (in) | - | - | 24.00 | - | - |
| | CFRP sheet width (in) | - | - | 24.00 | - | - |
| | | | | | | |
| **CFRP Longitudinal Sheets** | Location | - | - | - | - | - |
| | $t_f$ (in) | - | - | - | - | - |
| | No. of layer s | - | - | - | - | - |
| | $b_f$ (in) | - | - | - | - | - |
| | $E_f$ (ksi) | - | - | - | - | - |
| | $f_{fu}$ (ksi) | - | - | - | - | - |
| | $0.7A_f*f_{fu}$ (kip) | - | - | - | - | - |

Note: See Figure 5.36 for section location

**Table 5.52: Span 2 strengthening details**

| | Details / stations | S2P1 | S2.25 | S2.50 | S2.75 * | S2P2 ** |
|---|---|---|---|---|---|---|
| **CFRP BAR** | Location | top | top | - | - | - |
| | CFRP bar size | #8 | #8 | - | - | - |
| | No. of bars | 28.00 | 28.00 | - | - | - |
| | $f_{fu}$ (ksi) | 80.00 | 80.00 | - | - | - |
| | $0.7A_f*f_{fu}$ (kip) | 1,231.50 | 1,231.50 | - | - | - |
| | | | | | | |
| **U-WRAPS** | $\varepsilon_{fe}$ | - | - | 0.004 | 0.004 | 0.004 |
| | $E_f$ (ksi) | - | - | 10,700.00 | 10,700.00 | 10,700.00 |
| | $t_f$ (in) | - | - | 0.04 | 0.04 | 0.04 |
| | $S_f$ (in) | - | - | 24 | 24 | 24 |
| | CFRP sheet width (in) | - | - | 24.00 | 24.00 | 24.00 |
| | | | | | | |
| **CFRP Longitudinal Sheets** | Location | - | - | bottom | bottom | bottom |
| | $t_f$ (in) | - | - | 0.04 | 0.04 | 0.04 |
| | No. of layers | - | - | 2 | 3 | 4 |
| | $b_f$ (in) | - | - | 296 | 296 | 296 |
| | $E_f$ (ksi) | - | - | 10,700.00 | 10,700.00 | 10,700.00 |
| | $f_{fu}$ (ksi) | - | - | 150.00 | 150.00 | 150.00 |
| | $0.7A_f*f_{fu}$ (kip) | - | - | 2,822.40 | 4,233.60 | 4,233.60 |

*S2.75 would reach its maximum capacity by May 2022.

**This is the most critical section along the box girder. At least 4 layers of longitudinal sheets are required to strengthen the section to sustain the predicted settlement up to May 2022.

**Table 5.53: Span 3 strengthening details**

| | Details / stations | S3P2 | S3.25 | S3.50 | S3.75 | S3P3 |
|---|---|---|---|---|---|---|
| **CFRP BAR** | Location | - | - | - | - | - |
| | CFRP bar size | - | - | - | - | - |
| | No. of bars | - | - | - | - | - |
| | $f_{fu}$ (ksi) | - | - | - | - | - |
| | $0.7A_f*f_{fu}$ (kip) | - | - | - | - | - |
| | | | | | | |
| **U-WRAPS** | $\varepsilon_{fe}$ | 0.004 | 0.004 | 0.004 | 0.004 | - |
| | $E_f$ (ksi) | 10,700.00 | 10,700.00 | 10,700.00 | 10,700.00 | - |
| | $t_f$ (in) | 0.04 | 0.04 | 0.04 | 0.04 | - |
| | $S_f$ (in) | 24.00 | 24.00 | 24.00 | 24.00 | - |
| | CFRP sheet width (in) | 24.00 | 24.00 | 24.00 | 24.00 | - |
| | | | | | | |
| **CFRP Longitudinal Sheets** | Location | bottom | bottom | bottom | bottom | bottom |
| | $t_f$ (in) | 0.04 | 0.04 | 0.04 | 0.04 | 0.04 |
| | No. of layers | 4 | 3 | 2 | 2 | 1 |
| | $b_f$ (in) | 296 | 296 | 296 | 296 | 296 |
| | $E_f$ (ksi) | 10,700.00 | 10,700.00 | 10,700.00 | 10,700.00 | 10,700.00 |
| | $f_{fu}$ (ksi) | 150.00 | 150.00 | 150.00 | 150.00 | 150.00 |
| | $0.7A_f*f_{fu}$ (kip) | 4,233.60 | 2,822.40 | 1,411.20 | 1,411.20 | 1,411.20 |

**Table 5.54: Span 4 strengthening details**

| | Details / stations | S4P3 | S4.25 | S4.50 | S4.75 | S4A2 |
|---|---|---|---|---|---|---|
| **CFRP BAR** | Location | - | - | - | - | top |
| | CFRP bar size | - | - | - | - | #8 |
| | No. of bars | - | - | - | - | 14.00 |
| | $f_{fu}$ (ksi) | - | - | - | - | 80.00 |
| | $0.7A_f*f_{fu}$ (kip) | - | - | - | - | 615.75 |
| | | | | | | |
| **U-WRAPS** | $\varepsilon_{fe}$ | - | - | 0.004 | - | - |
| | $E_f$ (ksi) | - | - | 10,700.00 | - | - |
| | $t_f$ (in) | - | - | 0.04 | - | - |
| | $S_f$ (in) | - | - | 24.00 | - | - |
| | CFRP sheet width (in) | - | - | 24.00 | - | - |
| | | | | | | |
| **CFRP Longitudinal Sheets** | Location | bottom | bottom | bottom | bottom | - |
| | $t_f$ (in) | 0.04 | 0.04 | 0.04 | 0.04 | - |
| | No. of layers | 1.00 | 1.00 | 1.00 | 1.00 | - |
| | $b_f$ (in) | 296 | 296 | 296 | 296 | - |
| | $E_f$ (ksi) | 10,700.00 | 10,700.00 | 10,700.00 | 10,700.00 | - |
| | $f_{fu}$ (ksi) | 150.00 | 150.00 | 150.00 | 150.00 | - |
| | $0.7A_f*f_{fu}$ (kip) | 1,411.20 | 1,411.20 | 1,411.20 | 1,411.20 | - |

In the following, interaction curves for both un-strengthened and strengthened sections are provided. Equation 5.8A and Equation 5.10A are used to calculate the strengthened section capacity. Section S1A1, shown in Figure 5.36, has sufficient strength for April 2017 and predicted settlement in May 2022. Therefore, no T-V interaction curve for strengthened section is added.
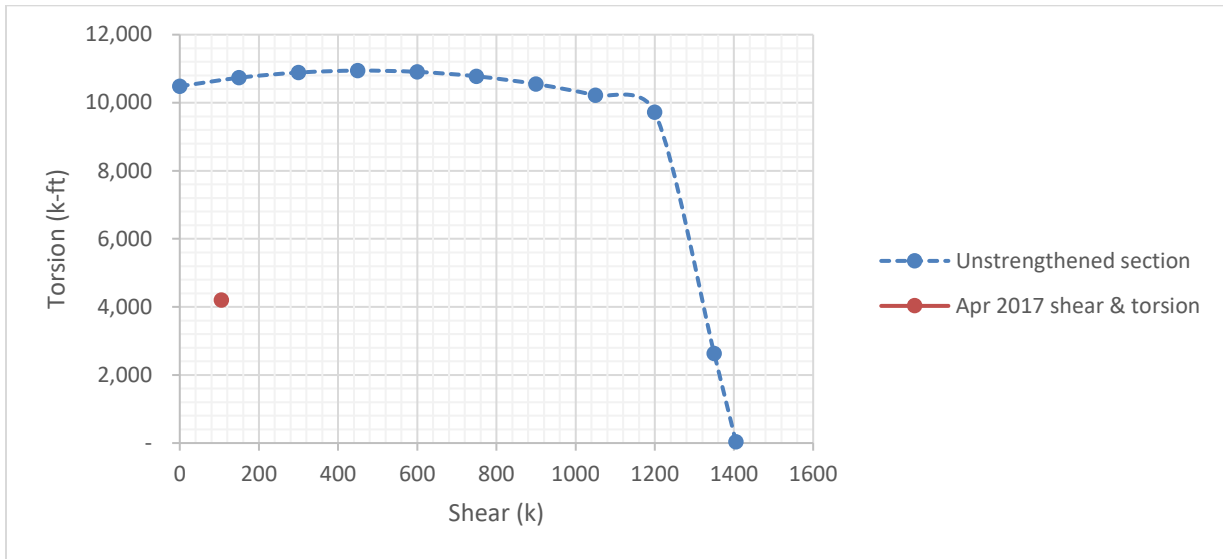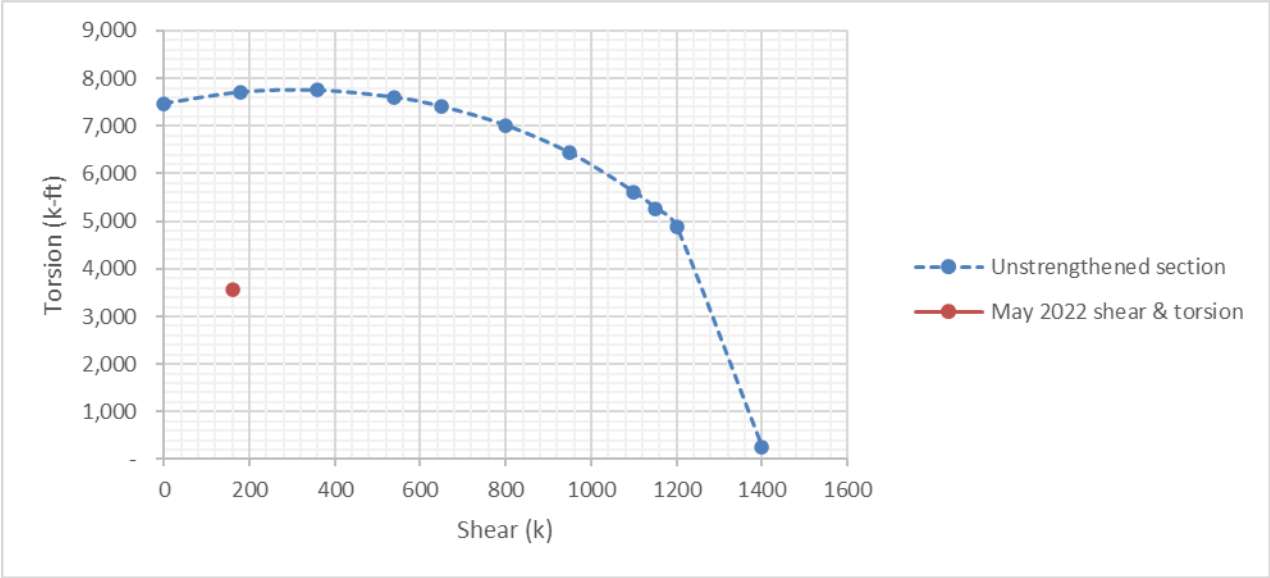


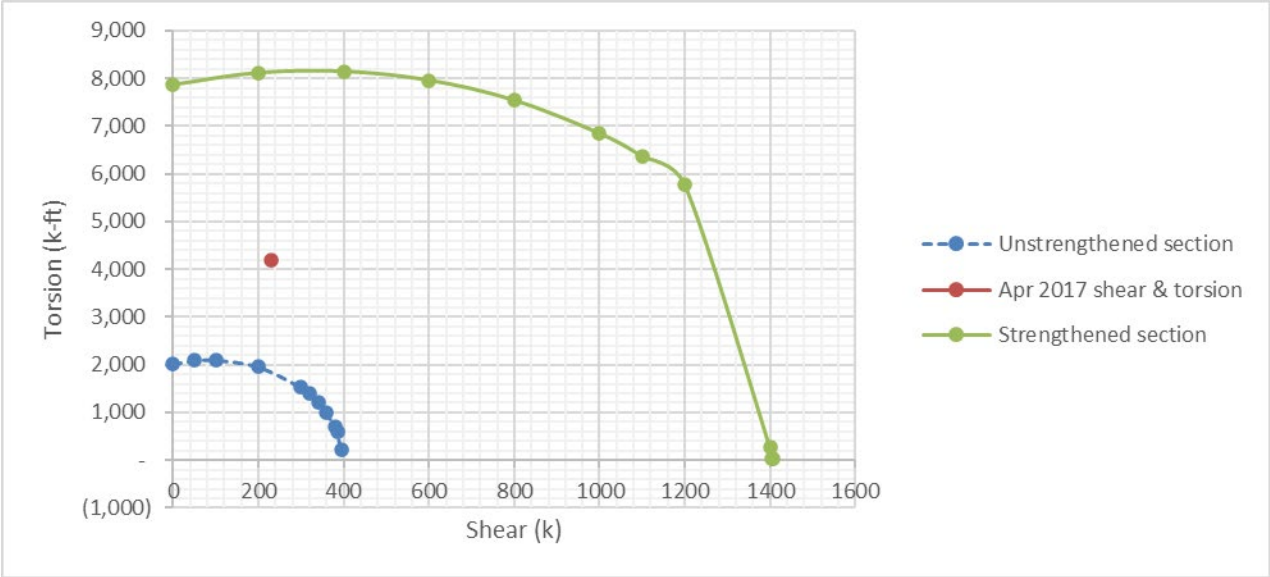**Figure 5.41: T-V interaction diagram for S1A1 based on April 2017 data**
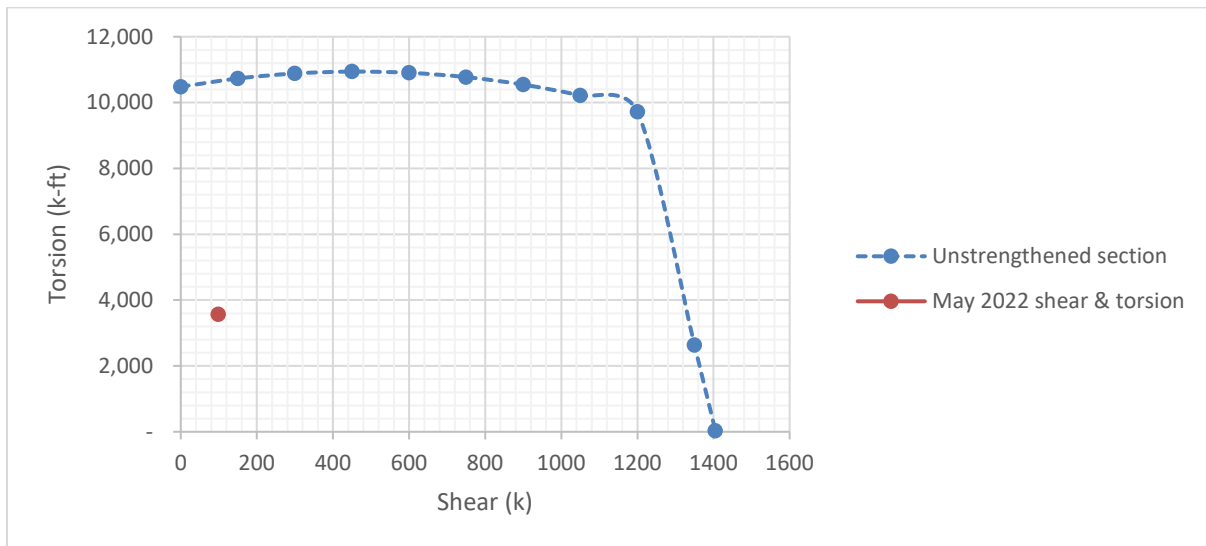


**Figure 5.42: Predicted T-V interaction diagram for S1A1 in May 2022**
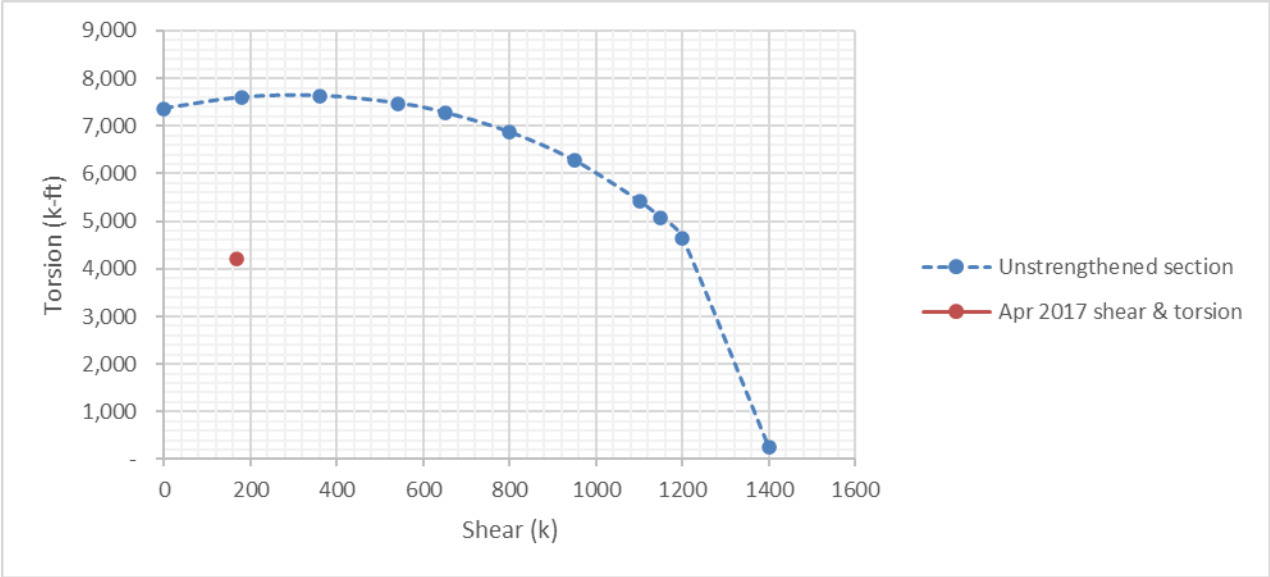
**Figure 5.43: T-V interaction diagram for S1.25 based on April 2017 data**



**Figure 5.44: Predicted T-V interaction diagram for S1.25 in May 2022**

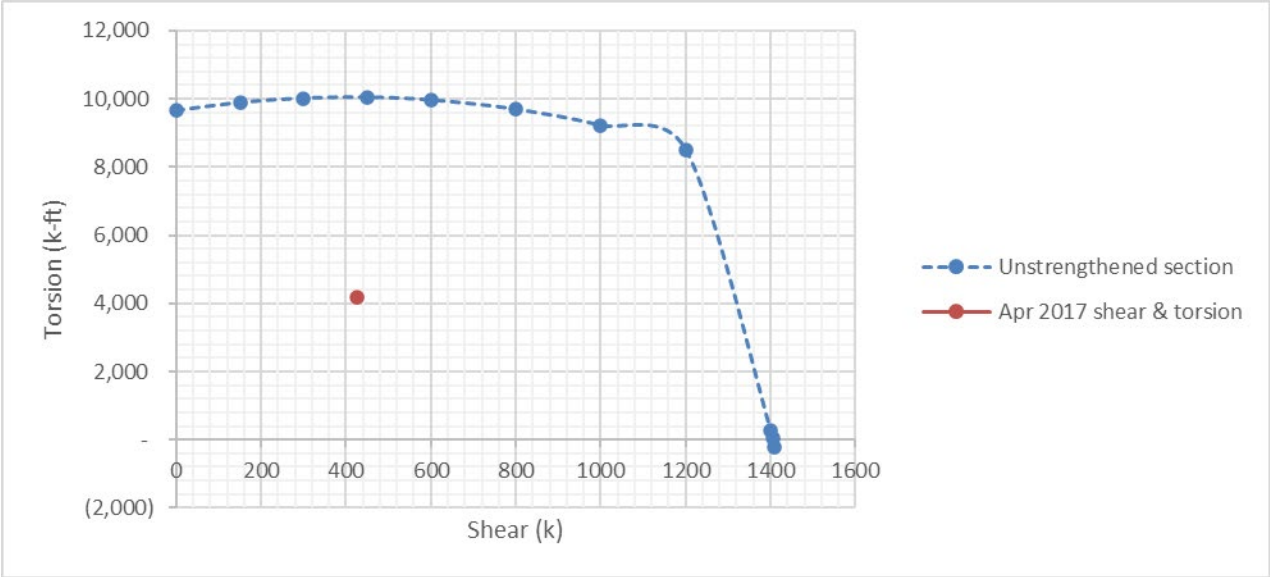**Figure 5.45: T-V interaction diagram for S1.50 based on April 2017 data**
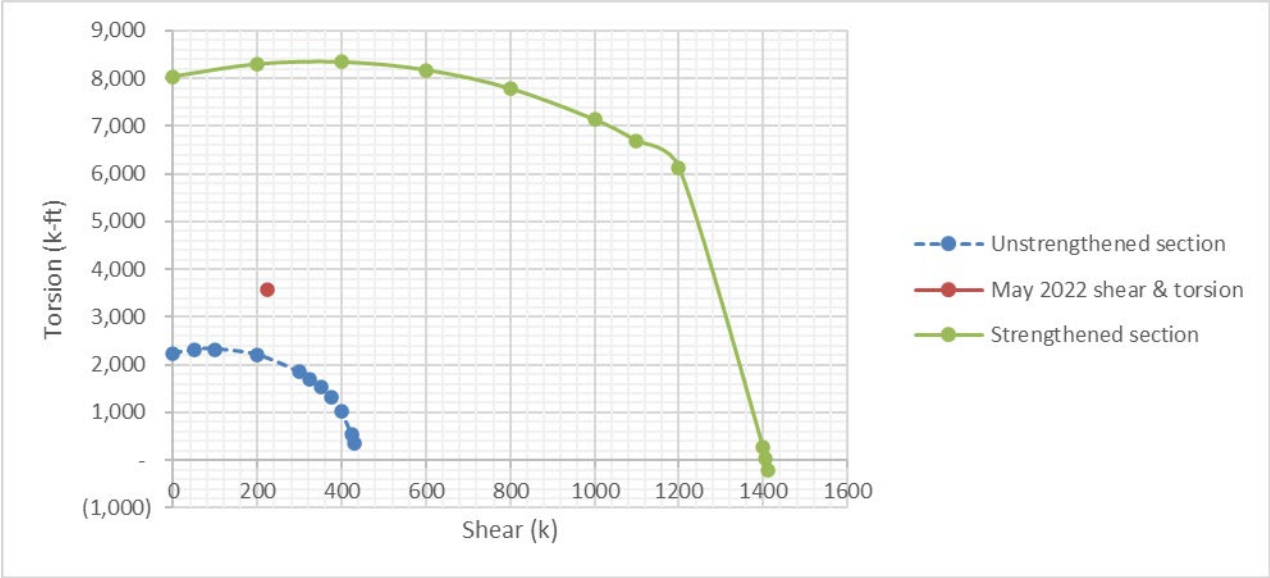


**Figure 5.46: Predicted T-V interaction diagram for S1.50 in May 2022**
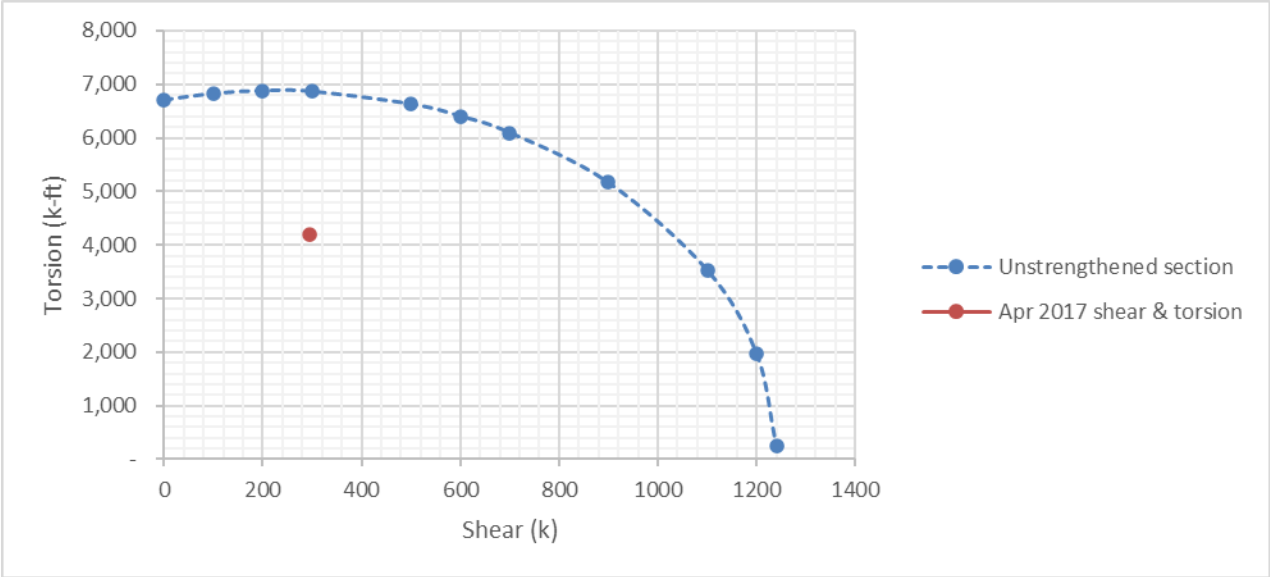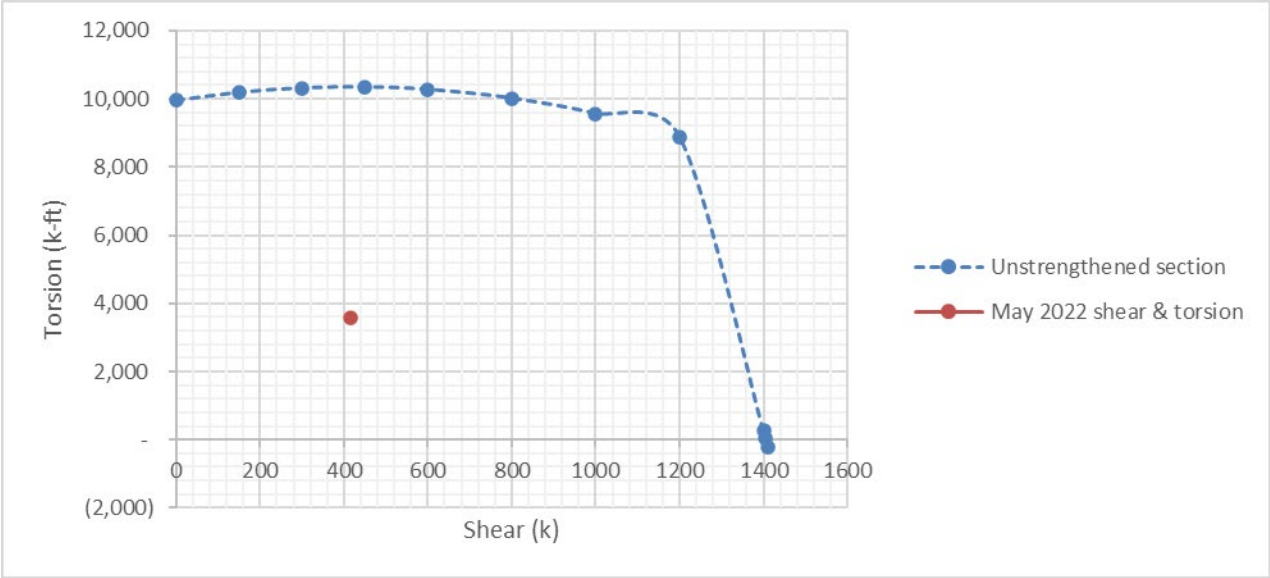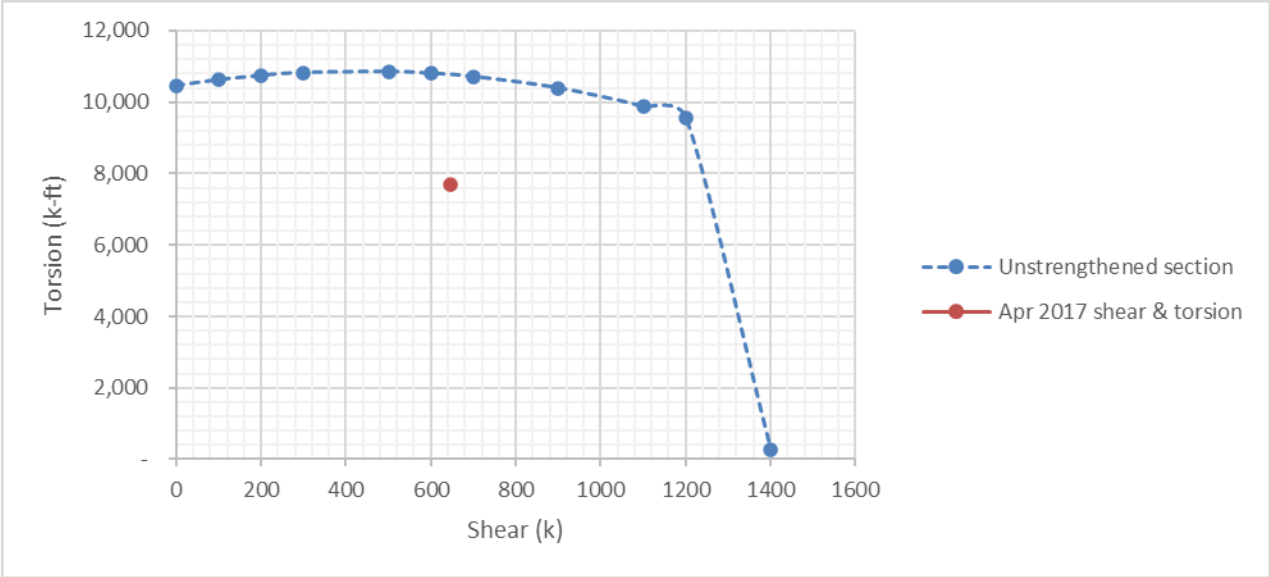
**Figure 5.47: T-V interaction diagram for S1.75 based on April 2017 data**
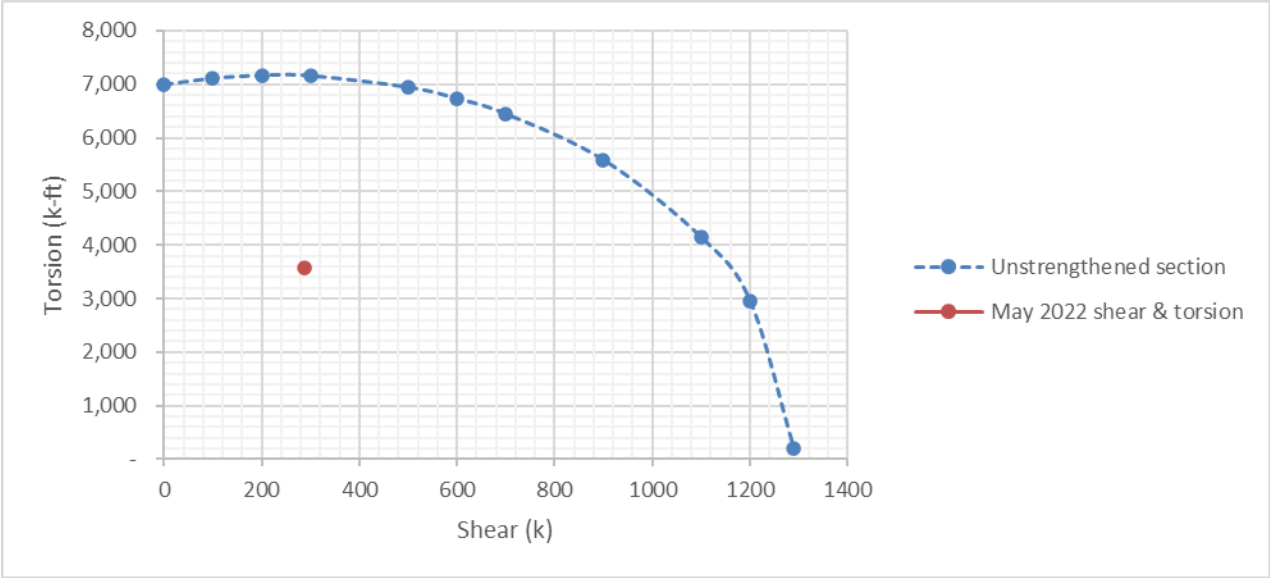


**Figure 5.48: Predicted T-V interaction diagram for S1.75 in May 2022**

**Figure 5.49: T-V interaction diagram for S1P1 based on April 2017 data**
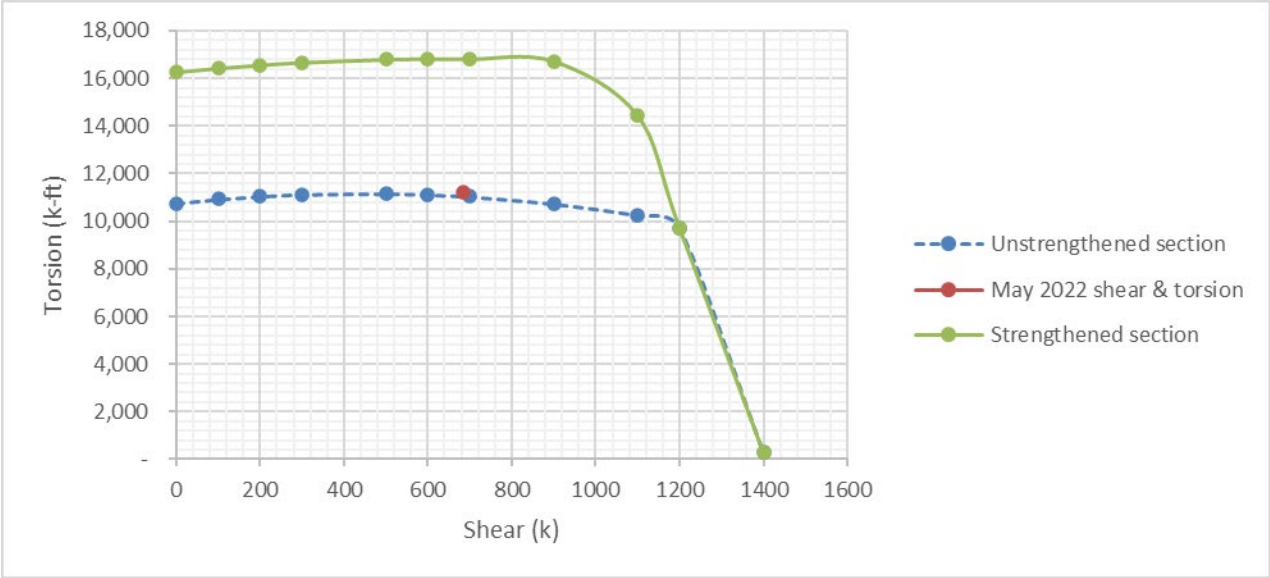


**Figure 5.50: Predicted T-V interaction diagram for S1P1 in May 2022**

**Figure 5.51: T-V interaction diagram for S2P1 based on April 2017 data**



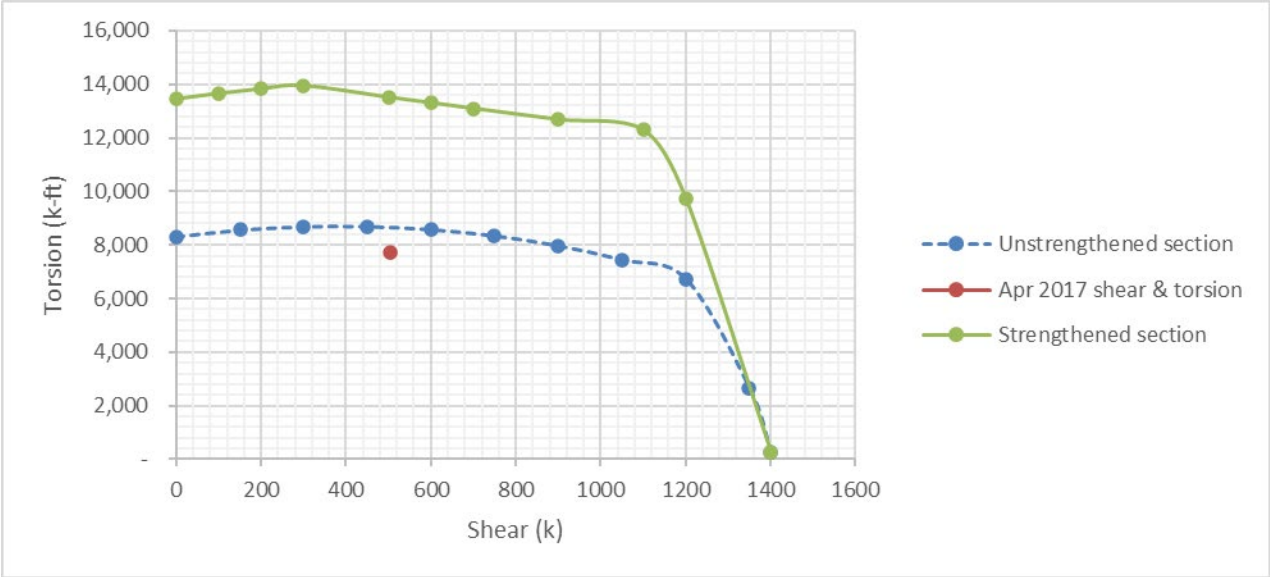**Figure 5.52: Predicted T-V interaction diagram for S2P1 in May 2022**

**Figure 5.53: T-V interaction diagram for S2.25 based on April 2017 data**
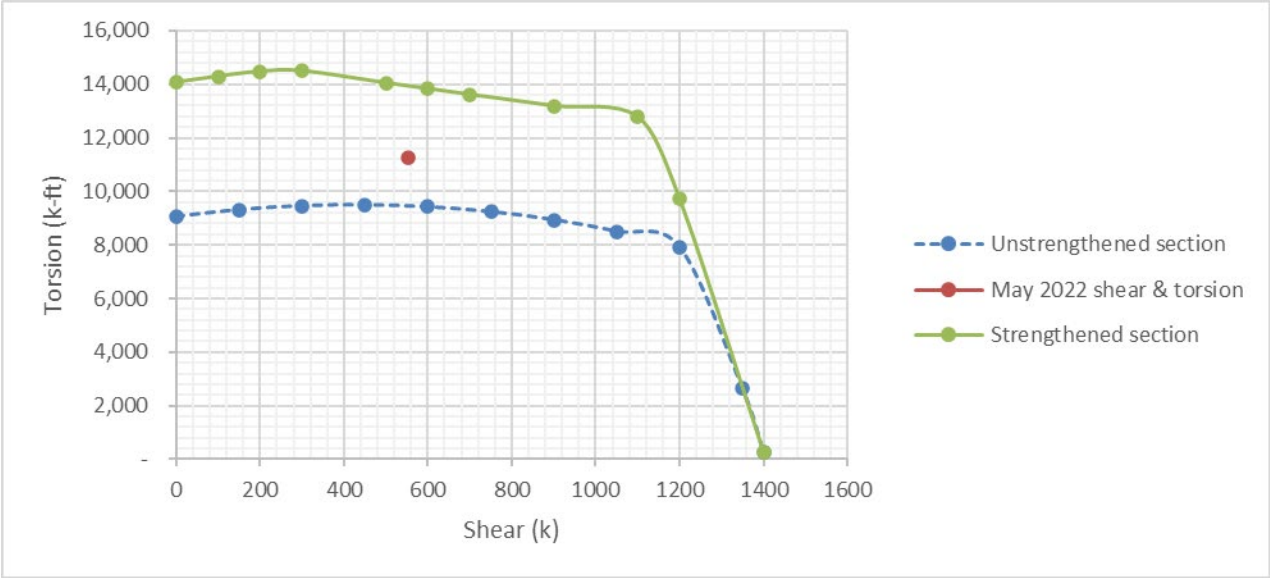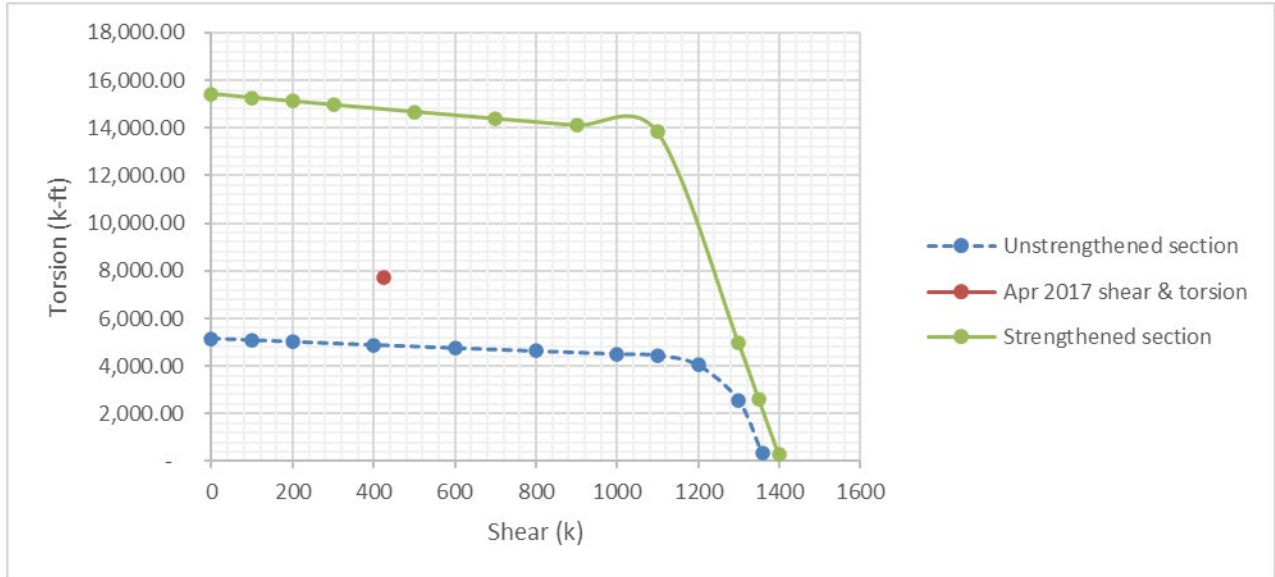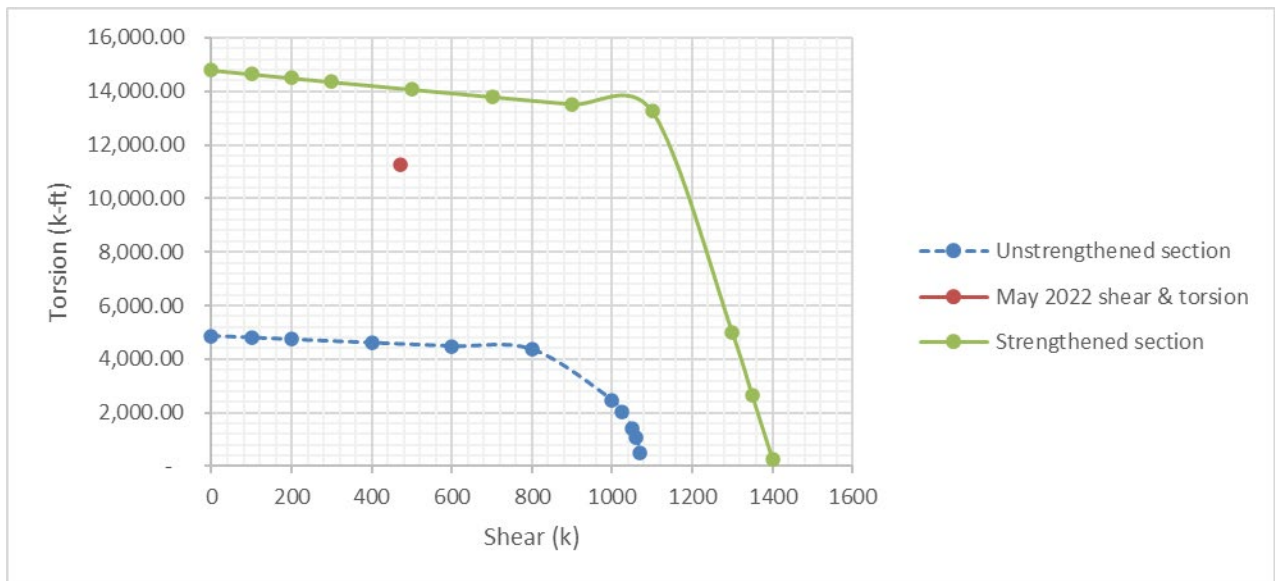


**Figure 5.54: Predicted T-V interaction diagram for S2.25 in May 2022**

**Figure 5.55: T-V interaction diagram for S2.50 based on April 2017 data**



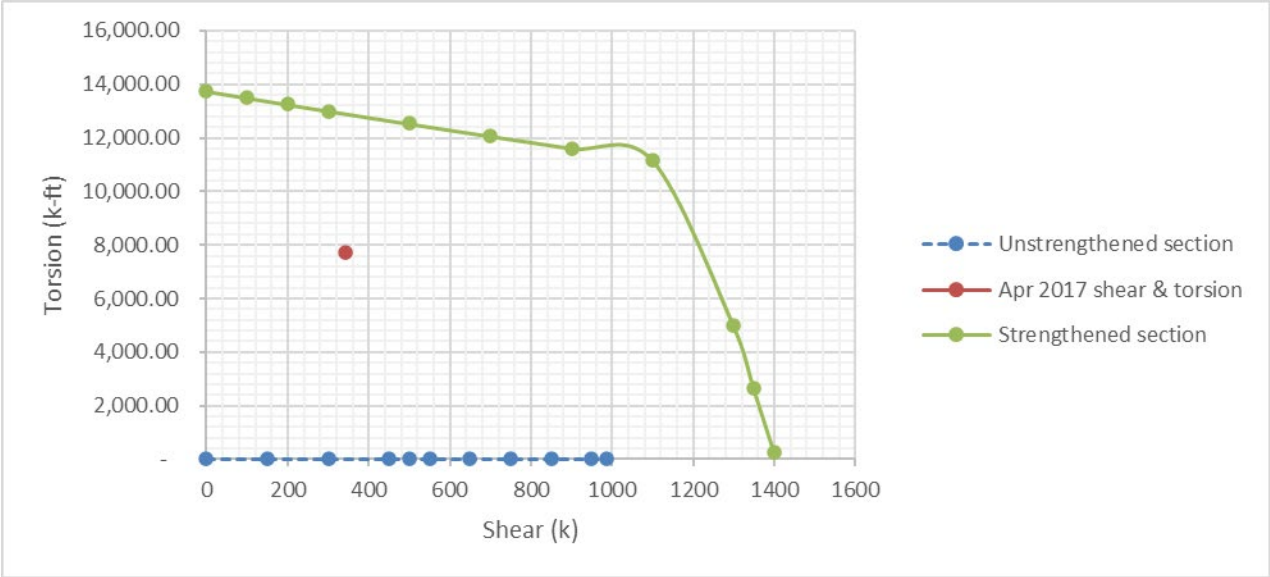**Figure 5.56: Predicted T-V interaction diagram for S2.50 in May 2022**

**Figure 5.57: T-V interaction diagram for S2.75 based on April 2017 data**



**Figure 5.58: Predicted T-V interaction diagram for S2.75 in May 2022**

**Figure 5.59: T-V interaction diagram for S2P2 based on April 2017 data (4-layers of CFRP C200H sheet)**



**Figure 5.60: Predicted T-V interaction diagram for S2P2 in May 2022 (4-layers of CFRP C200H sheet)**

**Figure 5.61: T-V interaction diagram for S3P2 based on April 2017 data**



**Figure 5.62: Predicted T-V interaction diagram for S3P2 in May 2022**

**Figure 5.63: T-V interaction diagram for S3.25 based on April 2017 data**



**Figure 5.64: Predicted T-V interaction diagram for S3.25 in May 2022**

**Figure 5.65: T-V interaction diagram for S3.50 based on April 2017 data**



**Figure 5.66: Predicted T-V interaction diagram for S3.50 in May 2022**

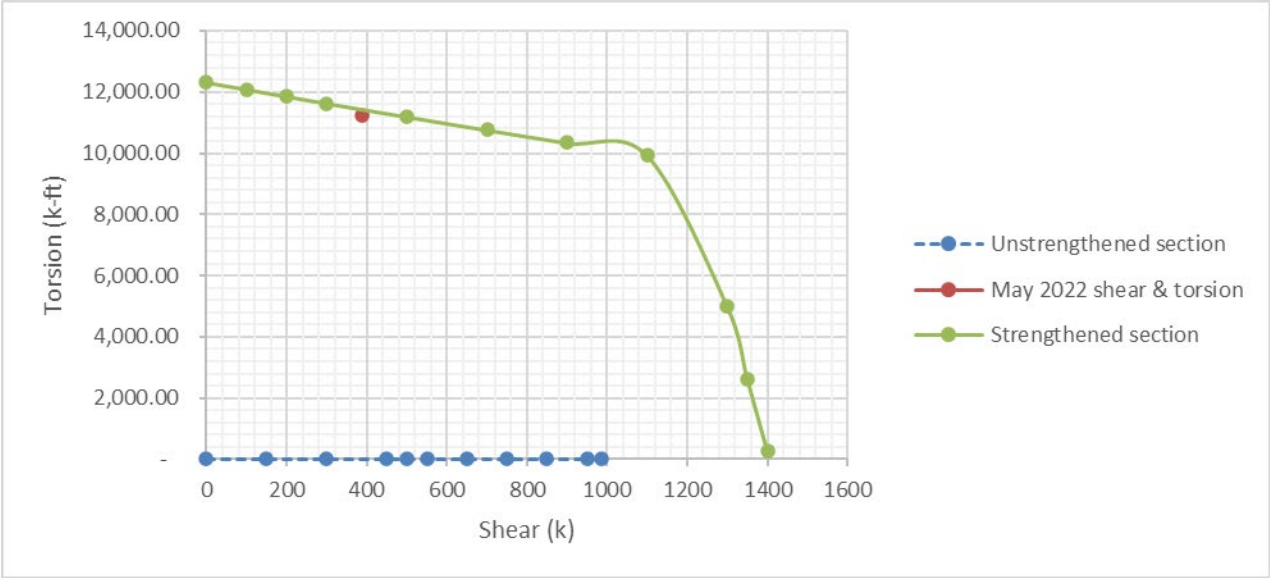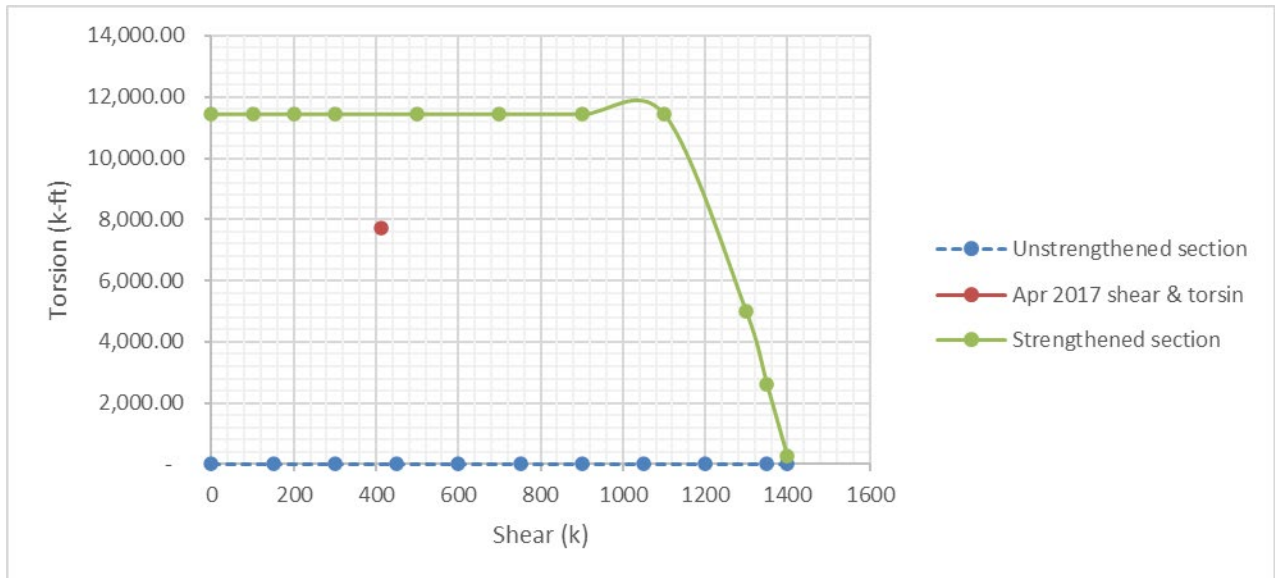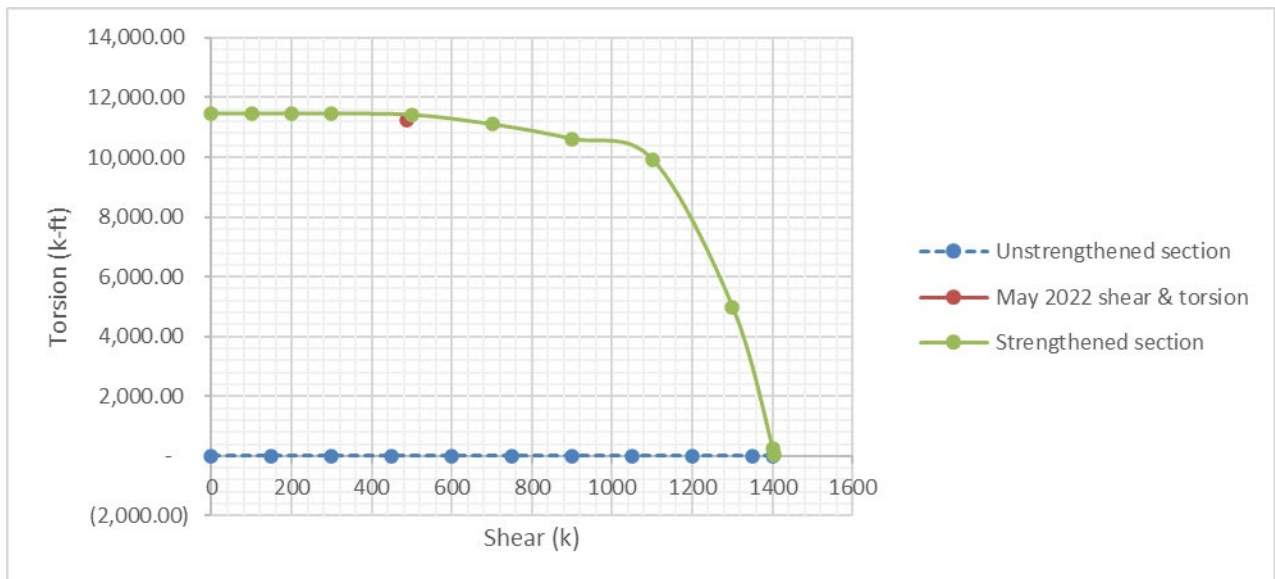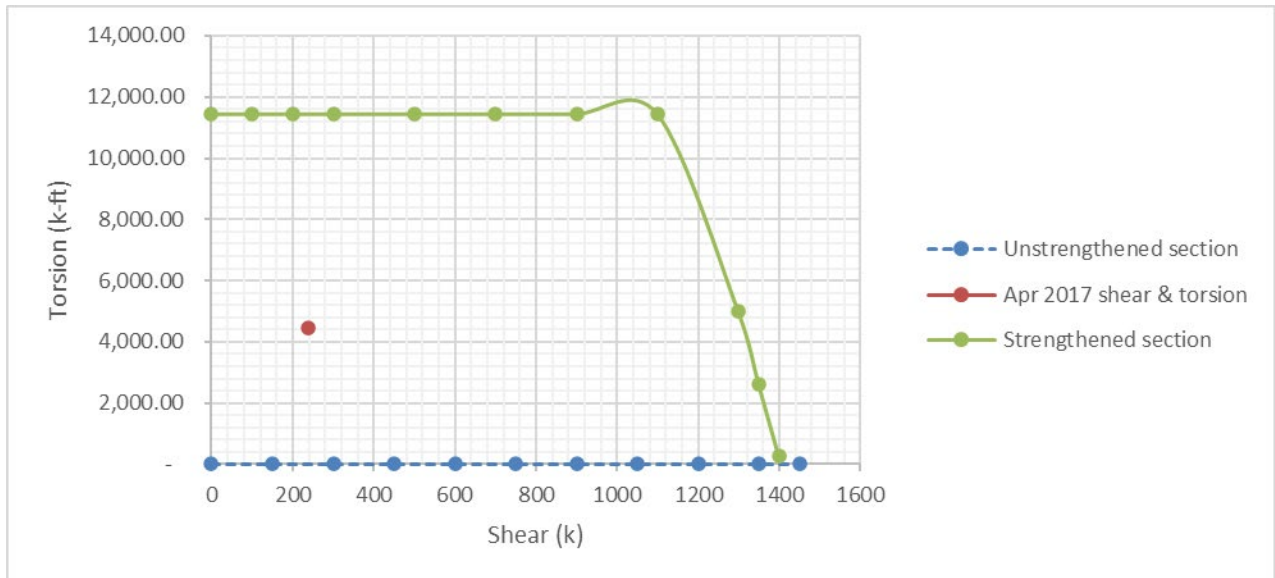**Figure 5.67: T-V interaction diagram for S3.75 based on April 2017 data**



**Figure 5.68: Predicted T-V interaction diagram for S3.75 in May 2022**

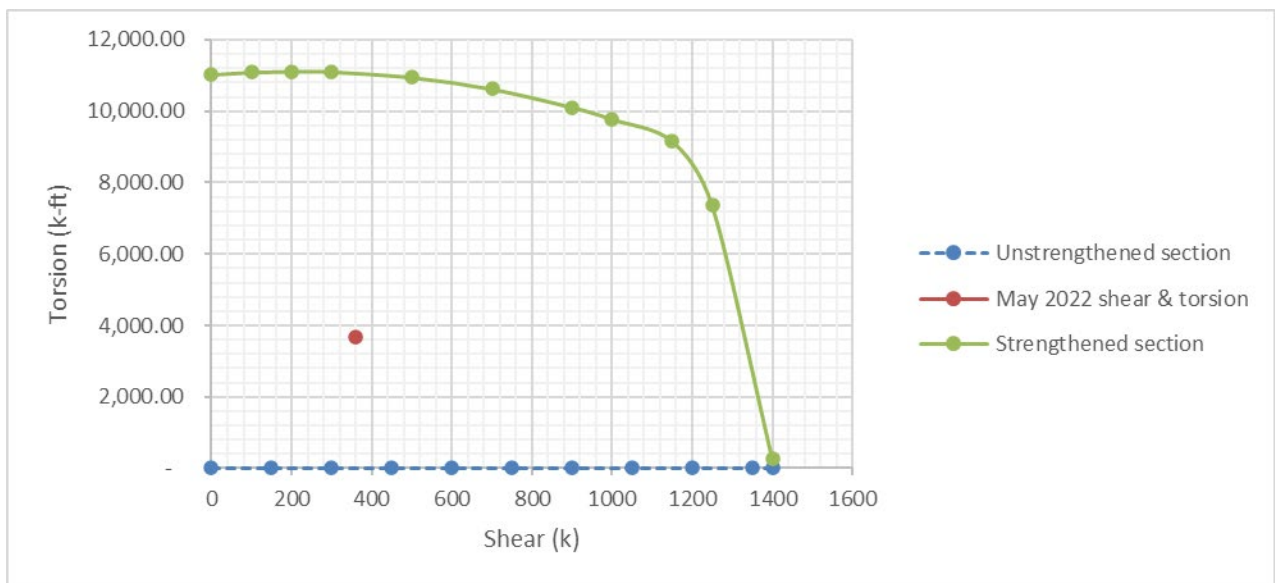**Figure 5.69: T-V interaction diagram for S3P3 based on April 2017 data**
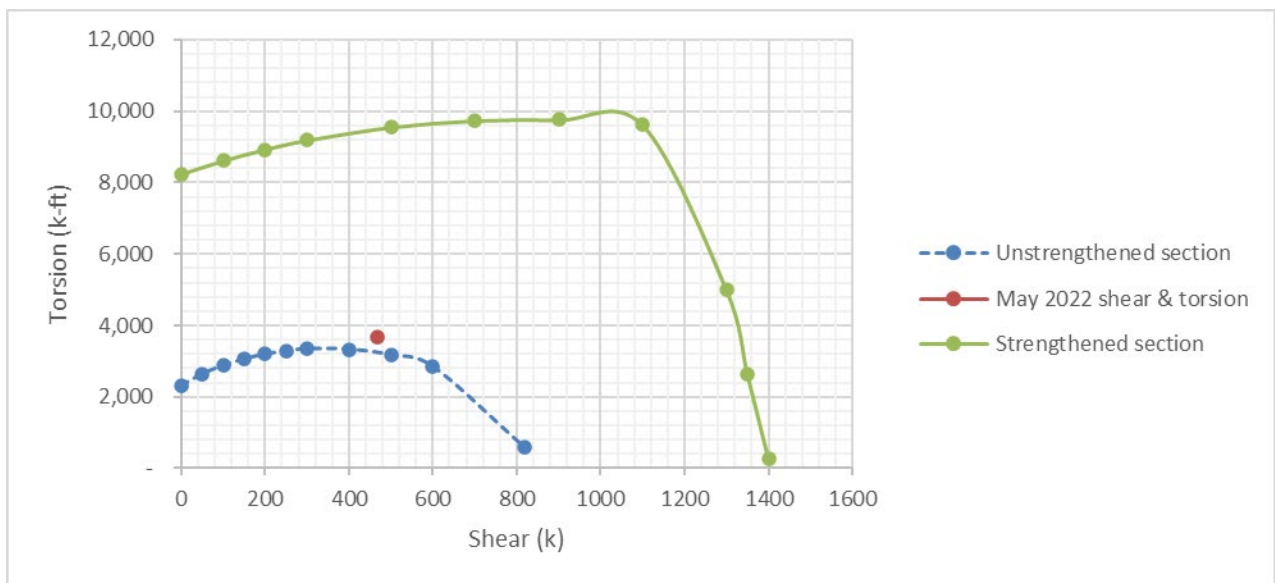


**Figure 5.70: Predicted T-V interaction diagram for S3P3 in May 2022**
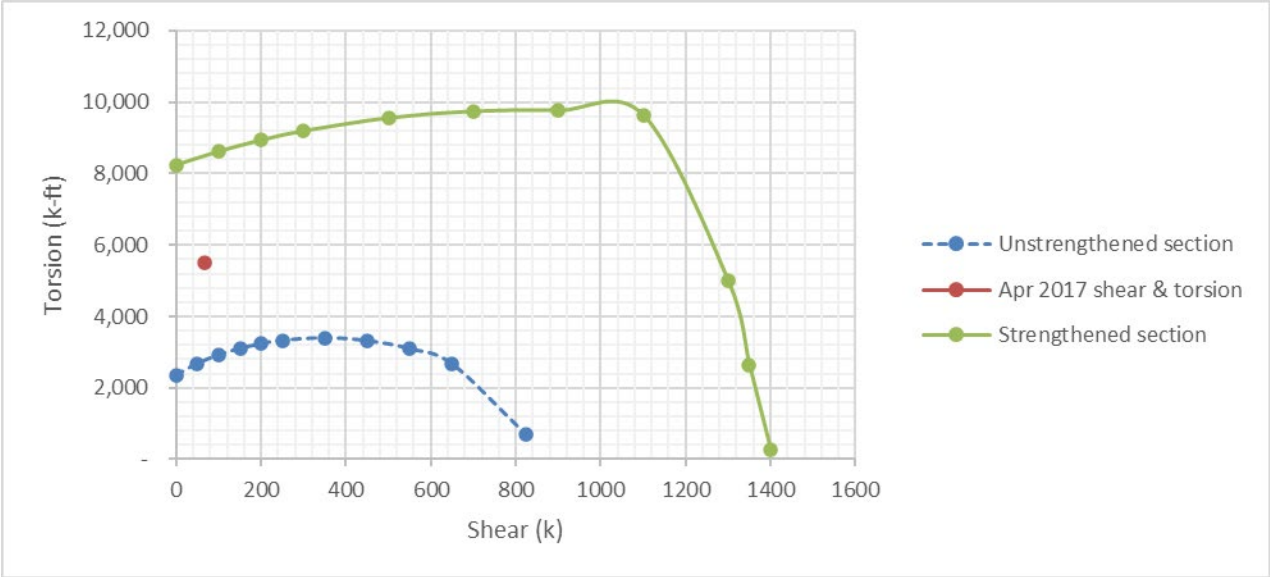
**Figure 5.71: T-V interaction diagram for S4P3 based on April 2017 data**
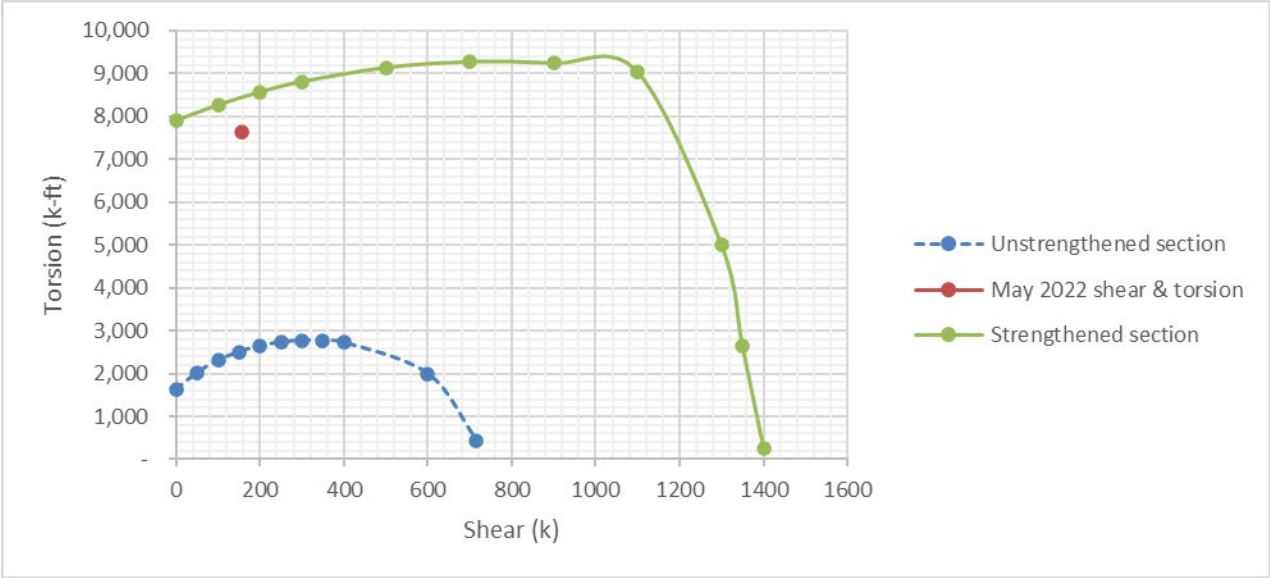


**Figure 5.72: Predicted T-V interaction diagram for S4P3 in May 2022**
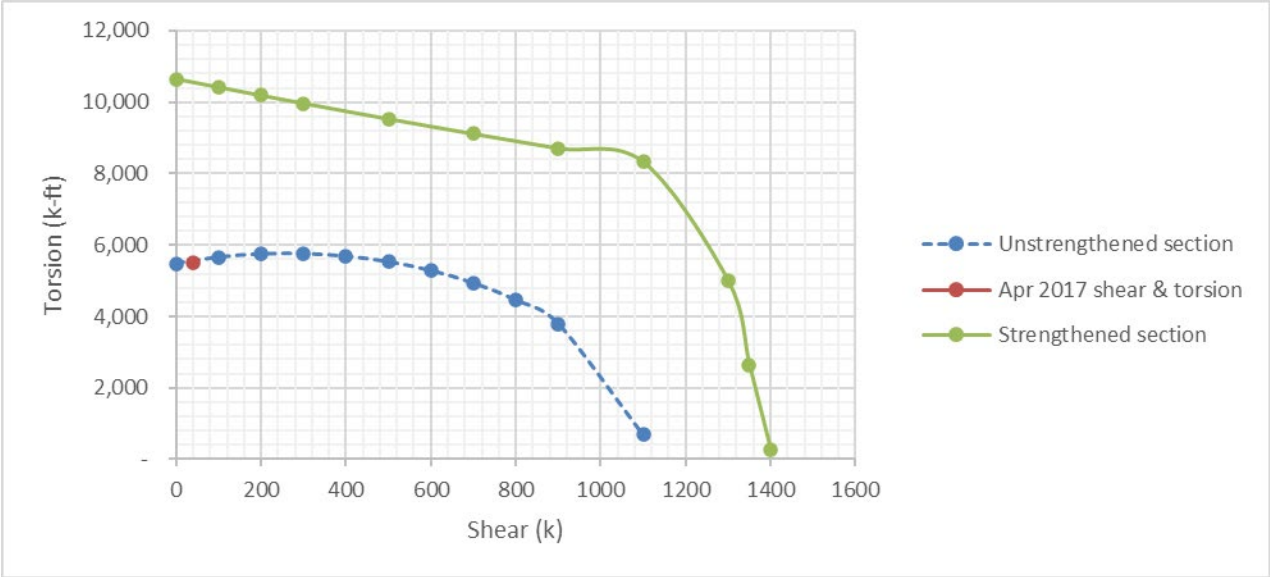
**Figure 5.73: T-V interaction diagram for S4.25 based on April 2017 data**
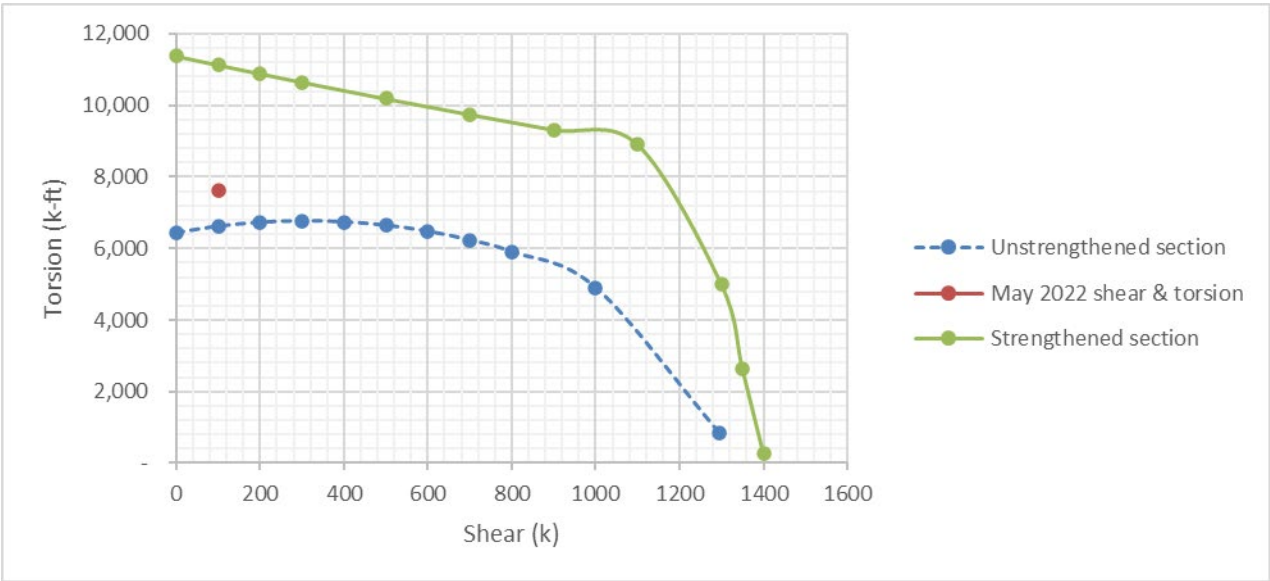


**Figure 5.74: Predicted T-V interaction diagram for S4.25 in May 2022**
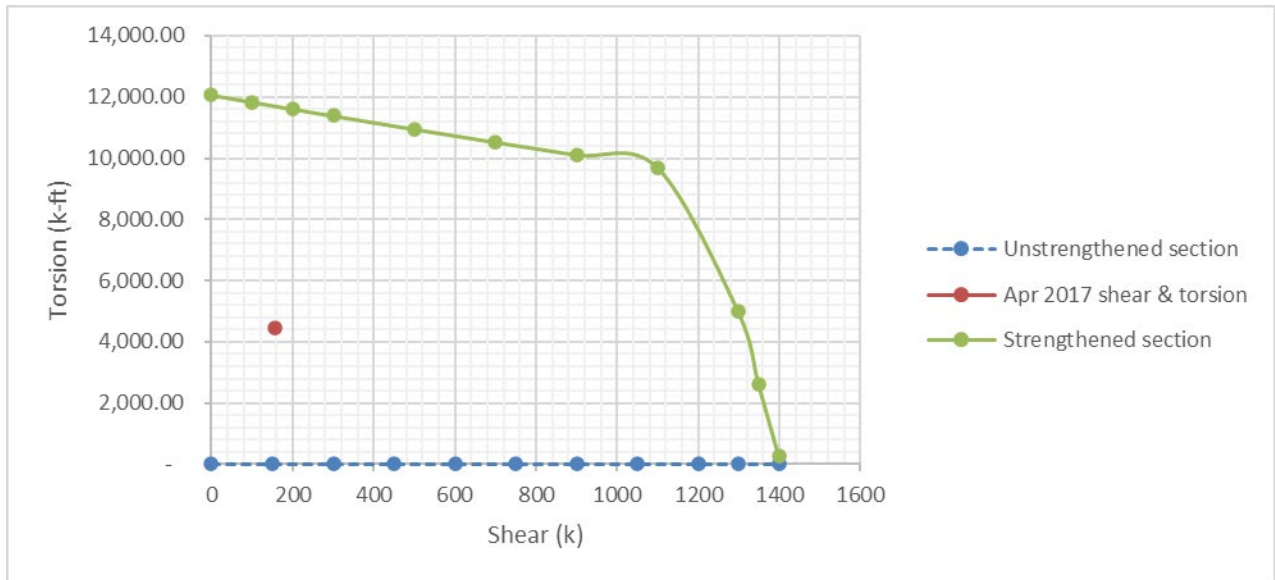
94
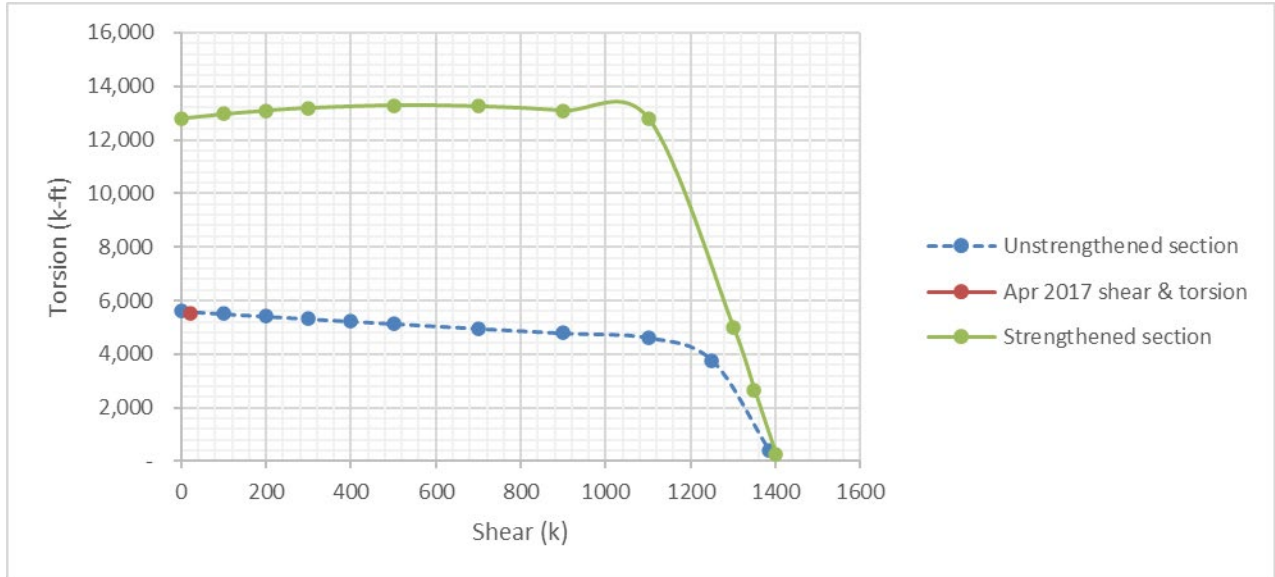
**Figure 5.75: T-V interaction diagram for S4.50 based on April 2017 data**
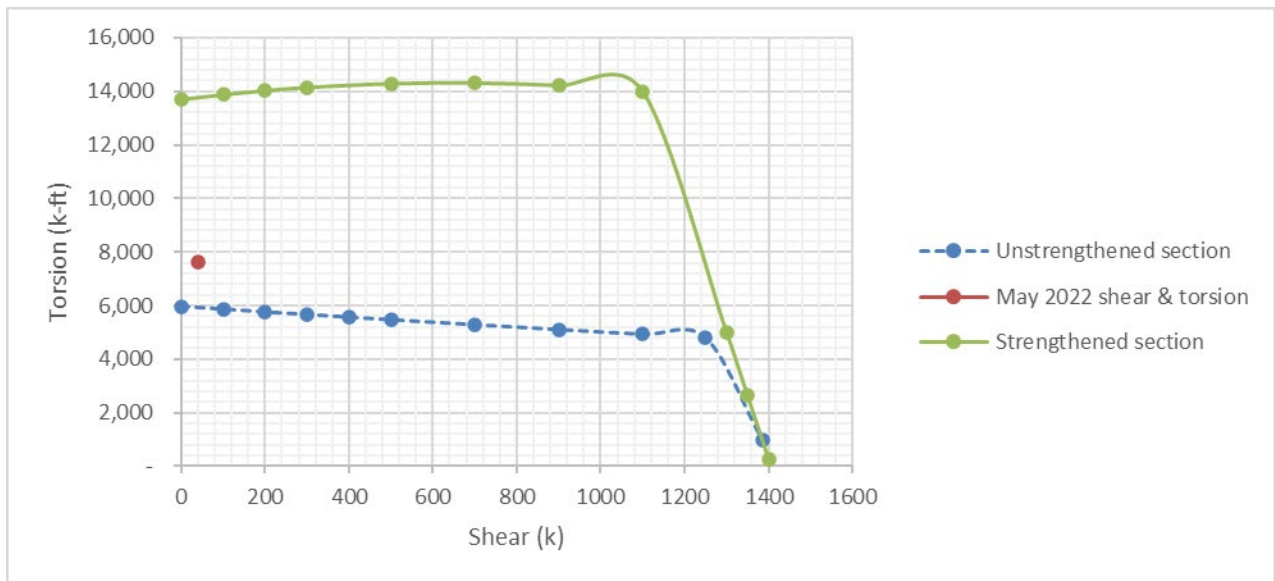


**Figure 5.76: Predicted T-V interaction diagram for S4.50 in May 2022**
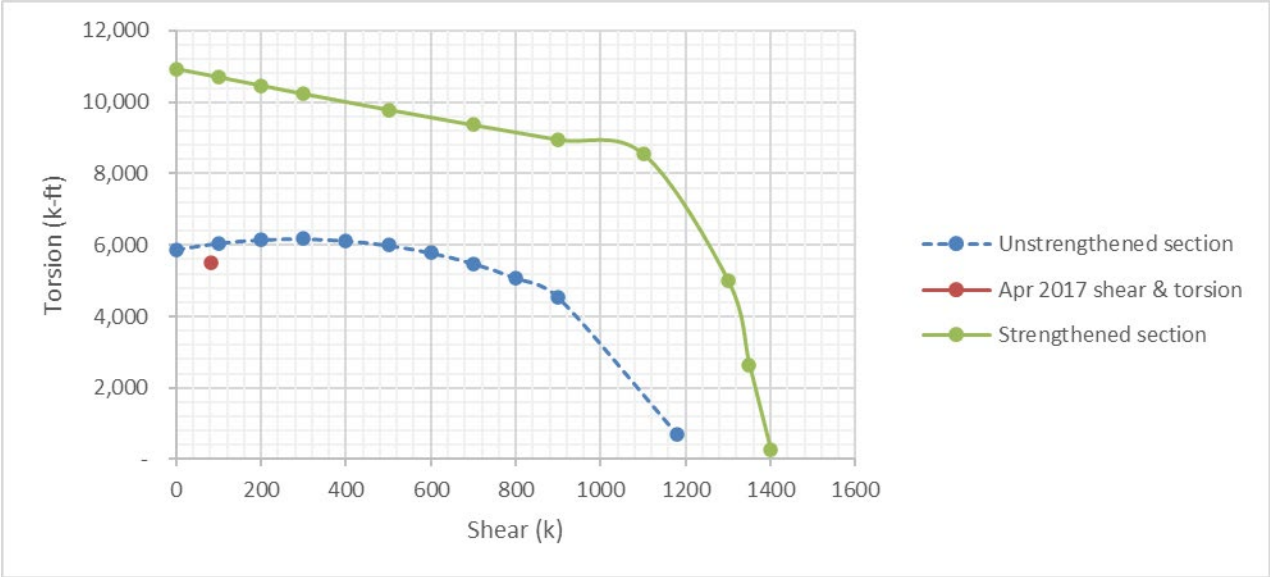
**Figure 5.77: T-V interaction diagram for S4.75 based on April 2017 data**
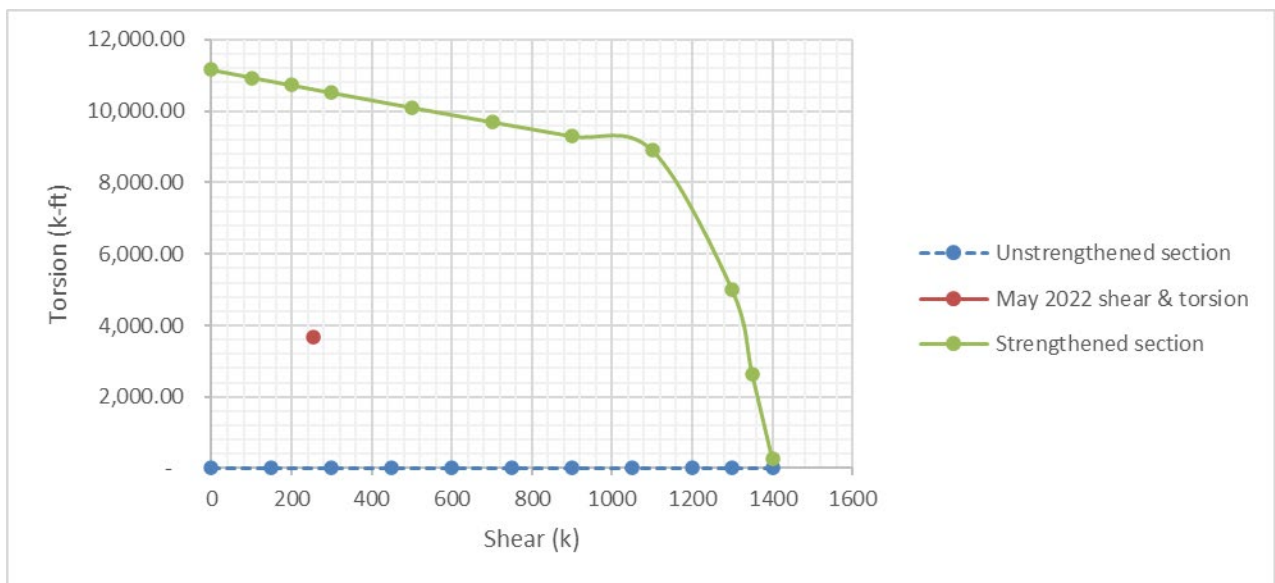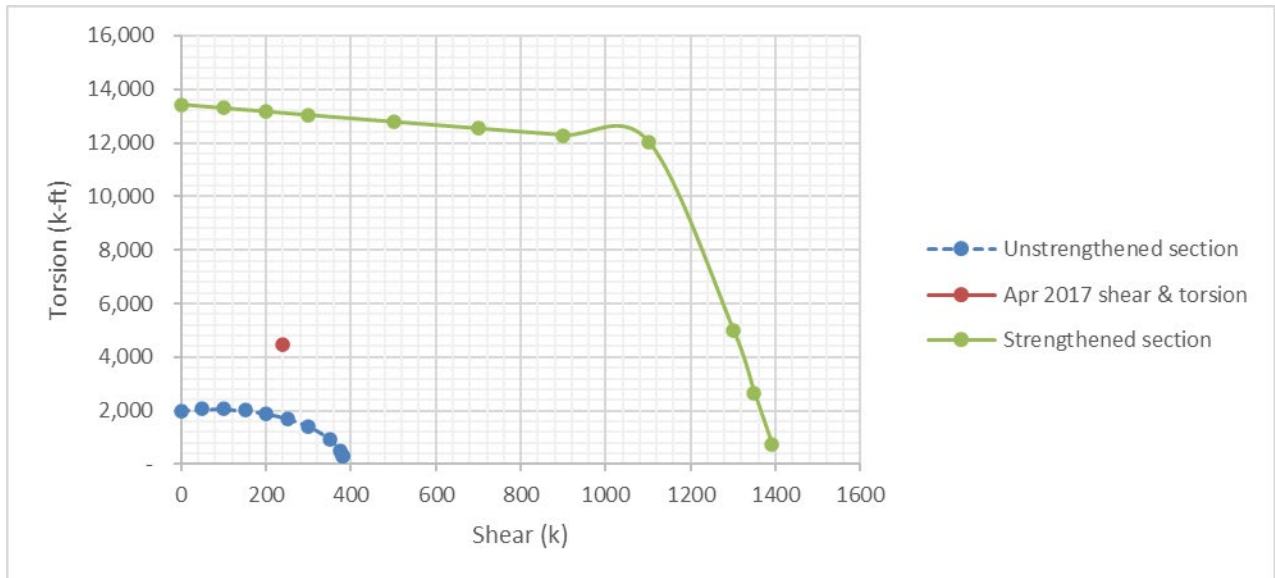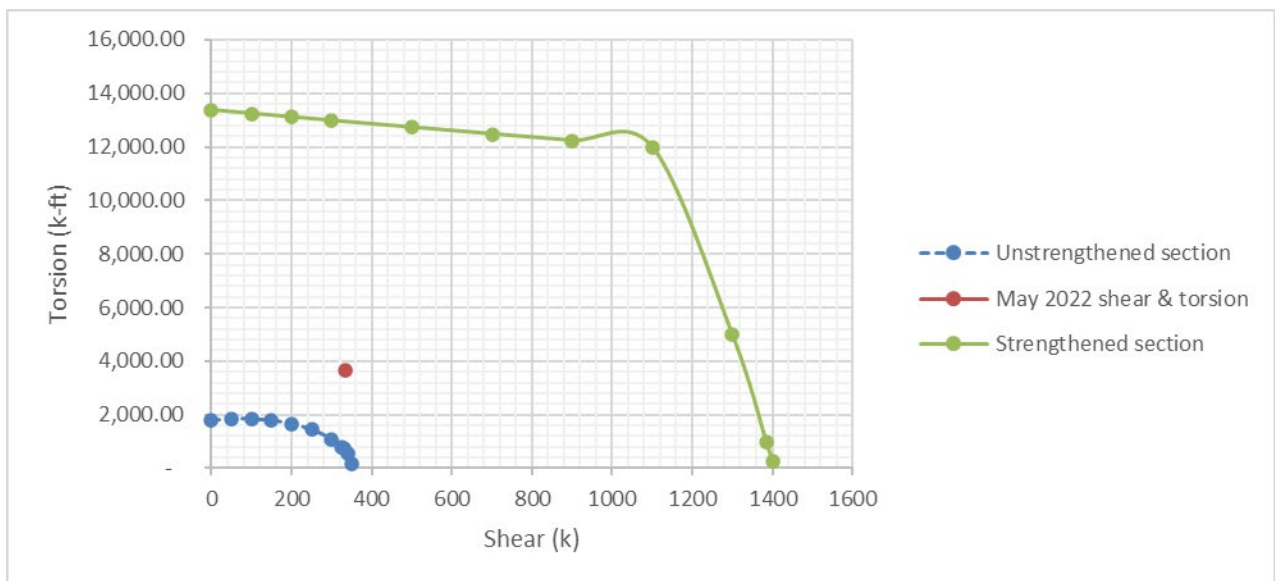


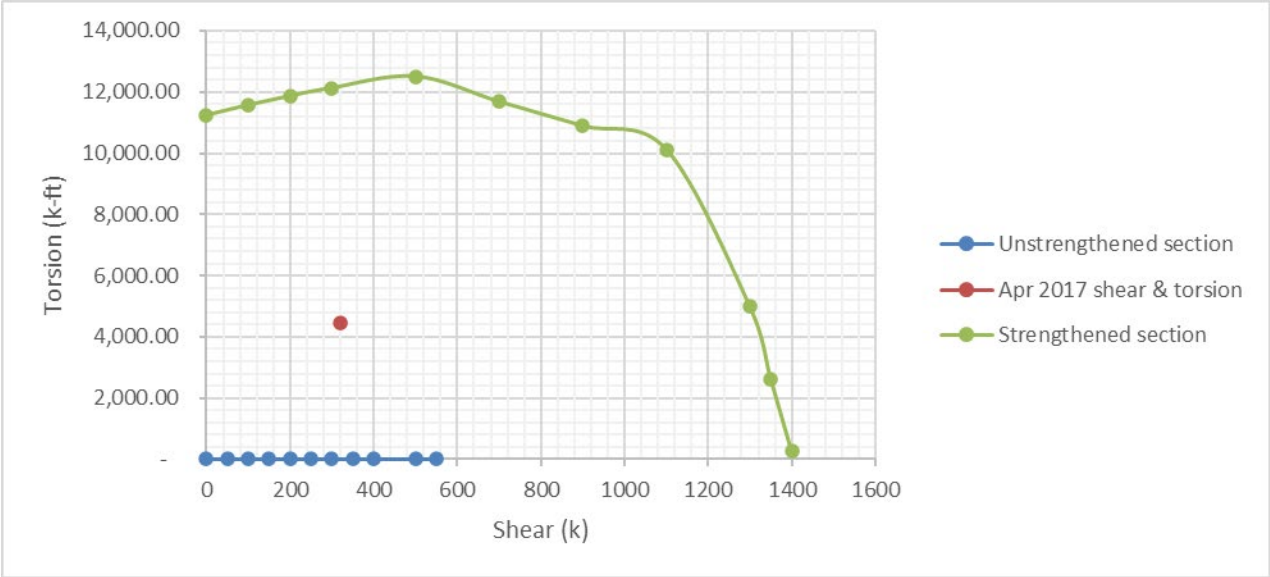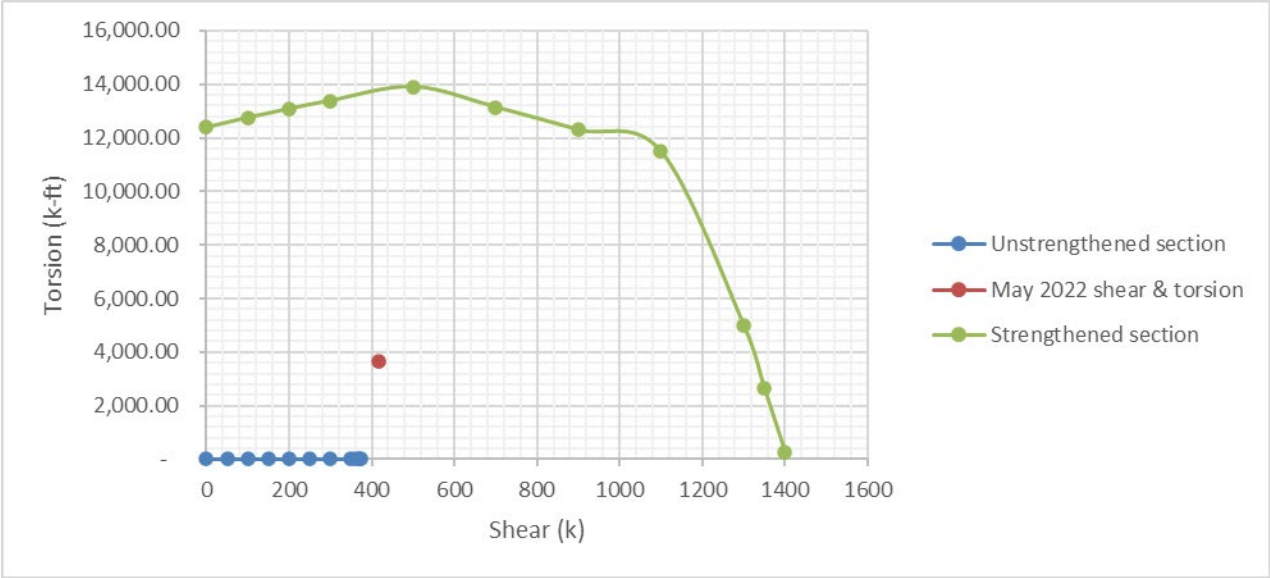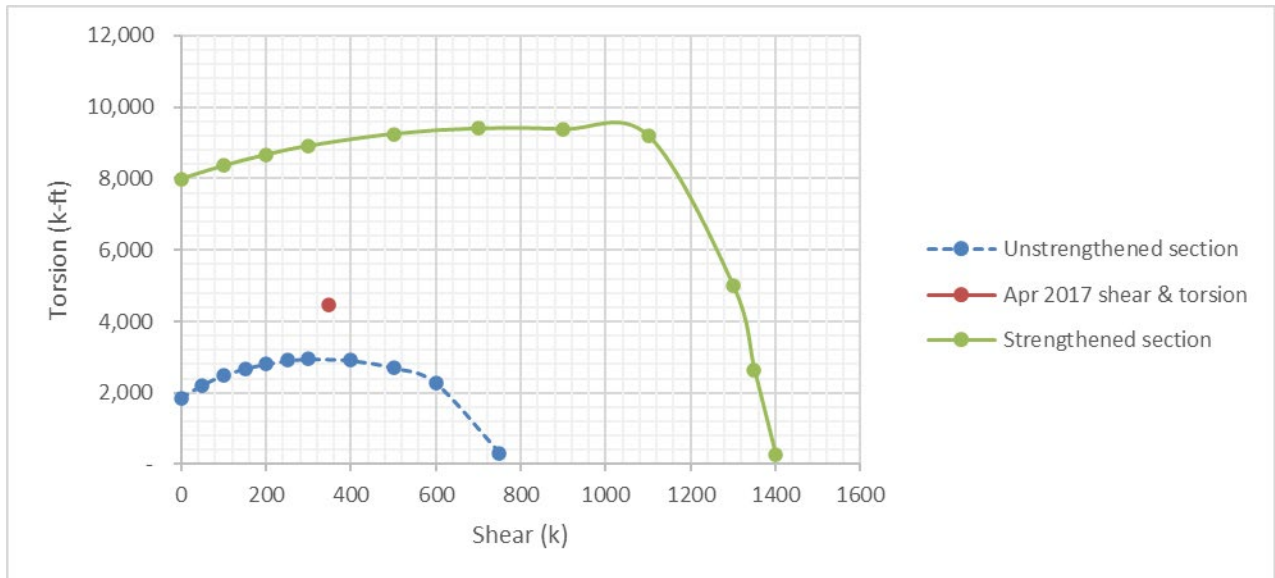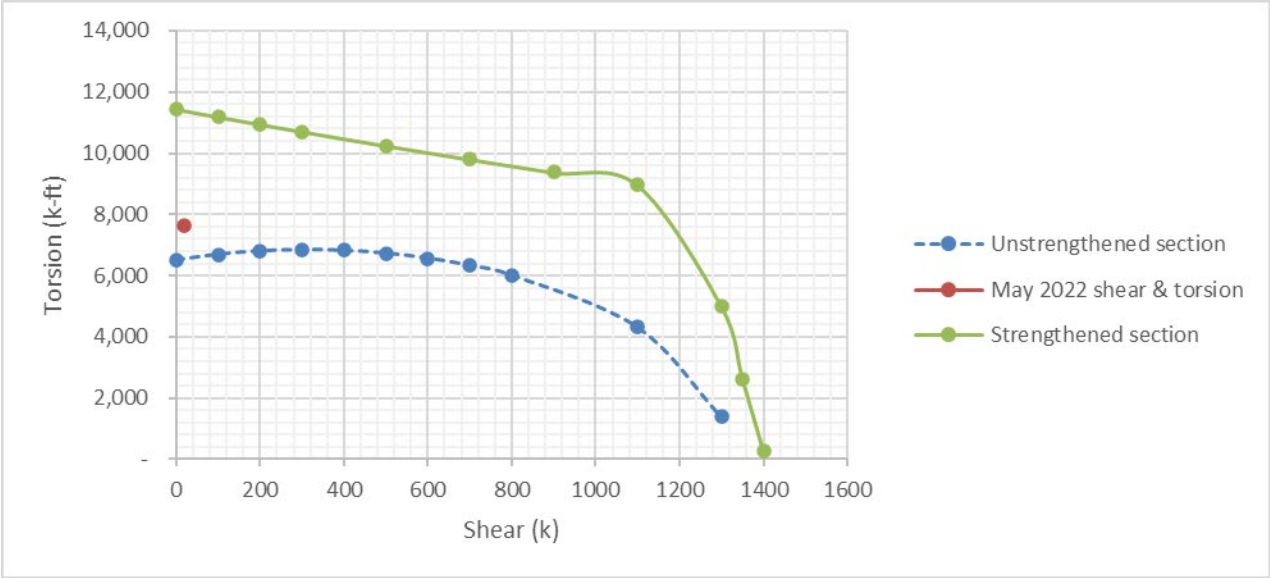**Figure 5.78: Predicted T-V interaction diagram for S4.75 in May 2022**
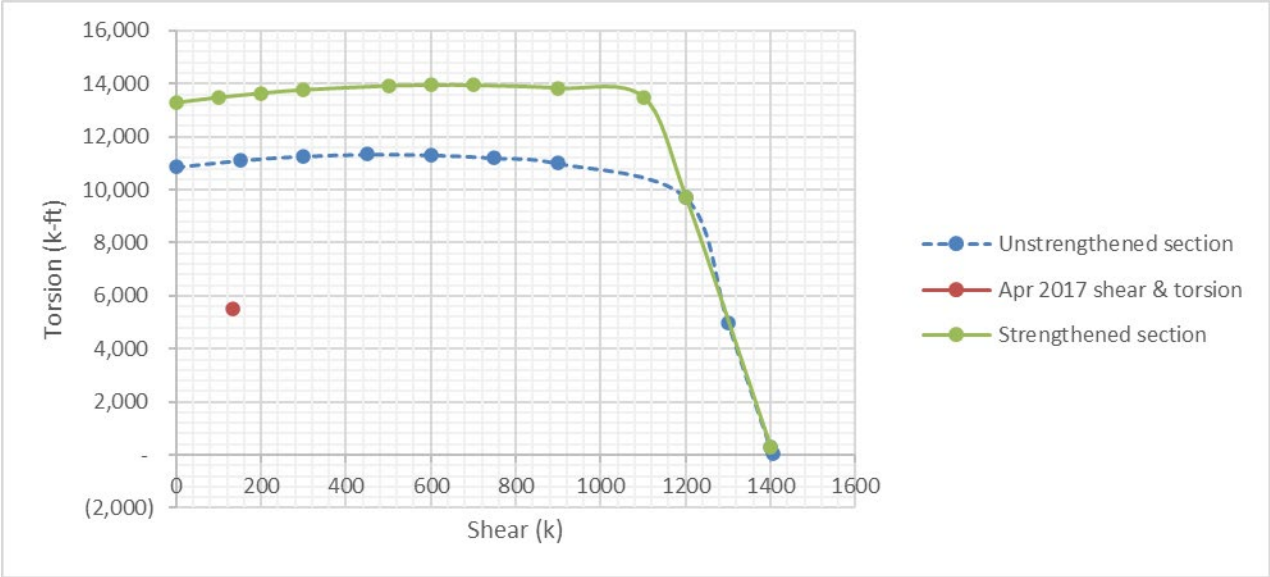
**Figure 5.79: T-V interaction diagram for S4A2 based on April 2017 data**
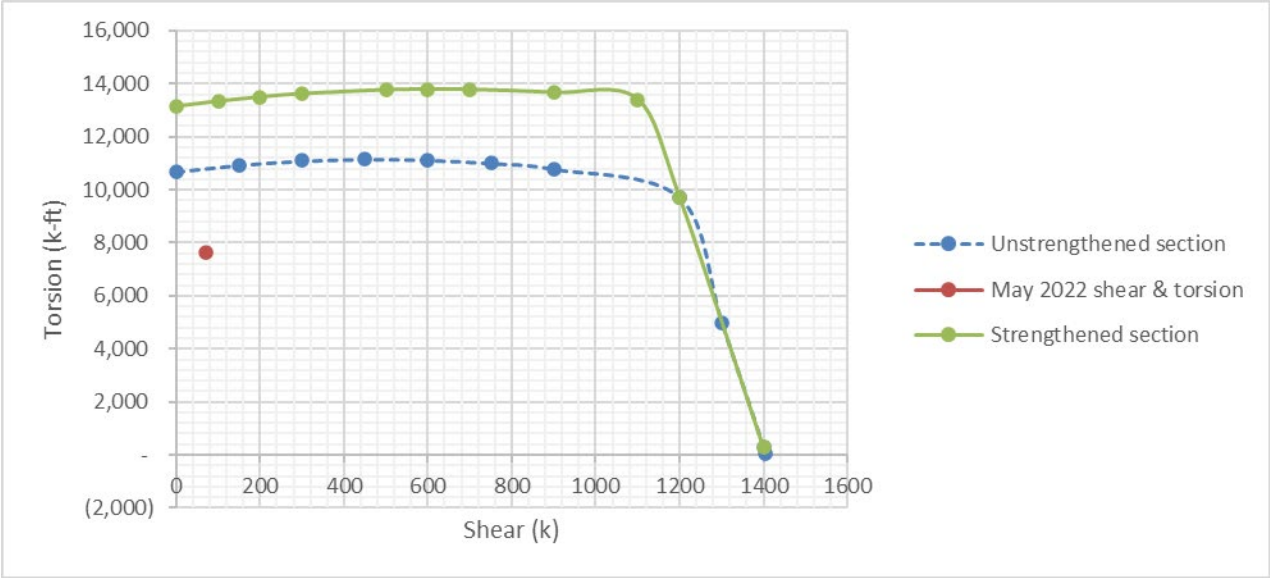


**Figure 5.80: Predicted T-V interaction diagram for S4A2 in May 2022**

### 5.2.1.3 Pier Results

The piers are the most critical components for the safety of the bridge. The results of the April 2017 settlements in terms of pier forces and moments are shown in Table 5.55. These data points are mapped onto the interaction diagram in Figure 5.81.

The pier column section has a diameter of 30 inches and a clear cover to reinforcement of 2 inches. The longitudinal reinforcement of nine #8 bars is used to plot the interaction diagram. Figure 5.81 shows that one of the piers has reached the critical state in tension under April 2017 settlements.

**Table 5.55: Pier results for April 2017 conditions**

|  | Axial (k) | Moment (k-ft) |
|---|---|---|
| Pier 1 South | 715.26 | 0 |
| Pier 1 North | 302.34 | 0 |
| Pier 2 South | −343.5 | 0 |
| Pier 2 North | 51.86 | 0 |
| Pier 3 South | −319 | 0 |
| Pier 3 North | 871.32 | 0 |
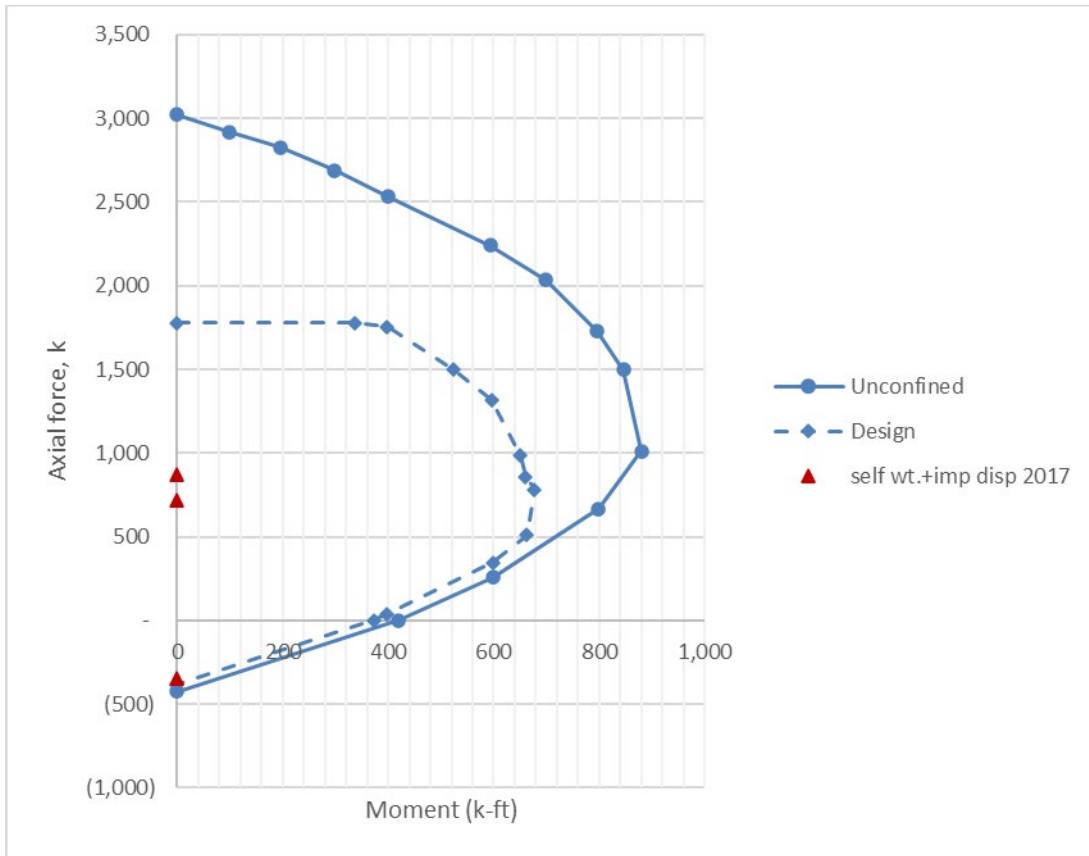
**Figure 5.81: Approximate Interaction diagram for the pier columns (April 2017)**

### 5.2.1.4 Results of Piles under Piers

The cross section of the steel H-piles used under the piers is shown in Figure 5.16. The interaction diagram for this cross section is computed using Excel assuming a uniaxial moment-axial compression force with fy = 36 ksi. The tabulated values of the force-moment in these piles are given in Table 5.56. Figure 5.82 presents the points mapped on the interaction diagram. It is evident that the pier piles are all safe since they are well within the interaction diagram.

**Table 5.56: Pier pile loads for 2017 settlement**

|  | Axial force, n (k) | Moment, mpc (k-ft) | n/ny | Mpc/mp |
|---|---|---|---|---|
| Pier 1 South | 182.35 | 0.101 | 0.325 | 0.000 |
| Pier 1 North | 79.09 | 0.041 | 0.41 | 0.000 |
| Pier 2 South | −79.42 | −0.047 | −0.142 | 0.000 |
| Pier 2 North | 16.46 | 0.007 | 0.029 | 0.000 |
| Pier 3 South | −73.29 | −0.043 | −0.131 | 0.000 |
| Pier 3 North | 221.33 | 0.122 | 0.395 | 0.001 |
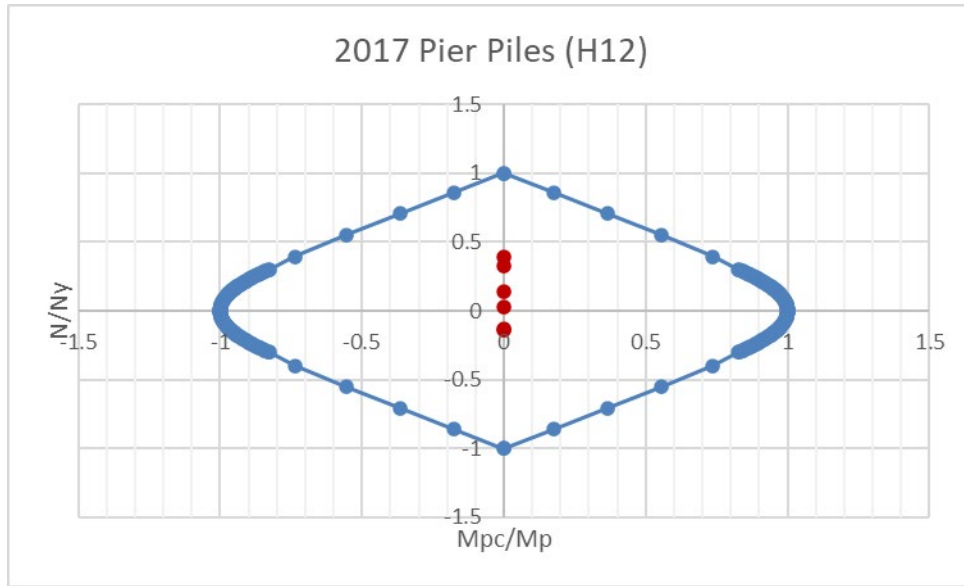
**Figure 5.82: Interaction diagram for the pier piles (April 2017 settlement)**

### 5.2.1.5 Results of Piles under Abutments

The cross section of the steel H-piles used under the abutments is shown in Figure 5.17. The interaction diagram for this cross section is computed using Excel assuming a uniaxial moment–axial compression force with fy = 36 ksi. The tabulated values of the force-moment in these piles are given in Table 5.57. Figure 5.83 presents the points mapped on the interaction diagram. It is evident from the figure that the abutment piles are generally safe.

**Table 5.57: Abutment pile loads for 2017 settlement**

| | | Axial force, n (k) | Moment, mpc (k-ft) | n/ny | Mpc/mp |
|---|---|---|---|---|---|
| Abutment 1 | South | 122.20 | −45.15 | 0.27 | −0.32 |
| | | 56.41 | −43.16 | 0.13 | −0.30 |
| | | −7.97 | −40.67 | −0.02 | −0.29 |
| | | −75.03 | −38.06 | −0.17 | −0.27 |
| | North | −147.46* | −35.64 | −0.33 | −0.25 |
| Abutment 2 | South | 227.94 | 39.91 | 0.51 | 0.28 |
| | | 114.26 | 40.45 | 0.26 | 0.28 |
| | | 39.16 | 40.37 | 0.09 | 0.28 |
| | | −33.33 | 40.31 | −0.08 | 0.28 |
| | North | −138.095 | 40.70 | −0.31 | 0.28 |

*Force is greater than the calculated pullout strength for the north abutment piles. This is due to the imposed displacement at the bottom of the piles to match the intended deformed shape. In reality there is no such a force in the piles, hence points lying outside interaction diagrams in Figure 5.85 to Figure 5.88 are believed to be of no concern. Pullout strength for abutment piles is calculated in section 5.1.1.4 of this report.
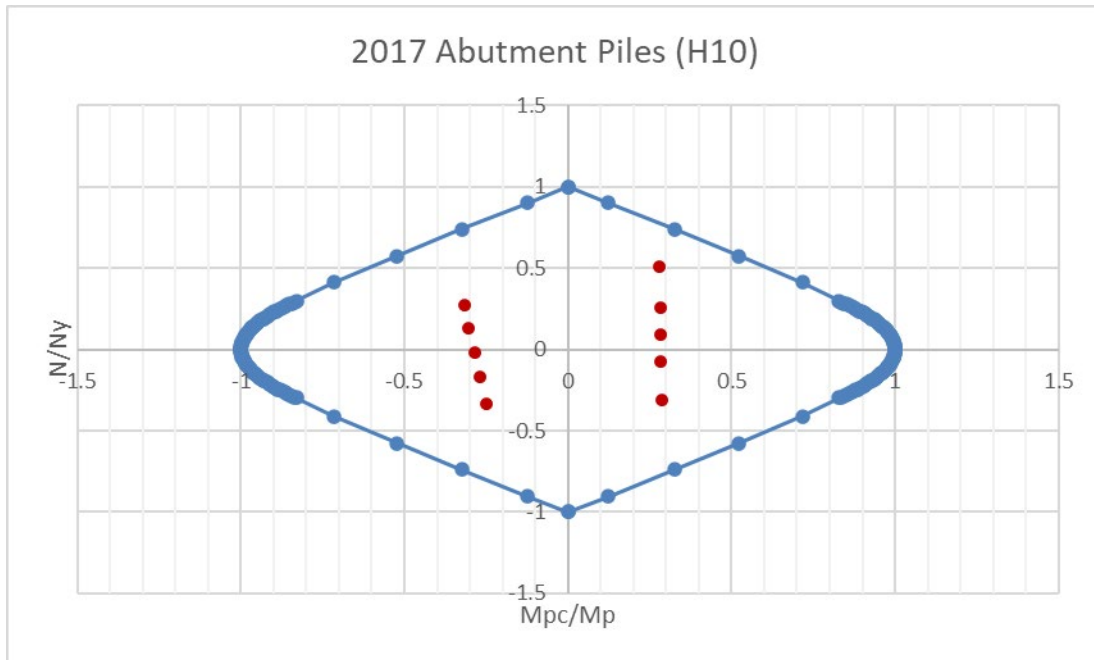


**Figure 5.83: Interaction diagram for the abutment piles (April 2017 settlement)**

## 5.2.2 Superimposing Live Load

As done earlier, the most critical truck loading case is selected for presentation and discussion. This is the case for which the rear axle loading is adjacent to Pier 2 while the truck is on Span 2 (Figure 5.84.)
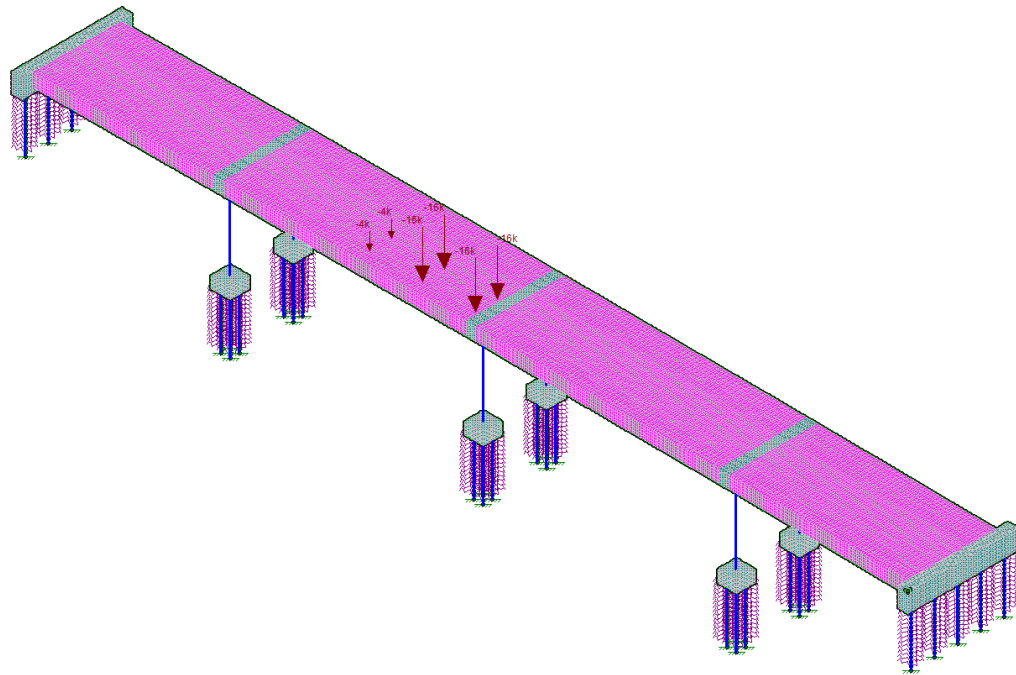


**Figure 5.84: Truck load location studied in this report (April 2017 settlement + truck loading)**

### 5.2.2.1 Pier Results

The results of April 2017 settlements plus the truck loading at the critical location in terms of pier forces and moments are shown in Table 5.58. These data points are mapped onto the interaction diagram in Figure 5.85 prepared using Excel.

**Table 5.58: Pier results for combined truck loading and April 2017 settlement**

|  | Axial (k) | Moment (k-ft) |  |
|---|---|---|---|
| Pier 1 South | 727.63 | 0 |  |
| Pier 1 North | 305.1 | 0 |  |
| Pier 2 South | −297.84 | 0 |  |
| Pier 2 North | 69.02 | 0 |  |
| Pier 3 South | −318.26 | 0 |  |
| Pier 3 North | 867.48 | 0 |  |
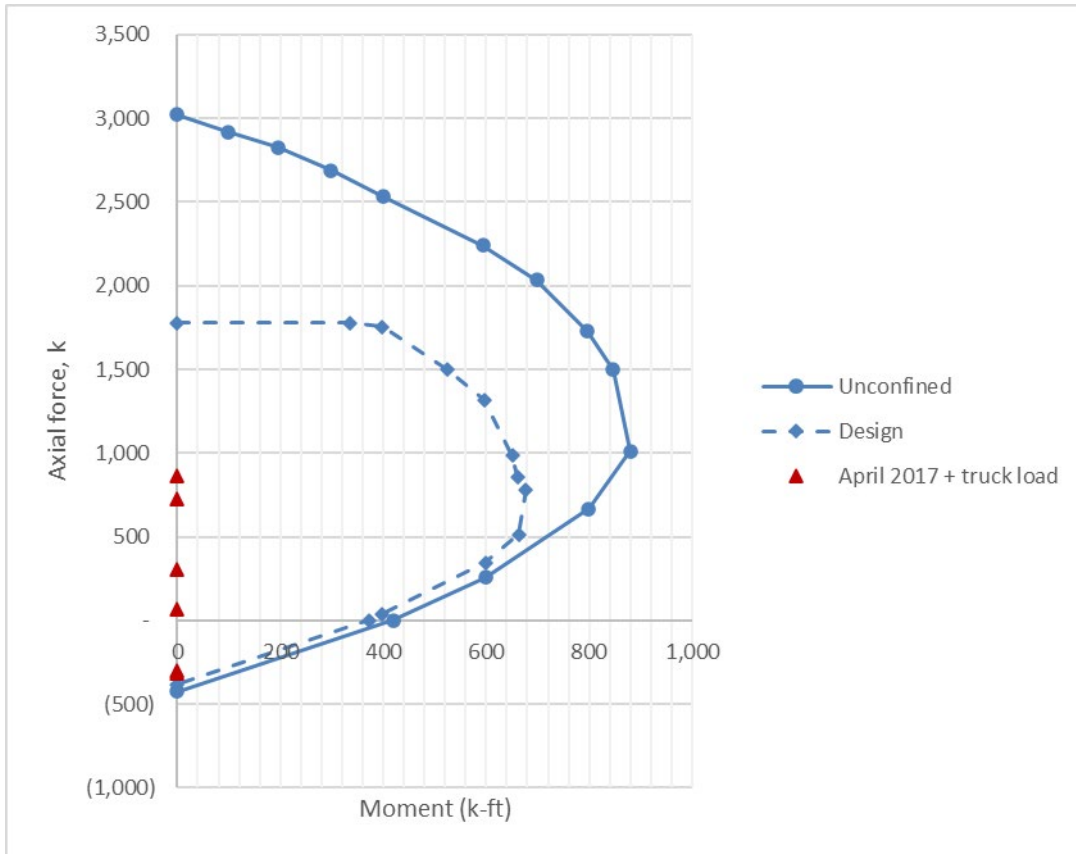


**Figure 5.85: Approximate Interaction diagram for piers (April 2017 + truck)**

### 5.2.2.2 Results of Piles under Piers

The tabulated values of the force-moment in these piles are given in Table 5.59. Figure 5.86 presents the points mapped on the interaction diagram.

**Table 5.59: Pile results under pier for combined truck loading and April 2017 settlement**

| | Axial, n (k) | Moment, mpc (k-ft) | n/ny | mpc/mp |
|---|---|---|---|---|
| Pier 1 South | 185.378 | 0.103 | 0.33081 | −0.00047 |
| Pier 1 North | 79.7417 | 0.042 | 0.141969 | −0.00019 |
| Pier 2 South | −90.859 | −0.051 | −0.16249 | −0.00023 |
| Pier 2 North | 20.714 | 0.01 | 0.036937 | −4.1E-05 |
| Pier 3 South | −73.477 | −0.043 | −0.13117 | −0.00035 |
| Pier 3 North | 220.376 | 0.122 | 0.393111 | 0.00126 |
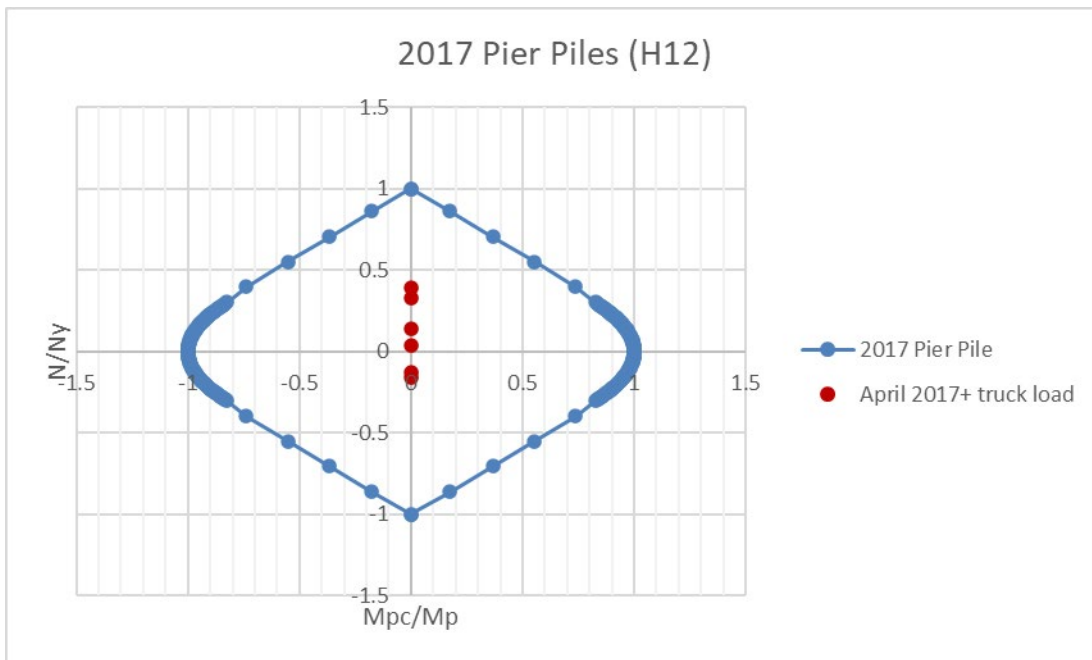


**Figure 5.86: Interaction diagram for piles under piers (April 2017 + truck)**

### 5.2.2.3 Results of Piles under Abutments

The tabulated values of the force-moment in these piles are given in Table 5.60. Figure 5.87 presents the points mapped on the interaction diagram.

**Table 5.60: Abutment pile results truck loading conditions**

| | | Axial, n (k) | Moment, mpc (k-ft) | n/ny | mpc/mp |
|---|---|---|---|---|---|
| Abutment 1 | South | 122.379 | −45.168 | 0.275434 | −0.31697 |
| | | 56.147 | −43.538 | 0.126351 | −0.30534 |
| | | −7.356 | −40.701 | −0.01644 | −0.28595 |
| | | −73.954 | −38.419 | −0.16642 | −0.27044 |
| | North | −145.971 | −65.686 | −0.32834 | −0.46086 |
| Abutment 2 | South | 228.463 | 40.095 | 0.513914 | 0.281594 |
| | | 114.492 | 40.139 | 0.257141 | 0.281545 |
| | | 39.222 | 40.348 | 0.088161 | 0.284275 |
| | | −33.209 | 40.278 | −0.07445 | 0.282906 |
| | North | −138.571 | 40.431 | −0.3125 | 0.284016 |
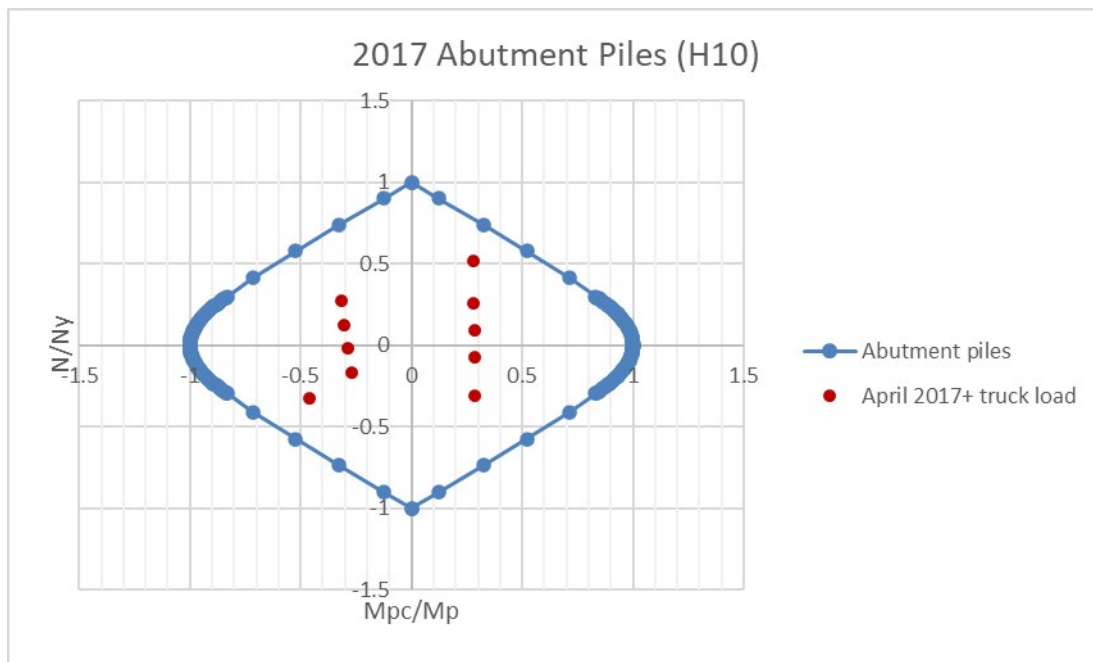


**Figure 5.87: Interaction diagram for the piles under the abutments (April 2017 + truck)**

## 5.2.3 Applying Projected Settlements

### 5.2.3.1 Pier Results

The results of the April 2017 settlements plus the incremental settlements up to May 2022 at the critical location in terms of pier forces and moments are shown Table 5.61. These data points are mapped onto the interaction diagram prepared using Excel (Figure 5.88).

**Table 5.61: Pier results for May 2022 settlement**

| Pier | Axial (k) | Moment (k-ft) |
|---|---|---|
| Pier 1 South | 979.84 | 0 |
| Pier 1 North | 77.23 | 0 |
| Pier 2 South | −672.2 | 0 |
| Pier 2 North | 234.94 | 0 |
| Pier 3 South | −314 | 0 |
| Pier 3 North | 1028.2 | 0 |
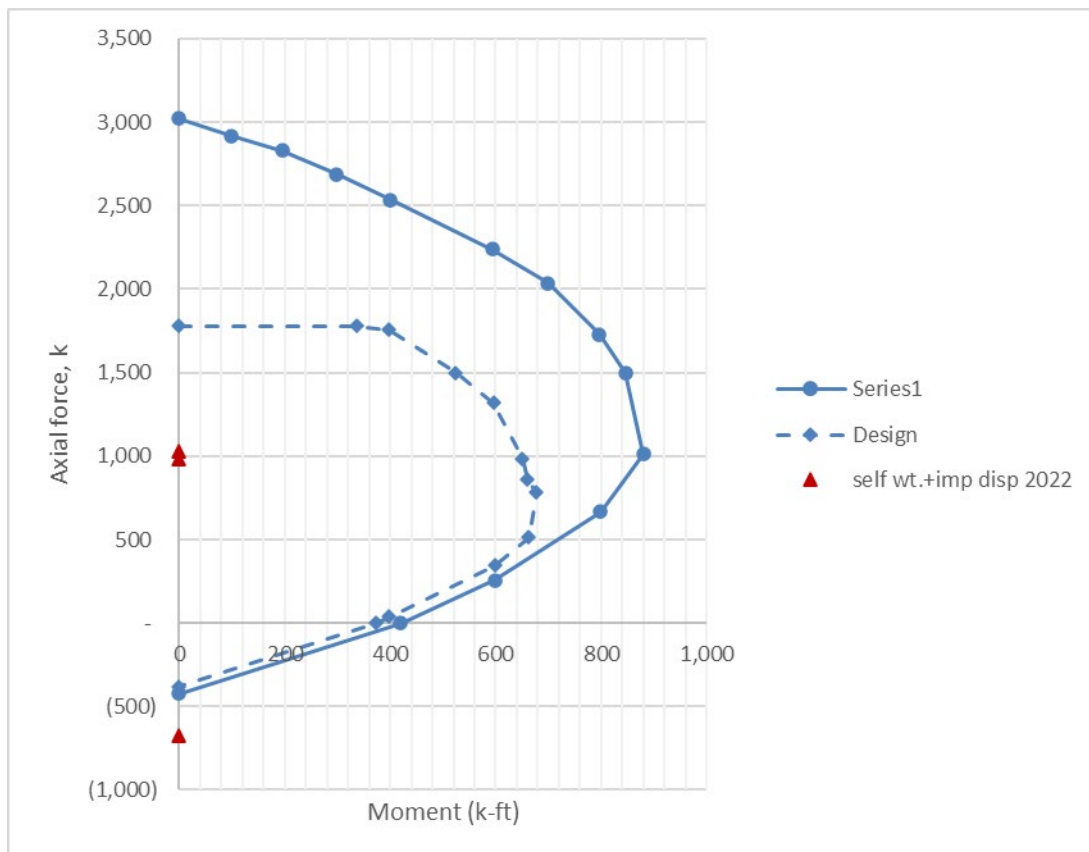


**Figure 5.88: Approximate interaction diagram for the pier columns (May 2022 Settlement)**

### 5.2.3.2 Results of Piles under Piers

The tabulated values of the force-moment in these piles are given in Table 5.62. Figure 5.89 presents the points mapped on the interaction diagram.

**Table 5.62: Results of piles under pier for May 2022 condition**

|  | Axial, n (k) | Mpc, (k-ft) | n/ny | mpc/mp |
|---|---|---|---|---|
| Pier 1 South | 248.469 | 0.138 | 0.443 | 0.001 |
| Pier 1 North | 22.818 | 0.010 | 0.041 | 0.000 |
| Pier 2 South | −161.590 | −0.094 | −0.288 | 0.000 |
| Pier 2 North | 62.231 | 0.033 | 0.111 | 0.000 |
| Pier 3 South | −72.051 | −0.043 | −0.128 | 0.000 |
| Pier 3 North | 260.564 | 0.145 | 0.465 | 0.001 |
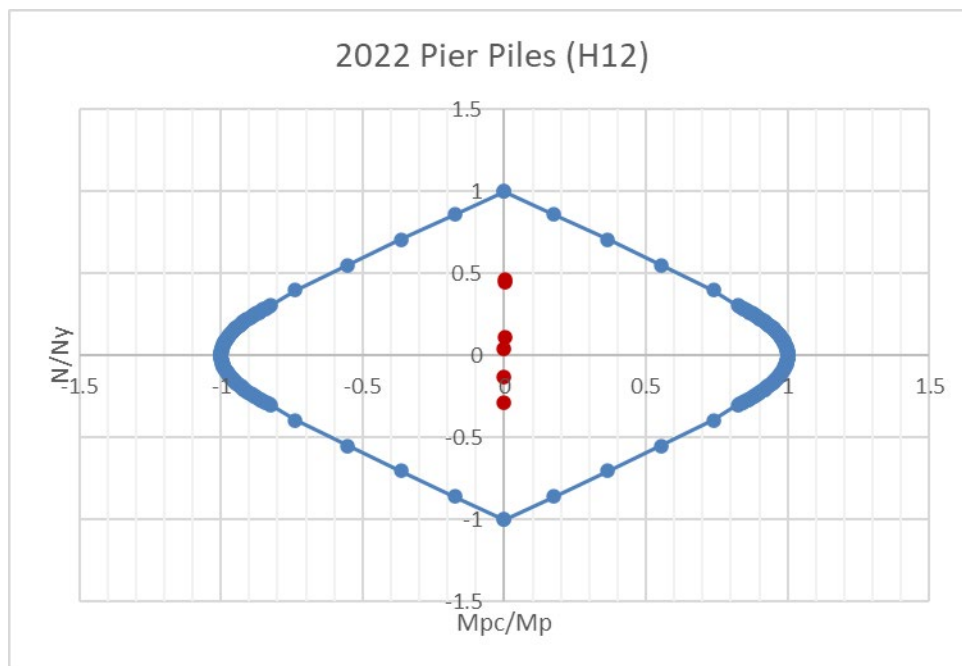


**Figure 5.89: Interaction diagram plot for the piles under the piers (May 2022)**

### 5.2.3.3 Results of Piles under Abutments

Tabulated values of the force-moment in these piles are given below in Table 5.63. Figure 5.90 presents the points mapped on the interaction diagram.

**Table 5.63: Tabulated values of force-moment in piles under the abutments**

|  |  | n | mpc | n/ny | mpc/mp |
|---|---|---|---|---|---|
| Abutment 1 | South | 103.592 | −48.371 | 0.233 | −0.340 |
|  |  | 47.938 | −46.348 | 0.108 | −0.326 |
|  |  | −6.580 | −43.896 | −0.015 | −0.308 |
|  |  | −63.732 | −41.324 | −0.143 | −0.290 |
|  | North | -125.959 | −38.854 | −0.283 | −0.273 |
| Abutment 2 | South | 282.798 | 42.780 | 0.636 | 0.301 |
|  |  | 133.838 | 44.331 | 0.301 | 0.312 |
|  |  | 27.600 | 43.772 | 0.062 | 0.308 |
|  |  | −77.677 | 43.190 | −0.175 | 0.304 |
|  | North | −220.306 | 43.230 | −0.496 | 0.304 |
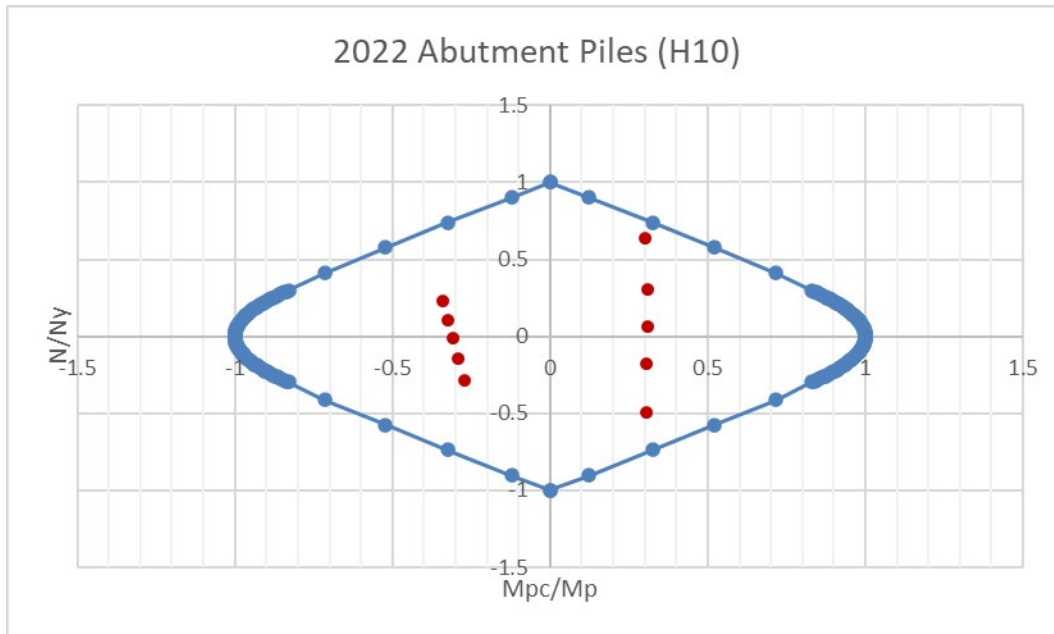


**Figure 5.90: Interaction diagram plot for the piles under the abutments (May 2022)**

*5.2.4 FRP Layouts*

Figure 5.92 shows the required number of GFRP bars to be applied at the top of each section. All bars are No. 8 Aslan 100 GFRP and applied on both directions with the given spacing as shown. For ease of construction, longitudinal CFRP sheets are considered at the bottom. V-Wrap C200H sheets shall be used for flexural and shear strengthening. They will be epoxied on to the existing surface as shown in Figure 5.93 and Figure 5.95. CRFP splay anchors with 3/4" diameter and 4" embedment shall be used at the bottom along each sheet as shown in Figure 5.94.

In addition, 3/4" splay anchors are used at the two edges to anchor GFRP bars to the U-Wraps as shown in Figure 5.91. It is also recommended to use the V-Wrap C200H sheets around the top of the piers. The wrapping would consist of a single sheet attached to the top two feet of each pier. This wrap would increase the strength of the piers by confining the concrete where the cracking is occurring on the bridge and the high stress concentration occurs in the Abaqus model.

NOTE:
Drill 3/4" hole through the top slab. Fill the hole with epoxy and and place splay anchors spaced every 3 ft along the edge where U-Wraps are needed.

use 2 zip-ties to fasten splay anchor with GRFP bars at the top

6 in.

CFRP splay anchors (total length 19")

Apply 4" concrete after cleaning & roughening the existing surface (f'c=4 ksi)

ASLAN 100 GFRP bar No. 8 @ 20" O.C

0.0156%

3/4" CFRP splay anchors spaced 3ft along the edge with 6" splay at the top and bottom (total length=19")

U-Wrap (C200H V-Wrap, strctural tech. inc.)

**Figure 5.91: Cross section of the box girder with U-wrap and GFRP bars shown**
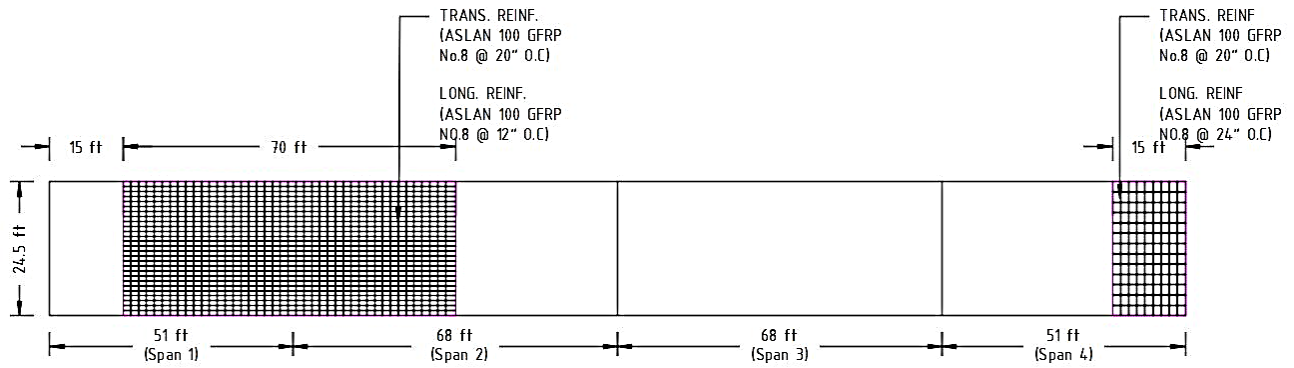
**Figure 5.92: Layout of GFRP bars required at the top along box girder**
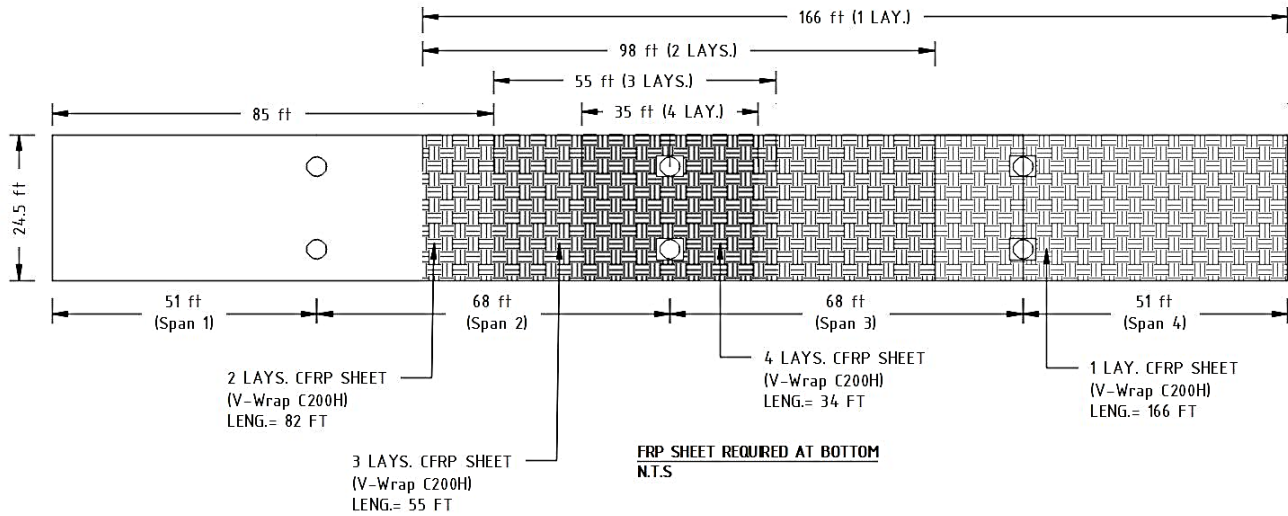


**Figure 5.93: Layout of CFRP sheets applied at the bottom along box girder**

110

NOTE:
1. ½" CFRP splay anchors with 4 in. embedment and 10 in. total length shall be used along 2, 3, and 4 layers of CFRP longitudinal sheets.
2. spacing of splay anchors are given in the figure.
3. splay should be facing towards pier 2 on both sides.
4. splay anchors are not needed for single layer of CRFP longitudinal sheets.
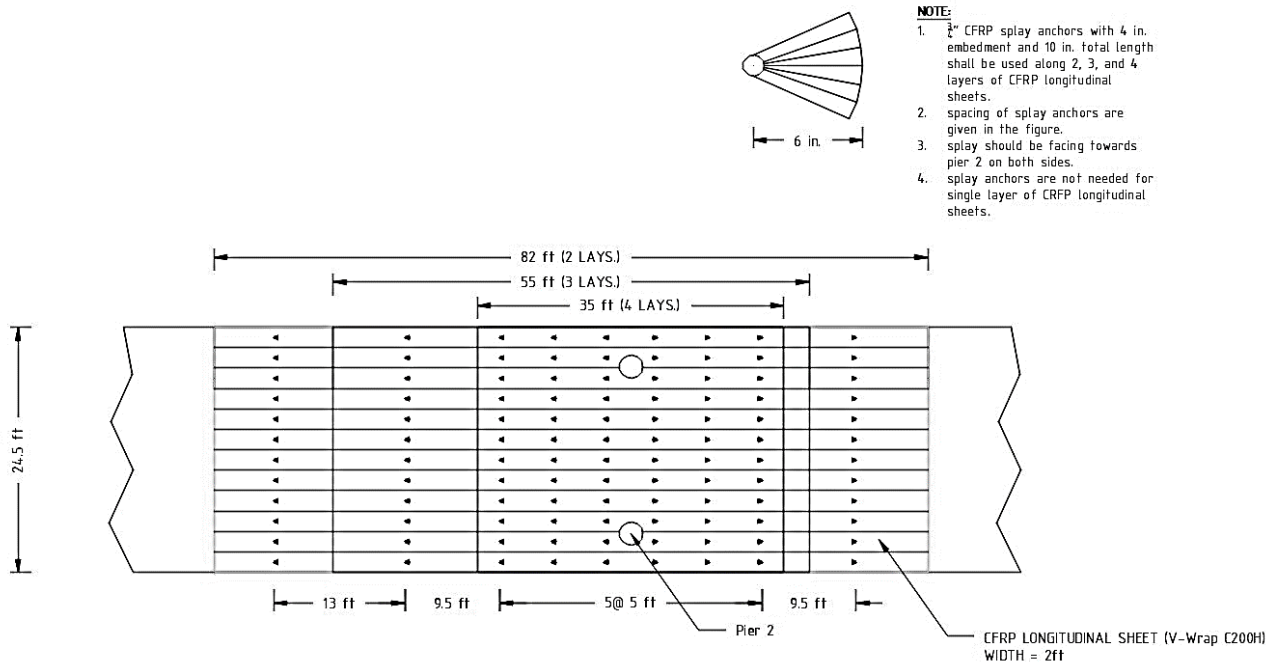
**Figure 5.94: Proposed CFRP splay anchor layout for 2, 3, and 4 layers of CFRP longitudinal sheets**
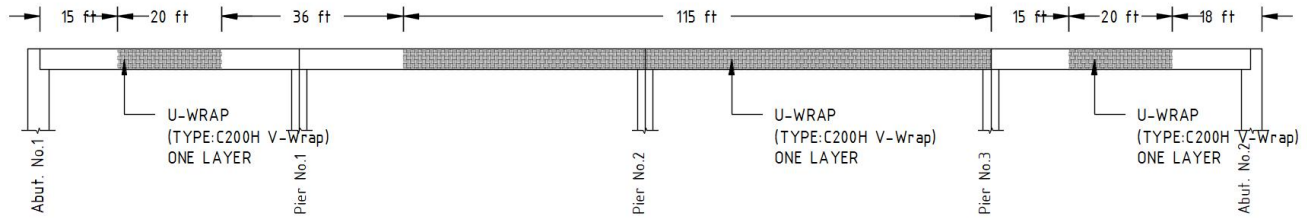


**Figure 5.95: Layout of U-Wraps along the box girder**

111

**Table 5.64: The current status and strengthening status of each section (April 2017)**

| Section designation* | Section status | Strengthening status |
|---|---|---|
| S1A1 | Capacity within range as of April 2017 | No strengthening needed |
| S1.25 | Capacity within range as of April 2017 | No strengthening needed |
| S1.50 | Yield capacity exceeded as of April 2017 | Strengthening needed |
| S1.75 | Capacity within range as of April 2017 | No strengthening needed |
| S1P1 | Capacity within range as of April 2017 | No strengthening needed |
| S2P1 | Capacity within range as of April 2017, however, yield capacity to exceed in May 2022 | No strengthening needed |
| S2.25 | Capacity within range as of April 2017, however, yield capacity to exceed as of May 2019 | No strengthening needed |
| S2.5 | Yield capacity exceeded as of April 2017 | Strengthening needed |
| S2.75 | Yield capacity exceeded as of April 2017 | Strengthening needed |
| S2P2 | Yield capacity exceeded as of April 2017 | Strengthening needed |
| S3P2 | Yield capacity exceeded as of April 2017 | Strengthening needed |
| S3.25 | Yield capacity exceeded as of April 2017 | Strengthening needed |
| S3.50 | Yield capacity exceeded as of April 2017 | Strengthening needed |
| S3.75 | Yield capacity exceeded as of April 2017 | Strengthening needed |
| S3P3 | Yield capacity exceeded as of April 2017 | Strengthening needed |
| S4P3 | Yield capacity exceeded as of April 2017 | Strengthening needed |
| S4.25 | Yield capacity exceeded as of April 2017 | Strengthening needed |
| S4.50 | Yield capacity exceeded as of April 2017 | Strengthening needed |
| S4.75 | Capacity within range as of April 2017, however, yield capacity to exceed as of May 2019 | No strengthening needed |
| S4A2 | Capacity within range as of April 2017 | No strengthening needed |

*See Figure 5.36 for section location along the bridge

### 5.2.5 Cost Analysis

In Table 5.65 through Table 5.68, an estimate for CFRP sheets applied longitudinally at the bottom, U-Wraps on sides, and GFRP bars along with splay anchors is given. Material and installation costs are provided separately in Table 5.69 and Table 5.70.

**Table 5.65: Estimate of GFRP bar and splay anchors required at the top**

|  | Length of bar (ft) | Span (ft) | Spacing (in.) | No. of bars | Total bar length (ft) | No. of FRP anchors (19") |
|---|---|---|---|---|---|---|
| Long. bar-L | 70 | 30 | 12 | 30 | 2,100 |  |
| Trans. bar_L | 30 | 70 | 20 | 42 | 1,260 | 46.67 |
| Long. bar-R | 15 | 30 | 24 | 15 | 225 |  |
| Trans. bar_R | 30 | 15 | 20 | 9 | 270 | 10 |
|  |  |  |  | **Sum** | **3,855** | **57** |

**Table 5.66: CFRP anchors at the bottom (length=10")**

|  | No. of FRP anchors (10") |
|---|---|
| Total no of anchors (dia. 3/4") | 108 |

**Table 5.67: CFRP sheet required at the bottom**

|  | Length of sheet (ft) | Width (ft) | Area (ft$^2$) |
|---|---|---|---|
| 1-layer | 166 | 24.5 | 4,067 |
| 2-layer | 98 | 24.5 | 2,401 |
| 3-layer | 55 | 24.5 | 1,348 |
| 4-layer | 35 | 24.5 | 858 |
|  |  | **Sum** | **8,673** |
| FRP sheets are manufactured having 24" width | | | |

**Table 5.68: CFRP U-Wraps required on sides**

|  | U-Wrap length (ft) | Span covered (ft) | Area (ft$^2$) |
|---|---|---|---|
| U-Wrap (Left) | 40 | 20 | 800 |
| U-Wrap (Middle) | 40 | 115 | 4,600 |
| U-Wrap (Right) | 40 | 20 | 800 |
|  |  | **Sum** | **6,200** |

**Table 5.69: Material cost***

| | | | |
|---|---|---|---|
| CFRP sheet required at the bottom (ft$^2$) | 8,673 | $5.00 | $43,365.00 |
| CFRP U-Wraps (ft$^2$) | 6,200 | $5.00 | $31,000.00 |
| GFRP bar, No. 8 (ft) | 3,855 | $1.75 | $6,746.25 |
| CFRP anchors at top (3/4" dia, length=19") | 57 | $21.00 | $1,190.00 |
| CFRP anchors at bottom (3/4" dia, length=10") | 108 | $13.25 | $1,431.00 |
| | | **Total:** | **$83,732.25** |

*Quotation for CFRP sheet and anchor including epoxy was obtained from Structural Technologies. Owens Corning provided the cost estimate for No. 8 CFRP bars.

**Table 5.70: Estimated installation cost**

| | | | |
|---|---|---|---|
| CFRP sheet required at the bottom (ft2) | 8,673 | $50.00 | $433,650.00 |
| CFRP U-Wraps (ft2) | 6,200 | $50.00 | $310,000.00 |
| GFRP bar, No. 8 (ft) | 3,855 | *$0.50 | $1,927.50 |
| CFRP anchors at top ( 3/4" dia, length=19") | 57 | $25.00 | $1,416.67 |
| CFRP anchors at bottom ( 3/4" dia, length=10") | 108 | $50.00 | $5,400.00 |
| | | **Total:** | **$752,394.17** |

Installation cost for GFRP bar and CFRP anchors are provided as an estimate by authors.

# Chapter 6: Conclusions and Recommendations

## 6.1 Conclusions

The following conclusions may be drawn from the present study:

1. The Abaqus analysis shows that the concrete maximum strength of 4 ksi is not exceeded in any component of the bridge except for the junction of the piers with the crossbeams under the April 2017 settlements. This is believed to be a stress concentration from the analysis. Tensile piles are not prone to pulling out as well.

2. The Abaqus analysis shows that the concrete maximum strength of 4 ksi is not exceeded in any component of the bridge except for the junction of the piers with the crossbeams under the April 2017 settlements plus HS20-44 truck loading. This is believed to be a stress concentration from the analysis. Tensile piles are not prone to pulling out as well.

3. The Abaqus analysis shows that the concrete maximum strength of 4 ksi is not exceeded in any component of the bridge except for the junction of the piers with the crossbeams under the April 2017 settlements plus projected settlements up to 2022. This is believed not to be a stress concentration from the analysis since it is spread beyond a hot spot. Tensile piles are not prone to pulling out as well.

4. The shear-torsion interaction diagrams established for various sections of the box girder with FRP strengthening indicate that these sections are safe beyond May 2022. However, S2.50 and S2P2 are only safe up to May 2022 after the section is strengthened.

5. Sections along Spans 2 and 3 seem to have already reached the yield strength due to April 2017 settlement. The bridge is unsafe to use if not strengthened properly.

6. The 4-inch concrete topping as shown in Figure 5.91 will increase the self-weight of the bridge and deflection. However, the most critical section along the bridge is located on the top of the second pier (S2P2) which is

115

undergoing positive moment due to differential settlement. Therefore, adding the topping will help this type of section. However, it will add up to extra stresses at typical positive moment sections.

## 6.2 Recommendations

The following recommendations are proposed from the conclusions of the present study:

1. Sections of the bridge along Spans 2 and 3 seem to have already reached the yield strength. It is strongly recommended to keep the bridge closed for traffic until it is strengthened or removed.

2. An estimated cost for strengthening is given in Section 5.2.5 of this report. Knowing that the strengthening will only extend the bridge's life up to May 2022, considering the settlement rate, it is recommended to demolish the bridge instead of strengthening it.

# References

Aggour, M. S., & Aggour, M. S. (1986). Settlement of simply supported bridge. *Journal of Structural Engineering, 112*(8).

Armstrong, A., Surdahl, R., & Armstrong, H. G. (2009). Peering into the unknown. *Public Roads, 72*(6).

Bowles, J. E. (1996). *Foundation analysis and design* (5th ed., pp. 932–934). New York, NY: McGraw-Hill.

Dedo, D., & White, K. (2017). KSN investigates: The money pit. Retrieved from https://www.ksn.com/news/local/ksn-investigates/ksn-investigates-the-money-pit/

Gurbuz, A., & Paikowsky, S. G., (2016). New simple approach to prediction of axial settlement of single piles under design load. *Journal of Bridge Engineering, 21*(10).

Halim, A. H., Esmaeily, A., & Rasheed, H. A. (2012). Behaviour of RC beams under combined shear and torsion according to AASHTO LRFD and ACI equations. *The IES Journal Part A: Civil & Structural Engineering, 5*(2), 95–105.

Lefchik, T. E., Ruegsegger, L. R., & Henthorne, R. W. (2003). Avoiding voids. *Public Roads, 66*(6).

O'Shea, D. M. (2015). How could a pile of dirt cause a major interstate bridge to tilt? *Public Roads, 79*(1).

Rabbat, B. G., & Russell, H. G. (1985). Friction coefficient of steel on concrete or grout. *Journal of Structural Engineering, 111*(3), 505–515.

Wardle, G. (2001, March/April). Gold mining from 1900 presents challenges for road construction. *Civil Engineering: Magazine of the South African Institution of Civil Engineering, 3*, 15–16.